INFORMATION TO USERS

This reproduction was made from a copy of a document sent to us for microfilming. While the most advanced technology has been used to photograph and reproduce this document, the quality of the reproduction is heavily dependent upon the quality of the material submitted.

The following explanation of techniques is provided to help clarify markings or notations which may appear on this reproduction.

1. The sign or "target" for pages apparently lacking from the document photographed is "Missing Page(s)". If it was possible to obtain the missing page(s) or section, they are spliced into the film along with adjacent pages. This may have necessitated cutting through an image and duplicating adjacent pages to assure complete continuity.

2. When an image on the film is obliterated with a round black mark, it is an indication of either blurred copy because of movement during exposure, duplicate copy, or copyrighted materials that should not have been filmed. For blurred pages, a good image of the page can be found in the adjacent frame. If copyrighted materials were deleted, a target note will appear listing the pages in the adjacent frame.

3. When a map, drawing or chart, etc., is part of the material being photographed, a definite method of "sectioning" the material has been followed. It is customary to begin filming at the upper left hand corner of a large sheet and to continue from left to right in equal sections with small overlaps. If necessary, sectioning is continued again–beginning below the first row and continuing on until complete.

4. For illustrations that cannot be satisfactorily reproduced by xerographic means, photographic prints can be purchased at additional cost and inserted into your xerographic copy. These prints are available upon request from the Dissertations Customer Services Department.

5. Some pages in any document may have indistinct print. In all cases the best available copy has been filmed.

University Microfilms International
300 N. Zeeb Road
Ann Arbor, MI 48106

Downloaded from SHAREOK. Persistent Handle URL: https://hdl.handle.net/11244/5159

8324887

Ewumi, Joseph Olukayode

THE STUDY OF WAVE MOTION IN A BOUNDED ELASTIC MEDIUM USING A MONTE CARLO RAY TRACING APPROACH

The University of Oklahoma PH.D. 1983

University Microfilms International 300 N. Zeeb Road, Ann Arbor, MI 48106

Copyright 1983

by

Ewumi, Joseph Olukayode

All Rights Reserved

PLEASE NOTE:

In all cases this material has been filmed in the best possible way from the available copy. Problems encountered with this document have been identified here with a check mark __√__.

1. Glossy photographs or pages _____
2. Colored illustrations, paper or print _____
3. Photographs with dark background _____
4. Illustrations are poor copy _____
5. Pages with black marks, not original copy _____
6. Print shows through as there is text on both sides of page _____
7. Indistinct, broken or small print on several pages _____
8. Print exceeds margin requirements _____
9. Tightly bound copy with print lost in spine _____
10. Computer printout pages with indistinct print __✓__
11. Page(s) _____ lacking when material received, and not available from school or author.
12. Page(s) _____ seem to be missing in numbering only as text follows.
13. Two pages numbered _____. Text follows.
14. Curling and wrinkled pages _____
15. Other _____

University
Microfilms
International

THE UNIVERSITY OF OKLAHOMA

GRADUATE COLLEGE

THE STUDY OF WAVE MOTION IN A BOUNDED ELASTIC MEDIUM USING A MONTE CARLO RAY TRACING APPROACH

A DISSERTATION

SUBMITTED TO THE GRADUATE FACULTY

in partial fulfillment of the requirements for the

degree of

DOCTOR OF PHILOSOPHY

By

JOSEPH OLUKAYODE EWUMI

Norman, Oklahoma

1983

THE STUDY OF WAVE MOTION IN A BOUNDED ELASTIC MEDIUM

USING A MONTE CARLO RAY TRACING APPROACH

A DISSERTATION

APPROVED FOR THE SCHOOL OF AEROSPACE, MECHANICAL

AND NUCLEAR ENGINEERING

By

Darin M. Egle

Tom J. Sorn

J N Huffaker

C. W. Bert

M Rasmussen

ACKNOWLEDGMENTS

I am very grateful to those individuals who have contributed very immensely to my academic career and most especially to my adviser, Dr. Davis M. Egle, who suggested this research topic and gave me consistent support, guidance, and encouragement. Other individuals worthy of special thanks include the members of my dissertation committee, Drs. Tom J. Love, Charles W. Bert, Maurice L. Rasmussen, and James N. Huffaker, from whose wealth of experience I greatly benefited.

Due acknowledgments are given to Drs. William D. Turner and L.W. Stockham whose dissertations I have used to enrich my understanding of the Monte Carlo method and to Ms. Rose Benda for the patience with which she typed this work.

I give due acknowledgment to the Federal Government of Nigeria and the University of Ife, Ile-Ife, Nigeria for their sponsorship. This research investigation could not have been possible without the computer time from the Merrick Computer Center at the University of Oklahoma. To this I am very grateful.

Finally, I do express my thanks and appreciation to my wife, Anu; daughters, Tayọ and Yetunde; and my son, Ṣegun, for their encouragement and sacrifices.

ABSTRACT

In this investigation, the displacement response of a bounded elastic medium is analyzed using a ray-tracing method coupled to a Monte-Carlo technique. The medium is an elastic, homogeneous, and isotropic solid bounded by six arbitrarily inclined stress-free plane surfaces. The wave-front curvature transformations due to the mode conversions at the free surfaces are derived. For sampling the reflected rays at the free surface, the Russian-roulette algorithm is utilized.

Numerical calculations are given for the following three models:

a) A two-dimensional plate with stress-free boundaries. The force is an impulsive dilatational wave located at the point (0,0).

b) A two-dimensional plate with stress-free boundaries. The force is a unit normal stress acting at the point (0,15) of the free surface. The force and the receiver are located at the opposite sides of the plate.

c) A two-dimensional plate with stress-free boundaries. The force is a unit normal stress acting at the point (0,15) of the free surface. The force and the receiver are located at the upper surface of the plate.

Computer algorithms are developed and the solutions of the displacement-field components are plotted for three different locations of

the receiver for each model. Numerical results are compared with the generalized ray analyses conducted by Pao [4] and Pao et al. [5] for the same geometry and the load conditions.

TABLE OF CONTENTS

	Page
ACKNOWLEDGMENTS	iii
ABSTRACT	iv
TABLE OF CONTENTS	vi
LIST OF TABLES	viii
LIST OF FIGURES	x
NOMENCLATURE	xiii
Chapter	
I. INTRODUCTION	1
1.1 Literature Survey	1
1.1.1 Problem Definition	1
1.1.2 Survey of Previous Research	3
1.2 Geometrical-Ray Approach	5
1.3 Monte Carlo Technique	9
1.4 The Main Objective of Research	9
II. PHYSICS OF THE PROBLEM AND MATHEMATICAL FORMULATION	12
2.1 Monte Carlo Formulation	12
2.1.1 Ray Emission from a Point Source	15
2.1.2 Russian Roulette	22
2.2 Reflection of Plane Waves at a Stress-Free Surface	27
2.2.1 Point of Intersection	29
2.3 Wavefront Curvature Due to Reflection of P-SV Wave at a Stress-Free Surface	30
2.3.1 Displacement Amplitude	32
2.3.2 Wavefront Curvature due to Reflection	34
2.3.3 Wavefront Curvature for Multiple Reflected Rays	38
2.3.4 Wavefront Curvature due to Reflection: A Three-Dimensional Case	42

Chapter		Page
III.	COMPUTATION ALGORITHM AND NUMERICAL EXAMPLES	49
	3.1 Computation Algorithm	49
	3.2 Numerical Calculation	53
	3.2.1 Response of a Plate to a Compressional Point Source: Numerical Calculations	53
	3.2.2 Components of Displacement at the Boundary . .	64
	3.3 Response of a Plate to a Unit Stress Normal to the Surface of the Plate	74
	3.3.1 Derivation of the Far-Field Solution Compressional and Shear Waves	74
	3.3.2 Unit Stress Normal to the Surface of the Plate: Numerical Calculations	78
IV.	ANALYSIS OF THE RESULTS AND CONCLUSIONS	101
	4.1 Results and Analysis	101
	4.1.1 Case (i) Dilatation Point Source	101
	4.1.2 Case (ii) Response Due to Surface Force (Source and Receiver on the Opposite Sides of the Plate)	102
	4.1.3 Case (iii) Response Due to Surface Force (Source and Receiver at the Upper Plate Surface)	103
	4.2 Comparison of Results and Conclusions	104
	4.3 Recommendations for Future Research	105
REFERENCES	. . . . .	107
APPENDIX:	COMPUTER PROGRAM	111
	Computer Program List for Dilatational Case	117
	Computer Program List for Surface Load	133

LIST OF TABLES

Table		Page
2.1	Direction of Emission	23
3.1	Arrival Time ($\tau = tC_T/2h$) Dilatation Point Source (r=2). . . .	56
3.2	Arrival Time ($\tau = tC_T/2h$) Dilatation Point Source ($r = 5, r = 10$)	57
3.3	Peaks of the Displacement Field ($r = 2$) Point of Dilatation (0,0)	61
3.4	Peaks of the Displacement Field ($r = 5$) Point of Dilatation (0,0)	62
3.5	Peaks of the Displacement Field ($r = 10$) Point of Dilatation (0,0)	63
3.6	Arrival Time ($\tau = tC_L/2h$) Surface Loading - Source and Receiver on the Opposite Sides of the Plate	80
3.7	Peaks of the Displacement Field ($r = 2$) Surface Loading - Source and Receiver on Opposite Side	81
3.8	Peaks of the Displacement Field ($r = 4$) Surface Loading - Source and Receiver on Opposite Side	82
3.9	Peaks of the Displacement Field ($r = 6$) Surface Loading - Source and Receiver on Opposite Side	83
3.10	Arrival Time ($\tau = tC_L/2h$) Surface Loading - Source and Receiver at the Upper Plate Surface	91
3.11	Peaks of the Displacement Field ($r = 2$) Surface Loading - Source and Receiver on the Upper Plate Surface	92
3.12	Peaks of the Displacement Field ($r = 4$) Surface Loading - Source and Receiver on the Upper Plate Surface	93
3.13	Peaks of the Displacement Field ($r = 6$) Surface Loading - Source and Receiver on the Upper Plate Surface	94

Table Page

A-1 Computer Time (CPU 112

LIST OF FIGURES

Figure		Page
1.1	Ray tracing in a bounded solid medium	2
1.2	Plane waves incident upon a stress-free surface	7
1.3a	Conventional ray-tracing approach	8
1.3b	Ray tracing with an application of Russian roulette	8
2.1	Emission of ray from a point source	16
2.2	Direction of emission — two-dimensional case	20
2.3	Average energy transmission across ΔS with incident shear waves	20
2.4	Direction of the reflected ray	28
2.5a	P-wave emitted from a point source	33
2.5b	Mode conversion and the imaginary point source — P-SV waves	34
2.6	Displacement of the P-SV waves: geometrical derivation . .	35
2.7a	Mode conversion at a free surface. (a) PSP waves	39
2.7b	Mode conversion at a free surface. (b) PSPS waves	40
2.8	Curvature due to reflection. (a) Location of R_1'', (b) Rotation about z-axis	44
2.9	Inclined planes of reflection	46
2.10	Lines of curvature. (a) Principal normal curvatures, (b) Normal curvature in an arbitrary direction	47
3.1	Direct ray and a single reflected waveform	51
3.2	Monte Carlo decision variables. (a) For incident P-wave, (b) For incident SV-wave	51

Figure		Page
3.3	Ray paths and the locations of the receiver. Source is at point (0,0), r = AY/2h	54
3.4	Time function [$\Delta = f(\tau)$]. (a) Quadratic pulse, (b) Saw-tooth shape function	58
3.5	Reflections of the PSP waves due to: (a) dilatational force, (b) unit normal stress	60
3.6	Direction of the partical displacements. (a) Reflection is at the upper surface, (b) Reflection is at the bottom surface	65
3.7	Plates response to a unit dilatation point force. Point of dilatation (0,0) ($t_0 = t/\tau$). Vertical components, r = 2 . .	67
3.7a	Responses due to dilatational point source obtained by Pao et al. [4]	68
3.8	Plates response to a unit dilatation point force. Point of dilatation (0,0)($t_0 = t/\tau$). Horizontal components, r = 2 . .	69
3.9	Plates response to a unit dilatation point force. Point of dilatation (0.0)($t_0 = t/\tau$). Vertical components, r = 5 . .	70
3.10	Plates response to a unit dilatation point force. Point of dilatation (0,0)($t_0 = t/\tau$). Horizontal components, r = 5. .	71
3.11	Plates response to a unit dilatation point force. Point of dilatation (0,0)($t_0 = t/\tau$). Vertical components, r = 10 . .	72
3.12	Plates response to a unit dilatation point force. Point of dilatation (0,0)($t_0 = t/\tau$). Horizontal components, r = 10. .	73
3.13	Reflection of waves with: (a) odd number of segments, (b) even number of segments	79
3.14	Plates response to a unit surface force at (0,15). Receiver is located at point (60,-15). Vertical components, r = 2 .	84
3.15	Plate response to a unit surface force at (0.15). Receiver is located at point (60,-15). Horizontal components, r = 2.	85
3.16	Plate response to a unit surface force at (0.15). Receiver is located at point (120,-15). Vertical components, r = 4 .	86
3.16a	Responses due to Surface Load by Pao [5]	87

Figure		Page
3.17	Plate response to a unit surface force at (0,15). Receiver is located at point (120,-15). Horizontal components, r = 4	88
3.18	Plate response to a unit surface force at (0.15). Receiver is located at point (180,-15). Vertical components, r = 6	89
3.19	Plate response to a unit surface force at (0,15). Receiver is located at point (180,-15). Horizontal components, r = 6	90
3.20	Plate response to a unit surface force at (0,15). Receiver is located at point (60,15). Vertical components, r = 2	95
3.21	Plate response to a unit surface force at (0,15). Receiver is loacted at point (60,15). Horizontal components, r = 2	96
3.22	Plate response to a unit surface force at (0,15). Receiver is located at point (120,15). Vertical components, r = 4	97
3.23	Plate response to a unit surface force at (0,15). Receiver is located at point (120,15). Horizontal components, r = 4	98
3.24	Plate response to a unit surface force at (0,15). Receiver is located at point (180,15). Vertical components, r = 6	99
3.25	Plate response to a unit surface force at (0.15). Receiver is located at point (180,15). Horizontal components, r = 6	100

NOMENCLATURE

a	radius of the circular disc
A	area of the sphere
A_i, B_i, C_i, D_i	coefficients
AY	horizontal distance of the receiver from the source
A_0, A_1, A_2	displacement amplitudes
C_L, C_T	dilatational and torsional wave speeds, respectively
dA'	differential surface area
dx,dy,dz	differential elements
e	incident or reflected angle for a P-wave
f	incident or reflected angle for an SV-wave
f( ),g( )	density functions
F( ),G( )	cumulative distribution functions
h	one-half of the thickness of the plane
h_1, h_2, h_3	distances of the apparent point sources from the reflecting planes
H( )	heaviside unit step function
i	square root of -1
k	ratio of wave speeds
K	wavefront curvature factor
ℓ,m,n	direction cosines
n	number of reflections

N	total number of emissions
0	real point source
$0_1, 0_2, 0_3$	apparent point sources
P	dilatational wave
P_i, P_r	incident and reflected dilatational waves, respectively
$P(\ )$	probability function
r	horizontal distance of the receiver from the real point source (normalized)
r,z	cylindrical coordinates
r_o	radial distance between either the source and the pierce point or any two conservative points of reflection
$\vec{R}$	unit vector normal to the plane
R'_{eff}, R''_{eff}	effective radii of curvature
R_θ	random number
$R_{SS}, R_{PS}, R_{PP}, R_{SS}$	coefficients of reflection
S,SV	shear wave
S_i, S_r	incident and reflected shear waves
t	arrival time
t_c	cumulative time of arrival
t_o	the time it takes a wave, P or SV, to travel across the thickness of the plate
t_{max}	maximum time for ending the calculation
u,w	displacement components
u_r, u_θ	displacement components for P- and SV-waves, respectively
$\vec{U}$	incident vector

U_R, U_θ	radial displacement components for P- and SV-waves, respectively
U_{RH}, U_{RV}	horizontal and vertical components of displacements with an incident P-wave
$U_{\theta H}, U_{\theta V}$	horizontal and vertical components of displacements with an incident SV-wave
$U_{\theta R}, U_{\theta i}$	real and imaginary parts of the displacement component of an SV-wave
$U_{RPP}, U_{RPS}, U_{OPP}, U_{OPS}$	displacement contributions of the reflected rays
x, y, z	system coordinates
$X(\ )$	random variable
α	the Monte Carlo sampling parameter for an incident P-wave
β	Monte Carlo sampling parameter for an incident SV-wave
γ_i	ratio of the horizontal distance of the point of reflection to the horizontal distance of the transducer
δ	delta function
Δ	half duration of the source pulse
$\Delta S, \Delta S_0, \Delta S_1, \Delta S_2$	cross-sectional area
θ, ϕ	random variables
θ_i	i-th angle of reflection
λ	Hooke's constant
λ, μ, ν	direction numbers of a line
μ	Lamé's constant

ξ	angle between two consecutive planes of reflection
π	3.1415927
σ	normal stress
τ	time of arrival (normalized)
$\phi(\ )$	joint density function
ϕ_o, ϕ, ψ	displacement potentials
ω	radial frequency of waves
ω_i	i-th angle of incidence
Ω	sample space

CHAPTER I

INTRODUCTION

1.1 Literature Survey

In this chapter, the problem is defined with respect to non-destructive testing of materials followed by a review of early research works in the literature. Moreover, both the geometrical ray approach and the Monte Carlo techniques are explained with specific allusion to their applications in fluid and solid acoustics, neutron transport, and radiative heat transfer.

1.1.1 Problem Definition

The structural integrity of some materials can be characterized through the stress waves generated from sources (cracks, growth of defects) in the medium. In order to sense these waves, which are also called acoustic emission, transducers are often located on the surface of the medium. However, since the source is very often of a random nature, the transducer can only pick up such signals after they have gone through many reflections, see for example, Hsu [1] and Fig. 1.1.

In spite of the fact that cracks or defects are located in the material in a random fashion, analytic representations of acoustic emission signals are still based on deterministic functions. This often leads to inaccurate results and grossly limits its exploitation as a

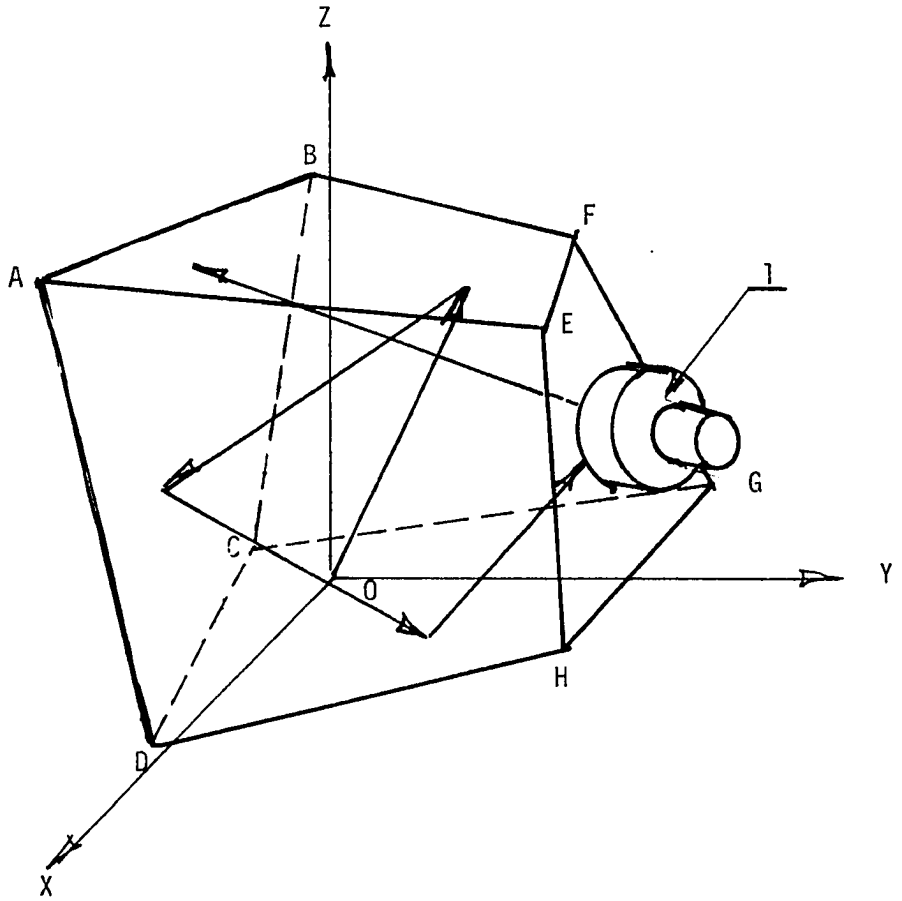

Fig. 1.1 Ray tracing in a bounded solid medium.

1 - transducer
O - point of origin

nondestructive testing technique. Moreover, it is extremely difficult to obtain details of the actual source of the mechanism.

Only recently has attention focused on representing acoustic emission by random processes. Egle [2,3] and Pao et al. [4,5,6] have suggested it might be best to correlate the wave behavior in the material with the observation on the transducer in order to realize the great potential of this technique in understanding mechanical properties of solids. In order to quantitatively analyze the response of the transducer to the source function inside the elastic solid (material), it is essential to simulate the source, identify the most predominant of the body waves, and characterize the stress waves in a probabilistic form.

The present investigation applies a ray-tracing technique coupled to the Monte Carlo method for determining the response at a point on the surface of a bounded elastic body excited by a compressional source. This method is further expanded to include other types of sources and so provides a valuable aid in acoustic emission research.

1.1.2 Survey of Previous Research

Since Lamb's classic paper [7] in 1904 on the propagation of a tremor over the surface of a semi-infinite elastic solid, tremendous efforts have been devoted to the study of the elastic wave motion and the resolving of the consequent complex integrals; see also [8,9].

Bromwich [10], for instance, expressed wave motion in a series of pulses by expanding the formal solution of elastic waves in negative powers of exponentials, a method which was used by Muskat and Pekeris [11,12,13] to obtain formal solutions to elastic wave problems. This method of expansion could be very tedious when solving the more complex but

but interesting problems. Also, in 1919, by representing sinusoidal spherical waves in terms of plane waves, Weyl [14] was able to study the propagation of radio waves generated by a dipole near the flat earth. His method was later extended to arbitrary wave shapes by Poritsky [15].

However, most of these techniques give solutions in a closed form not amenable to numerical calculations, since many parameters introduced can hardly be accounted for. Even after the development of direct methods of inversion of the relevant integrals by Cagniard [16], many investigators, like Lapwood [17], Pekeris et al. [18] and Pinney [19,20], still resorted to different asymptotic techniques. One of these methods often adopted by Pekeris uses plane-wave approximations which assume that the source function is either of a short duration or of high frequency content. In this case like in Lamb's work, Bessel functions in the integral are represented with their asymptotic expressions. In an attempt to give numerical calculations in his work on surface motion due to a point source in a semi-infinite elastic medium, Pinney [19,20], as it was later shown by Pekeris and Longman [12], used a method of evaluation of the integrals which became inaccurate just at the point of interest.

Knofoff, et al. [21] on the other hand adopted a generalized ray approach, a technique which considers only the predominant part of the wave motion near the arrival time. Both normal mode and the generalized-ray methods also required the Bromwich expansion. Besides, the generalized-ray method becomes increasingly inefficient for multi-reflected rays since, as Pao [4] pointed out, the number of integrals to evaluate increases as $2m + 1$ where m is the number of reflections

of each ray path. This also limits its use in studying long term response.

Another interesting method is a geometrical-ray approach which Chopra [22] used to give a formal solution for a compressional point source in an internal stratum. In the same work, assuming a harmonic source, he represented the potential for a point source of compressional waves by Sommerfeld's integral. Since this integral for a spherical point source can be regarded as a superposition of plane waves [13], he expanded it using Bromwich's method. He later evaluated the displacement corresponding to two of the successive terms in the expansion by the saddle-point approximation. He did conclude, however, that the two methods yielded the same result.

Although the geometric ray has some geometric involvement, it gives a better insight into the mode conversion phenomenon and is applied in this present research work.

1.2 Geometrical-Ray Approach

The geometrical-ray approach for solving wave propagation is an asymptotic approximation valid only in the far field of the source. The technique is well known and has been used extensively in optics and fluid acoustics. In solid acoustics, the geometrical-ray approach has not been as widely used as the more formal generalized-ray methods, summarized by Pao [4] or the Bromwich-expansion method (see, for example, Newlands [23], Hong [24,25]).

The major disadvantage of the simple ray-tracing approach is that it cannot account for several near field effects, including conical or head waves, and the generation of surface waves. It is shown in

the later chapters that this approach, when the refraction of mode conversions of waves transmitted into different media are properly accounted for, does yield the correct far-field results for body waves. This geometrical-ray approach, if modified to account for the generation of surface waves, can be used to compute the response at any point on the surface of a solid bounded by planes.

Given a point source, the direction cosines of a ray, and the defined geometry of the boundary planes, it is possible to determine the point of intersection of the ray and the impinged plane. Because of the mode conversion phenomenon in elastic waves after reflection (see Fig. 1.2), it becomes necessary to pursue two rays: both P- and S-waves after reflection. This makes the number of different rays to trace down after a few reflections enormous and, hence, ray tracing in the conventional sense becomes impracticable. This problem is avoided by using the Russian-roulette method—a special form of importance-sampling technique whereby functions of less importance are eliminated and the resulting bias reduced by increasing the weight of the remaining function. Thus, in this application, the Russian-roulette method is applied to select one of the reflected rays to continue tracing. This process is continued for a cumulative time $t_c \leq t_{max}$ where t_{max} is the predetermined time for ending the calculation (see Fig. 1.3).

This process of selecting a ray emanating from the source, weighting according to the source type and tracing that ray as it reflects from the boundaries of the media is repeated many times. Whenever a ray strikes the part of the surface on which the transducer is located, the time of hit is recorded and the displacement components

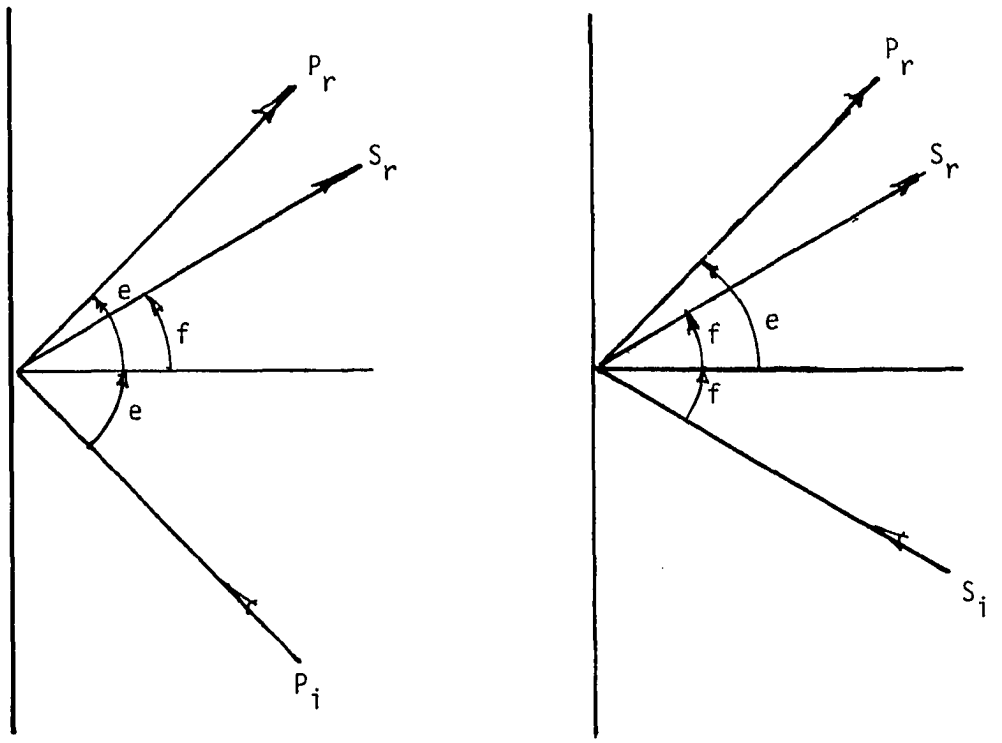

(a) Incident P-Waves (b) Incident SV-Waves

Fig. 1.2 Plane waves incident upon a stress-free surface.

P_i - incident P-waves
S_i - incident SV-waves
S_r - reflected SV-waves
P_r - reflected P-waves
e - incident or reflected angle for P-waves
f - incident or reflected angle for SV-waves

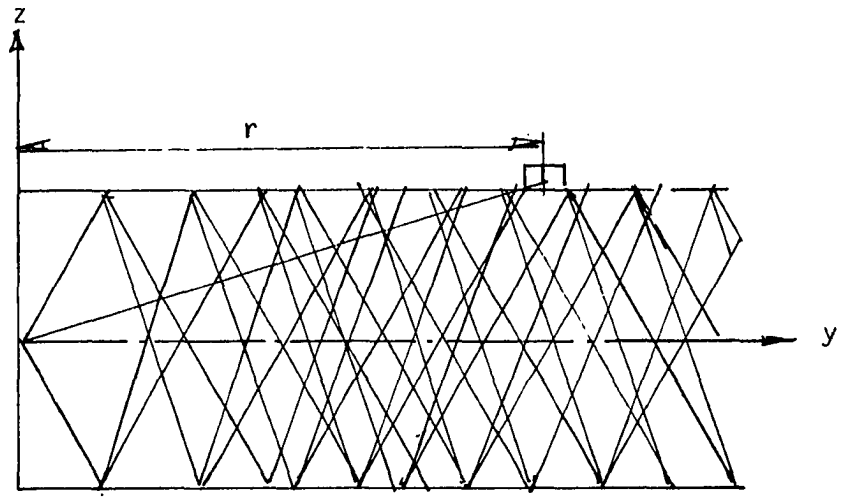

Fig. 1.3a. Conventional ray-tracing approach.

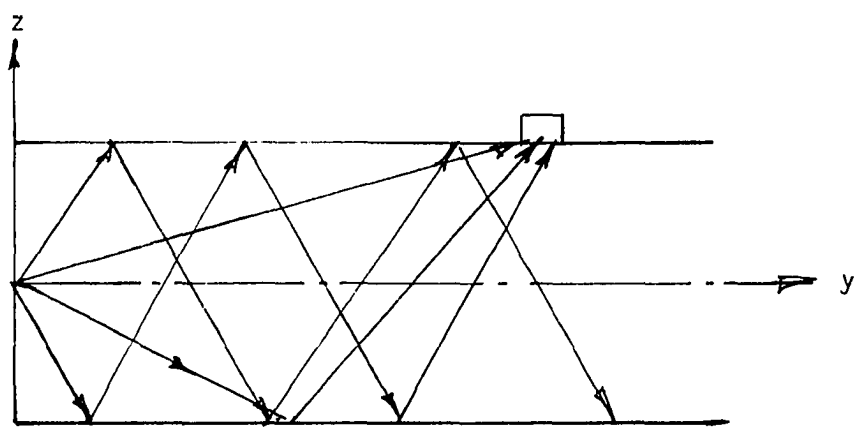

Fig. 1.3b. Ray tracing with an application of Russian roulette.

under the transducer are calculated. The cumulative displacement then gives the response of the solid to the source being simulated.

1.3 Monte Carlo Technique

This is a method of statistical trials used for solving problems of computational mathematics [26]. It involves the construction of some random process for the problem at hand and equating its parameters to the required physical quantities in the problem. By calculating the statistical characteristics from the observation of the parameters of the random process, those of the physical quantities can also be computed.

This technique has recently received wide application in neutron transport, fluid, and room acoustics [27,28]. Haviland et al. [28] proposed it for determining the acoustical pressure-time history in a spatial enclosure by tracing acoustical rays. They used it to calculate the ultimate average pressure in a given rectangular room and found their result to compare reasonably well with known solutions. They have only considered a simple case of reflection instead of complex cases like curved boundaries, cases involving refraction or elastic waves where modes of reflection should be taken into consideration. Stockham [29] and Turner [30] had also extended its application to radiative heat transfer.

1.4 The Main Objective of Research

In light of the above, it was considered best to attack this problem by combining the Monte Carlo method with a geometrical ray tracing technique. Therefore, the following tasks are the objectives

of this research:

1) Simulation of the compressional and the transverse (shear) waves emitting from an impulsive point source. The solid is assumed to be elastic, isotropic, and homogeneous.
2) The study of the response of a bounded elastic solid due to an impulsive compressional point source with specific reference to:
   a. An isotropic and homogeneous solid body bounded by six arbitrarily inclined planes. Surfaces are stress free.
   b. An isotropic and homogeneous elastic plate with the stress-free surfaces
3) Determination of mode conversion after reflection on a stress-free surface, using the Russian-roulette technique and computation of the displacements for both incident and reflected waves including P-P, P-SV, SV-SV, and SV-P.
4) Development of a computer algorithm for the ray tracing, boundary reflections, and displacement computations.
5) Application of the above methodology to give numerical calculations for:
   a. The response of an elastic plate due to an impulsive point source.
   b. Response of a plate to a unit normal stress with a square pulse time function applied to the surface of the plate.

6) Analysis of the results, comparison with known existing analytical and experimental results and recommendations for future research.

CHAPTER II

PHYSICS OF THE PROBLEM AND MATHEMATICAL FORMULATION

One of the distinguishing characteristics in the study of elastic waves in a bounded medium is the occurrence of the mode conversion phenomenon whereby two different types of waves are generated after reflection at a free surface. This does account for the relative complexities of its problems as compared to those of either acoustic or electro-magnetic waves. Therefore, due considerations are given to the physics involved when theoretical bases are formulated.

With this understanding in mind, in this chapter, bases for using a Monte Carlo approach for the ray emission from a point source are examined, followed by the Russian-roulette method for selecting the reflected ray, reflection of the plane waves at the free surface, and the curvature due to reflection of waves. Applications to both two- and three-dimensional cases are given.

2.1 Monte Carlo Formulation

In this section, we make use of a random number generator to determine the vector direction of each ray coming from a point source in such a way that it possesses an equal distribution over all directions of a sphere.

Firstly, let us recount some relevant portions of the theory

of probability (see Lindgren [31] and Shooman [32]).

A distribution function is defined as [31] the probability of a random variable $X(\omega)$ induced in a sample space Ω, i.e.,

$$F(\lambda) = P(X \leq \lambda),\ F(x) = P(X \leq x)$$

or

$$F(q) = P(X \leq q)$$

and obeying the following axioms of a probability space.

$$\begin{aligned} &\text{(a)}\quad 0 \leq F(x) \leq 1 \\ &\text{(b)}\quad F(-\infty) = 0,\quad F(\infty) = 1 \\ &\text{(c)}\quad F(x) \leq F(y) \quad \text{whenever } x < y \\ &\text{(d)}\quad \lim_{y \to x^{+}} F(y) = F(x) \end{aligned} \tag{2.1}$$

A distribution function could be discrete or continuous depending on whether the probability is assigned in discrete amounts at isolated places or 'spread' over an interval of values.

The derivative of a distribution function is called the density function which can be expressed as

$$\begin{aligned} f(x) &= \frac{d}{dx} F(x) = \frac{d}{dx} P(X \leq x) \\ f(x)dx &= P(X \leq x + dx) - P(X \leq x) \\ f(x)dx &= P(x < X < x + dx) \end{aligned} \tag{2.2}$$

In the case of a continuous function, the probability distribution can be set by specifying the density function which should satisfy the following properties:

$$f(x) \geq 0 \tag{2.3}$$

and

$$\int_{-\infty}^{\infty} f(x)dx = 1$$

Therefore, the distribution function can be defined as

$$F(x) = P(X \leq x) = \int_{-\infty}^{X} f(u)du$$

From here, it follows that

$$P(a \leq x < b) = \int_{a}^{b} f(\lambda)d\lambda \tag{2.4}$$

which shows that as a definite integral, a distribution function can be interpreted as an area under a curve.

Similarly, in the case of a multiple random variable, we can define a cumulative distribution function if the joint density function $\Phi(\theta,\phi)$ satisfies the following conditions:

$$\int_{-\infty}^{\infty}\int_{-\infty}^{\infty} \Phi(\theta,\phi)d\theta d\phi = 1$$

and

$$\Phi(\theta,\phi) \geq 0 \quad \text{for} \begin{cases} -\infty \leq \theta \leq \infty \\ -\infty \leq \phi \leq \infty \end{cases} \tag{2.5}$$

The random variables θ,ϕ could be dependent or independent.

If it is assumed that θ and ϕ are two independent random variables, then their density functions can be written as the product of the two marginal density functions.

$$\Phi(\theta,\phi) = g(\theta)f(\phi) \tag{2.6}$$

where

$$g(\theta)d\theta = [\int_{\alpha}^{\beta} \Phi(\theta,\phi)d\phi]d\theta$$

$$f(\phi)d\phi = [\int_{\alpha}^{\beta} \Phi(\theta,\phi)d\theta]d\phi \qquad (2.7)$$

and $g(\theta)$ and $f(\phi)$ are the marginal density functions. Hence, the probability (cumulative) distribution functions can be determined as

$$G(\theta) = \int_{0}^{\theta} g(\theta)d\theta \qquad (2.8a)$$

and

$$F(\phi) = \int_{0}^{\phi} f(\phi)d\phi \qquad (2.8b)$$

2.1.1 Ray Emission from a Point Source

In this analysis, the above probability principles are applied for both the three-dimensional and two-dimensional cases. See Turner [30] and Stockham [29] for more details.

A Three-Dimensional Case. Let us assume that a ray emanating from a point source at O is isotropic (see Fig. 2.1), i.e., both the cosine of the polar angle, θ, and the aximuthal angle, ϕ, are considered uniformly distributed in the interval (-1, +1) and (0.2π), respectively for

$$0 \leq \theta \leq \pi$$

$$\theta \leq \phi \leq 2\pi$$

Since the number of emissions from a point source through a differential area on the surface of a sphere is directly

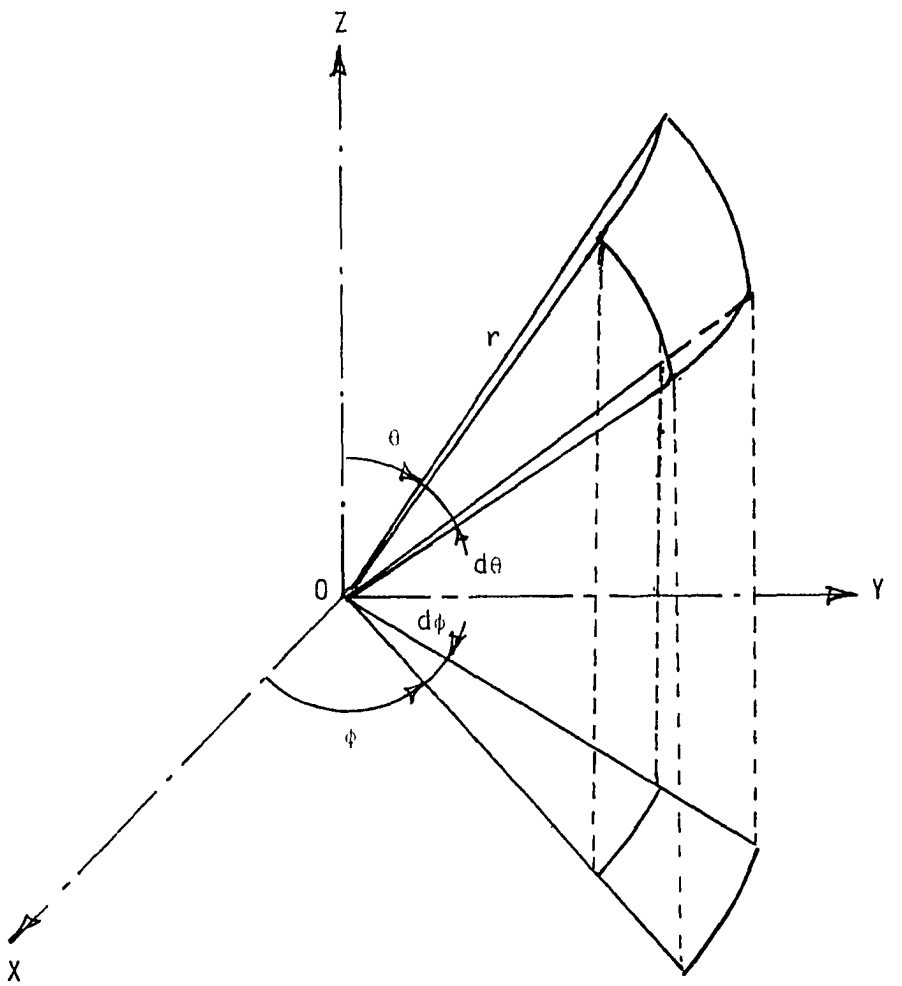

Fig. 2.1 Emission of ray from a point source.

ϕ - azimuthal angle
θ - polar angle
r - position vector
0 - point of origin

proportional to the area of the surface, then the number of emissions from a point O can be written as

$$N = \frac{dA'}{A} = \frac{r\sin\theta d\phi r d\theta}{4\pi r^2} = \frac{\sin\, d\phi d\theta}{4\pi} \tag{2.9}$$

where

N - total number of emissions

dA' - area of the differential surface

A - area of the sphere

Since

$$\int_0^{2\pi}\int_0^{\pi} \frac{\sin\theta d\theta d\phi}{4\pi} = 1$$

and

$$\frac{\sin\theta}{4\pi} \geq 0 \quad \text{for} \quad 0 \leq \theta \leq \pi \quad \text{and} \quad 0 \leq \phi \leq 2\pi$$

then, we can define

$$\Phi(\theta,\phi) = \frac{\sin\theta}{4\pi}$$

as the joint probability density function of the random variables θ and ϕ and determine its associated cumulative distribution function.

Determination of the Marginal Density Functions and Their Probability Distribution Functions

If we assume that θ and ϕ are two independent random variables, then their joint density function from equation (2.6) above, becomes

$$\Phi(\theta,\phi) = g(\theta)f(\phi)$$

where

$$g(\theta)d\theta = \left[\int_0^{2\pi} \Phi(\theta,\phi)d\phi\right]d\theta$$

and

$$f(\phi)d\phi = \left[\int_0^{\pi} \Phi(\theta,\phi)d\theta\right]d\phi$$

$g(\theta)$ and $f(\phi)$ are the marginal density functions

$$g(\theta) = \int_0^{2\pi} \frac{\sin\theta d\phi}{4\pi} = \frac{\sin\theta}{2} \tag{2.10}$$

Similarly,

$$f(\phi) = \int_0^{\pi} \frac{\sin\theta}{4\pi} d\theta$$

i.e.,

$$f(\phi) = \frac{1}{2\pi} \tag{2.11}$$

Therefore, the associated probability distributions can be determined by integrating equations (2.10) and (2.11) over θ and ϕ, respectively.

$$G(\theta) = \int_0^{\theta} \frac{\sin\theta}{2} d\theta = 1/2(1 - \cos\theta)$$

$$F(\phi) = \int_0^{\phi} \frac{d\phi}{2\pi} = \frac{\phi}{2\pi}$$

where $G(\theta)$, $F(\phi)$ are the probability distributions.

It could be observed that as $\cos\theta$ varies from -1 to +1, $G(\theta)$ varies from 1 to 0. Therefore, it is appropriate to set

$[1 - G(\theta)]$ which varies in the interval $[0,1]$ equal to a random number $R_\theta[0,1]$, say.

Similarly, since $F(\phi)$ varies in the interval $[0,1]$ as ϕ varies from 0 to 2, $F(\phi)$ can be equated to a random number R_ϕ in the interval $[1,0]$, i.e.,

$$R_\theta = 1 - G(\theta)$$

$$R_\theta = 1 - 1/2(1 - \cos\theta)$$

$$R_\theta = 1/2(\cos\theta + 1)$$

$$R_\phi = \frac{\phi}{2\pi} \tag{2.12}$$

The directions of emission can be determined by

$$\cos\theta = 2R_\theta - 1 \qquad (-1 \leq \cos\theta \leq +1)$$

$$\theta = 2\pi R_\phi \qquad (0 \leq \phi \leq 2\pi) \tag{2.13}$$

Hence, any ray emanating from the point, 0 can be represented by a vector,

$$\vec{r} = \ell\hat{i} + m\hat{j} + n\hat{k} \tag{2.14}$$

where ℓ, m, and n are the direction cosines

$$\ell = \cos\phi \sin\theta$$

$$m = \sin\phi \sin\theta$$

$$n = \cos\theta$$

A Two-Dimensional Case. In this case, the number of emissions is given as (see Fig. 2.2)

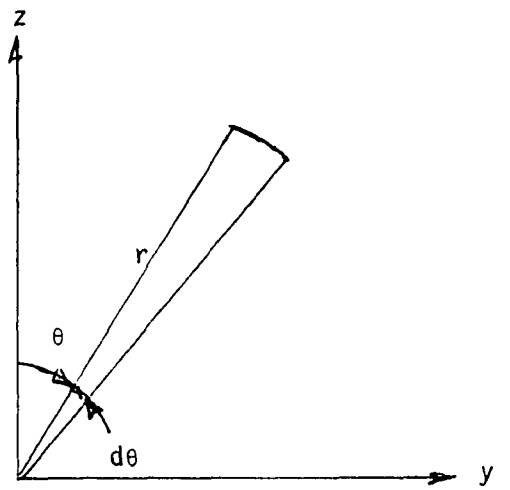

Fig. 2.2. Direction of emission - two-dimensional case.

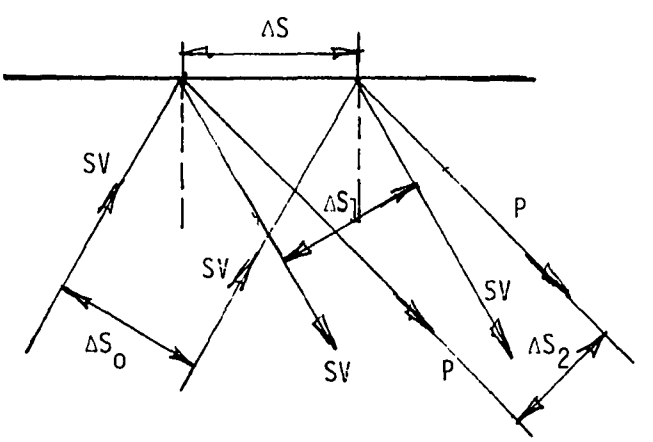

Fig. 2.3. Average energy transmission across ΔS with incident shear waves.

$$N \simeq \frac{A'}{A} = \frac{\frac{1}{2}\gamma^2 d\theta}{\pi\gamma^2} = \frac{d\theta}{2\pi}$$

Since

$$\int_0^{2\pi} \frac{d\theta}{2\pi} = 1$$

and

$$\frac{1}{2\pi} > 0 \quad \text{for} \quad 0 \leq \theta \leq 1$$

the density function $f(\theta)$ is taken as $1/2\pi$.

In order to find the distribution function, $G(\theta)$, equation (2.11) is integrated to give

$$G(\theta) = \int_0^{\theta} \frac{d\theta}{2\pi} = \frac{\theta}{2\pi}$$

Since $G(\theta)$ varies within the limits $[0,1/2]$ as θ varies between $(0 \leq \theta \leq \pi)$ and $G(\theta)$ varies between $[1/2,0]$ as θ varies between $(\pi < 0 < 2\pi)$, we can equate $G(\theta)$ to a random number R which varies between $R_\theta(0,1)$, see Fig. .

Thus, if R_θ falls between $(0 \leq R_\theta \leq 1/2)$,

$$\frac{\theta}{2\pi} = R_\theta$$

therefore,

$$\theta = 2\pi R_\theta$$

but if R_θ falls between $(1/2 < R_\theta < 1)$, the ray is emitted outside the plate.

Therefore, the direction cosines are

$$\ell = \cos \theta$$
$$n = \sin \theta \qquad (2.15)$$

Table 2.1 shows the summary of the distribution functions and the direction of emission.

2.1.2 Russian Roulette

The Russian-roulette technique is used in this work, as mentioned earlier, to select and trace down the path history of the more important of the two rays produced by each reflection. The frequency of occurrence of the waveform chosen depends on both the nature of the incident ray and the ratio of the energy distribution at the point of reflection. As mentioned in the earlier chapter, the incident ray on reflection at a free surface generates two other rays. Therefore, for energy considerations, we can assume that there is no energy loss at the point of reflection. Achenbach [33,34,35] represented this for incident P-waves as

$$\left(\frac{A_1}{A_0}\right)^2 + \left(\frac{A_2}{A_0}\right)^2 \frac{C_T}{C_L} \frac{\cos f}{\cos e} = 1 \qquad (2.16)$$

where A_0, A_1, and A_2 are the amplitudes of the incident P-wave, reflected P-wave and the reflected S-V wave, respectively.

C_T, C_L are the torsional wave speed and the dilatational wave speed, respectively.

e - angle of incidence for P-waves.

f - reflected angle for SV-waves.

Since in this work, the incident angle alternates after reflection depending on the reflected wave chosen, it is essential to derive a similar equation for the incident shear waves.

Table 2.1. Direction of Emission

CASES	JOINT PROB FUNCTION $\Phi(\theta,\phi)$	MARGINAL DENSITY FUNCTION $g(\theta)$, $f(\phi)$	DISTRIBUTION FUNCTION $G(\theta)$, $F(\phi)$	DIRECTION OF EMISSION
3-D	$\Phi = \frac{\sin\theta\, d\theta\, d\phi}{4\pi}$	$g(\theta) = \frac{\sin\theta}{2}$	$G(\theta) = \frac{1}{2}(1 - \cos\theta)$	$\cos\theta = 2R_\theta - 1$ $(1 - \leq \cos \leq + 1)$
		$f(\phi) = \frac{1}{2\pi}$	$F(\phi) = \frac{\phi}{2\pi}$	$\phi = 2\pi R_\theta$ $(0 \leq \phi \leq 2\pi)$
2-D	$f(\theta) = \frac{1}{2\theta}$		$G(\theta) = \frac{\theta}{2\pi}$	$\theta = 2\pi R_\theta$ $(0 \leq \theta \leq 2\pi)$

Energy Decomposition due to an Incident Shear Wave

Let us examine a beam of an incident SV-wave of cross-sectional area ΔS_o. After reflection, it generates both P- and SV-waves of cross-sectional areas ΔS_2 and ΔS_1, respectively. Assuming that the surface is traction free and the energy is conserved after reflection, the energy transmissions across ΔS becomes (see Fig. 2.3, page 20).

$$< P_T > \text{incident} = < P_T > \text{reflected} + < P_L > \text{reflected} \tag{2.17}$$

i.e.,

$$\frac{1}{2}\mu\frac{W^2}{C_T}(A_o)^2\Delta S_o = \frac{1}{2}\mu\frac{W^2}{C_T}(A_1)^2\Delta S_1 + \frac{1}{2}(\lambda+2\mu)\frac{W^2}{C_L}(A_2)^2\Delta S_2 \tag{2.17a}$$

But $\Delta S_o = \Delta S_1 = \Delta S \cos f$ for both the incident and the reflected shear waves and $\Delta S_p = \Delta S \cos e$ for the reflected P-waves where

f = incident or reflected angle for shear waves

e = angle of reflection for P-waves

Therefore, equation (2.17a) becomes

$$\frac{1}{2}\mu\frac{W^2}{C_T}(A_o)^2\Delta S\cos f = \frac{1}{2}\mu\frac{W^2}{C_T}(A_1)^2\Delta S\cos f + \frac{1}{2}(\lambda+2\mu)\frac{W^2}{C_L}(A_2)^2\Delta S\cos e \tag{2.17b}$$

Dividing equation (2.17b) through by $\frac{1}{2}\frac{W^2}{C_T}(A_o)^2\Delta S\cos f$ and noting that

$$(\lambda + 2\mu)/\mu = \left(\frac{C_L}{C_T}\right)^2 = k^2$$

we have

$$\left(\frac{A_1}{A_o}\right)^2 + \frac{k\cos e}{\cos f}\left(\frac{A_2}{A_o}\right)^2 = 1 \tag{2.18}$$

The terms A_2/A_0, A_1/A_0 are in fact the coefficients of reflections of the reflected P and SV waves, respectively. We would then rewrite the equation as:

$$(R_{SS})^2 + \frac{k \cos e}{\cos f} (R_{SP})^2 = 1 \tag{2.18a}$$

where

R_{SP} - coefficient of reflection of an incident shear wave reflected as a dilatational wave.

R_{SS} - coefficient of reflection of an incident shear wave reflected without a mode conversion.

According to Achenbach [33],

$$R_{SP} = - \frac{k \sin 4f}{\sin 2f \sin 2e + k^2 \cos^2 2f} \tag{2.19a}$$

$$R_{SS} = \frac{\sin 2f \sin 2e - k^2 \cos^2 2f}{\sin 2f \sin 2e + k^2 \cos^2 2f} \tag{2.19b}$$

Similarly, equation (2.16) could be rewritten as

$$(R_{PP})^2 + \frac{1}{k} \frac{\cos f}{\cos e} (R_{PS})^2 = 1 \tag{2.16a}$$

where R_{PP}, R_{PS} are the coefficients of reflection of P-waves reflected as P- and SV-waves, respectively.

$$R_{PP} = \frac{\sin 2e \sin 2f - k^2 \cos^2 2f}{\sin 2e \sin 2f + k^2 \cos^2 2f} \tag{2.20a}$$

$$R_{PS} = \frac{2k \sin 2e \cos 2f}{\sin 2e \sin 2f + k^2 \cos^2 2f} \tag{2.20b}$$

For computation purposes, let us put $\cos e = (1 - k^2 \sin^2 f)^{\frac{1}{2}}$ in

equations (2.19a, b).

Therefore, equations (2.17a, b) become

$$R_{SP} = - \frac{4 \sin f \cos f (1 - 2 \sin^2 f)}{(1 - 2 \sin^2 f)^2 + 4 \sin^2 f \cos f (a^2 - \sin^2 f)^{1/2}} \qquad (2.21a)$$

$$R_{SS} = - \frac{(1 - \sin^2 f)^2 - 4 \sin^2 f \cos f (a^2 - \sin^2 f)^{1/2}}{(1 - \sin^2 f)^2 + 4 \sin^2 f \cos f (a^2 - \sin^2 f)^{1/2}} \qquad (2.21b)$$

Similarly, by putting

$$\sin f = \sin e / k$$

$$\cos f = (1 - \sin^2 e / k^2)^{1/2}$$

and noting that $C_T / C_L = a$, we can write equations (2.20a, b) as

$$R_{PP} = - \frac{(1 - 2a^2 \sin^2 e) - 4a^3 \sin^2 e \cos e (1 - a^2 \sin^2 e)^{1/2}}{(1 - 2a^2 \sin^2 e) + 4a^3 \sin^2 e \cos e (1 - a^2 \sin^2 e)^{1/2}} \qquad (2.22a)$$

$$R_{PS} = \frac{4a \sin e \cos e (1 - 2a^2 \sin^2 e)}{(1 - 2a^2 \sin^2 e)^2 + 4a^3 \sin^2 e \cos e (1 - a^2 \sin^2 e)^{1/2}} \qquad (2.22b)$$

e, f are the incident angles for P- and SV-waves, respectively.

2.2 Reflection of Plane Waves at a Stress-Free Surface

In this section, equations are derived for locating the point of reflection and for determining the direction of the ray path after reflection.

Suppose that the equation of a plane is represented as

$$A_1 x + B_1 y + C_1 z + D = 0$$

where A_1, B_1, and C_1 are the direction numbers. Then, the normal vector to the plane is

$$A_1\hat{i} + B_1\hat{j} + C_1\hat{k}$$

Therefore, the unit normal vector is

$$\vec{R} = \frac{A_1\hat{i} + B_1\hat{j} + C_1\hat{k}}{\sqrt{A_1^2 + B_1^2 + C_1^2}} \tag{2.23}$$

The equation of the straight line incident on the plane with the direction numbers λ, μ, and ν from the point (x_1, y_1, z_1) can be written as

$$\frac{x - x_1}{\lambda} = \frac{y - y_1}{\mu} = \frac{z - z_1}{\nu}$$

The unit vector $\vec{U}$ incident on the plane becomes

$$\vec{U} = \frac{\lambda\vec{i} + \mu\vec{j} + \nu\vec{k}}{\sqrt{\lambda^2 + \mu^2 + \nu^2}} \tag{2.24}$$

Having known the incident ray, $\vec{U}$ and the unit normal vector to the plane, $\vec{R}$ then the reflected ray, $\vec{V}$ from Fig. 2.4 can be represented as

$$\vec{V} = A_R\,\vec{R} + B_R\,\vec{Y} \tag{2.25}$$

where $A_R = -\vec{U}\cdot\vec{R}$ and

$$B_R = \frac{\vec{U}\cdot\vec{Y}}{\vec{Y}\cdot\vec{Y}}$$

But

$$\vec{Y} = \vec{R} \times (\vec{U} \times \vec{R}) \tag{2.26}$$

Therefore,

$$\vec{V} = -(\vec{U}\cdot\vec{R})\vec{R} + \frac{\vec{U}\cdot(\vec{R} \times \vec{U} \times \vec{R})\,\vec{Y}}{\vec{Y}\cdot\vec{Y}} \tag{2.27}$$

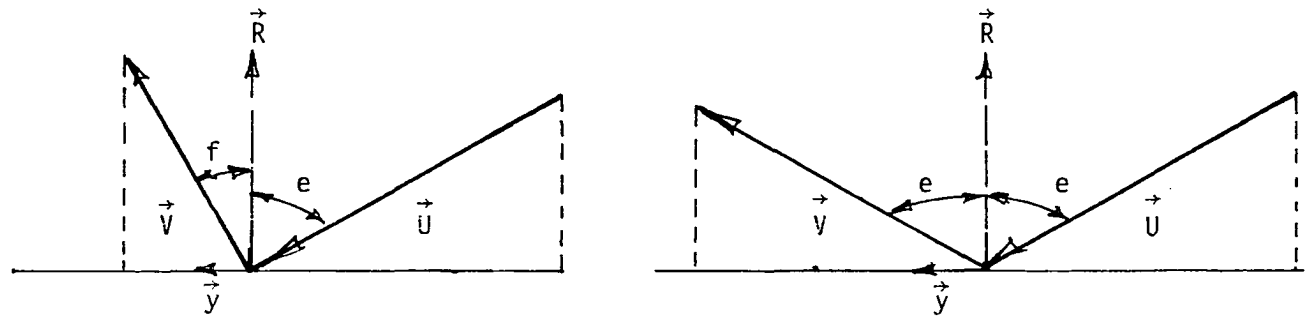

Fig. 2.4. Direction of the reflected ray.

(a) P-wave is incident and SV-wave is reflected
(b) P-wave is incident and reflected

For a plane case,

$$\vec{R} = (\xi, \eta)$$

$$\vec{U} = (\mu, \nu)$$

Therefore,

$$\vec{Y} = \vec{R} \times (\vec{U} \times \vec{R})$$

$$\therefore \quad \vec{Y} = [\mu(\eta)^2 - \nu(\eta)(\xi)]\hat{j} - [\mu(\xi)(\eta) + \nu(\xi)^2]\hat{k}$$

But the vector R has no component in the j direction, i.e.,

$\vec{R} = (0, \eta)$

$$\therefore \quad \vec{Y} = \mu\eta^2 \hat{j}$$

Hence,

$$B_R = \frac{(\mu\hat{j} + \nu\hat{k}) \cdot \mu(\eta)^2 \hat{j}}{[\mu(\eta)^2]^2} = \frac{1}{(\eta)^2}$$

$$\vec{V} = (-\vec{U} \cdot \vec{R})\,\vec{R} + \frac{\mu(\eta)^2 \hat{j}}{(\eta)^2}$$

But $\eta = -1$ for the upper plane.

$$\therefore \quad \vec{V} = \mu\hat{j} - \nu\hat{k} \tag{2.28}$$

2.2.1 Point of Intersection

We know from elementary geometry that the point of intersection between a plane

$$A_i x + B_i y + C_i z + D_i = 0$$

and the line

$$x = x' + \lambda r_o$$

$$y = y' + \mu r_o$$

$$z = z' + \nu r_o$$

could be obtained by substituting for x, y, and z in the equation of the former, i.e., $A_i(x' + \lambda r_o) + B_i(y' + \mu r_o) + C_i(z' + \nu r_o) + D_i = 0$. From here

$$r_o = - \frac{A_i x' + B_i y' + C_i z' + D_i}{A_i \lambda + B_i \mu + C_i \nu} \tag{2.29}$$

Therefore, the point of impingement becomes

$$\begin{aligned} x &= x' + \lambda r_o \\ y &= y' + \mu r_o \\ z &= z' + \nu r_o \end{aligned} \tag{2.30}$$

It is worth noting here that since $\vec{U}$ is a directed ray, r_o is in fact the radial distance from the origin to the point of impingement. This fact is later used as a criterion for finding which of the six possible inclined planes is impinged by the ray.

2.3 Wavefront Curvature Due to Reflection of P-SV Wave at a Stress-Free Surface

The solution to the problem of reflection in an elastic homogeneous isotropic semi-infinite medium has been studied by Chopra [22]. In his work, he used harmonic point source and treated the problem by using the Sommerfield technique of deforming the contours and approximating the branch line by saddle-point approximation. He has demonstrated that the ray-theory approach gives the same result without the complexity of the former.

Therefore, the application of the ray-theory approximation is used in this section to calculate the displacements of an impulsive P-SV wave reflected from an elastic isotropic plane and the result

is extended to the form applicable for our purpose.

For an isotropic solid body, the equation of the wave propagation can be represented as

$$(\lambda + u)\nabla\nabla\cdot\vec{u} + \mu\nabla\vec{u} + P\vec{f} = \rho\ddot{\vec{u}} \tag{2.31}$$

where

$\vec{u}$ - displacement vector

ρ - density of the medium

μ,λ - Lamé's constants for the material

$\vec{f}$ - body force vector

For the case of an impulsive dilatational point source with axial symmetry about the z-axis, the equation can be reduced in cylindrical coordinates to (see [22,36,37]):

$$C^2\nabla^2\phi + f_\phi = \ddot{\phi}$$

$$C^2\nabla^2\psi + f_\psi = \ddot{\psi}$$

where

$$\nabla^2 = \frac{\partial^2}{\partial r^2} + \frac{1}{r}\frac{\partial}{\partial r} + \frac{\partial}{\partial z^2}$$

$$f_\phi = \delta(z - z_o)\delta(r)\ H(R - C_L t)$$

$$f_\psi = 0$$

ϕ,ψ - are dilatational and shear wave displacement potentials, respectively.

$$u = \frac{\partial\phi}{\partial r} - \frac{\partial\psi}{\partial z} \quad , \quad w = \frac{\partial\phi}{\partial z} + \frac{\partial\psi}{\partial r} + \frac{\psi}{r}$$

u,w - displacement components

2.3.1 Displacement Amplitude

Let us suppose that the displacement potential of a ray emanating from a point source, O (see Fig. 2.5) is represented as

$$\Phi_o = \frac{1}{R} H(R - C_L t) \tag{2.32}$$

H(t) - heaviside unit function
R - total distance from point, O to the point of impingement
C_L - velocity of dilatation waves
t - time of arrival

At point A, the intersection of the ray and the plane boundary, the displacement due to the wave is

$$\frac{\partial \Phi_o}{\partial R} = \frac{1}{R} \delta(R - C_L t) - \frac{1}{R^2} H(R - C_L t)$$

If it is assumed that the distance OA is very large as compared with the wavelength of the waves, we can then assume that the term $1/R^2$ tends to zero. Therefore,

$$\frac{\partial \Phi_o}{\partial R} = \frac{1}{R} \delta(R_1 - C_L t)$$

where R_1 is the distance from the point O to the point of intersection of the ray and the first plane. Therefore, the amplitude of the wave at A is given as

$$A_A = \frac{1}{R_1} \tag{2.33}$$

The displacement amplitude at A after reflection can be gotten by multiplying equation (2.33) by the appropriate coefficient of reflection.

The reflection at the free surface is treated as a plane wave problem. The respective displacement amplitudes of the dilatational

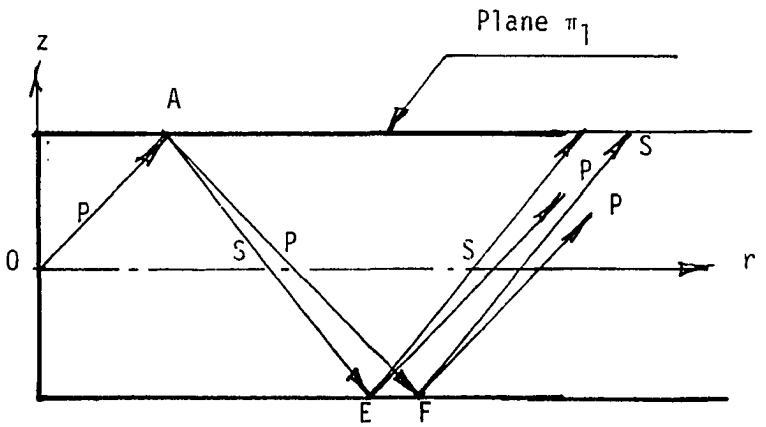

Fig. 2.5a. P-wave emitted from a point source.

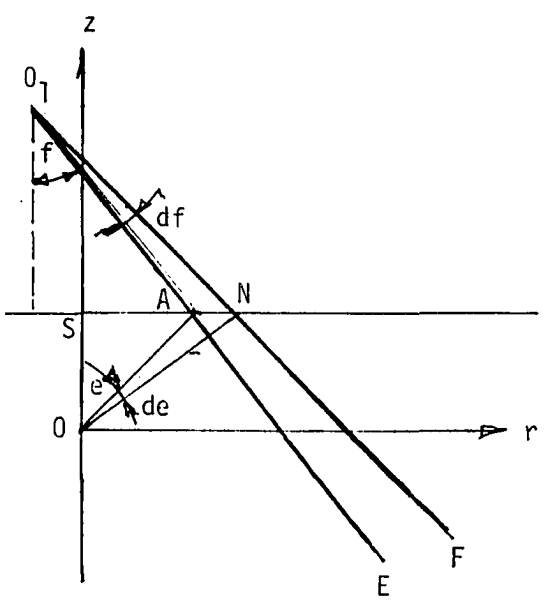

Fig. 2.5b. Mode conversion and the imaginary point source — P-SV waves.

and the equivoluminal waves are

$$A_{APP} = A_A \, R_{PP} \tag{2.34a}$$

$$A_{APS} = A_A \, R_{PS} \tag{2.34b}$$

where

A_{APP} - displacement amplitude of the reflected P-P waves at point A.

A_{APS} - displacement amplitude of reflected P-SV waves at point A.

R_{PP}, R_{PS} - corresponding coefficients of reflection, see equations (2.22a, b)

Therefore, it may be possible to find the displacement amplitude at a point, E (see Fig. 2.5), once the amplitude at point A has been determined. In other words, any subsequent amplitude can be written as

$$A_{EPS} = K^{1/2} \, A_A \, R_{PS} \tag{2.35}$$

where K is the curvature factor which is the subject matter of the next section.

2.3.2 Wavefront Curvature due to Reflection

If two close incident P rays, inclined at an angle de, and originating at the same point, O are examined, it can be observed that the reflected rays appear to have originated from the point O_1, instead of O; see also [38] and Bremmer [39].

Suppose there is a mode conversion after reflection, i.e., the P-waves are reflected as SV-waves (see Fig. 2.6). From geometry (see [40,41])

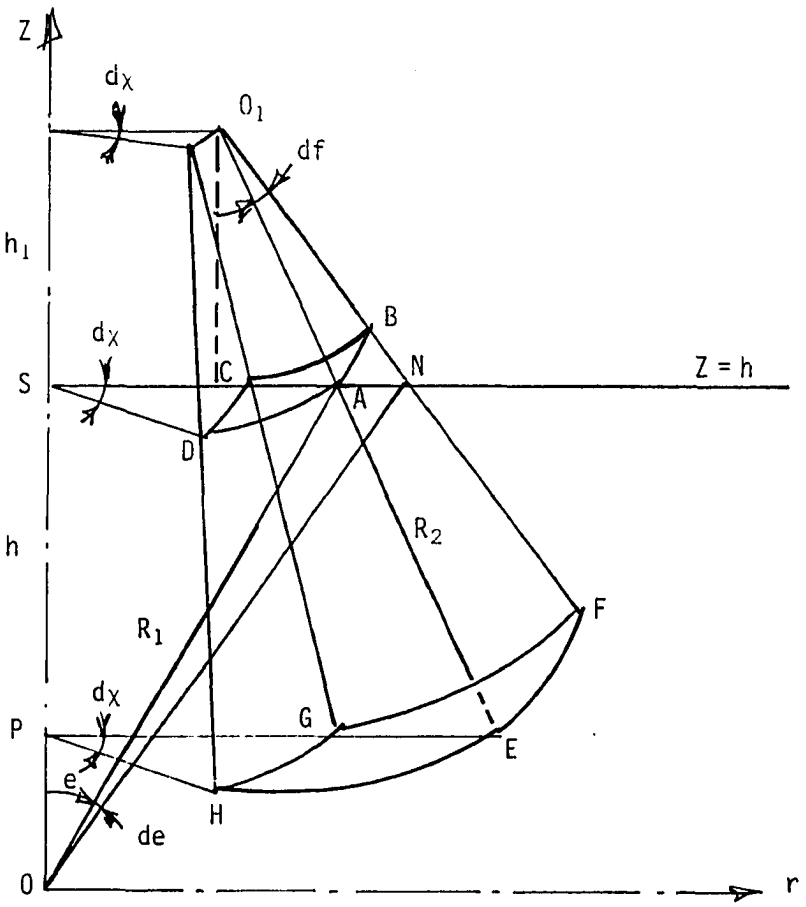

Fig. 2.6. Displacement of the P-SV waves: geometrical derivation

O — real point source
O_1 — apparent point source
h_1 — distance of the apparent point source from the horizontal plane
h — distance of the true point source from the horizontal plane
e — incident angle of the P-waves
f — reflected angle of the S-waves

$$R_1 \, de \sec e = R' \, df \sec f$$

But

$$R_1 = h \sec e$$

and

$$R' = h_1 \sec f$$

where

e - incident angle

f - reflected angle

$$\frac{df}{de} = \frac{h \sec^2 e}{h_1 \sec^2 f} \tag{2.36}$$

From Snell's law

$$C_T \sin e = C_L \sin f \tag{2.37}$$

By differentiating equation (2.37), we have

$$\frac{df}{de} = \frac{C_L \cos e}{C_T \cos f} = \frac{\sin f \cos e}{\sin e \cos f} \tag{2.38}$$

By combining equations (2.36) and (2.38), we arrive at

$$h_1 = \frac{h \cos^3 f \sin e}{\sin f \cos^3 e} \tag{2.39}$$

When the incident angle, e and reflected angle, f are equal, i.e., a case of PP-waves, then

$$h_1 = h \tag{2.39a}$$

If the area O_1EF is rotated about the z-axis, it could be seen that the same quantity of energy passes through the areas of both surfaces generated, ABCD and EFGH per unit time.

Therefore, the amplitudes in the ray P-SV of A and E after reflection, are in the limiting ratio of the square roots of their areas.

$$A_{EPS} = (\lim \frac{\text{area ABCD}}{\text{area EFGH}})^{\frac{1}{2}} A_{APS}$$

where A_{EPS} - amplitude of reflected P-SV waves at the point E. Therefore,

$$A_{EPS} = [\frac{(O_1A)(SA)}{(O_1E)(PE)}]^{\frac{1}{2}} A_{APS}$$

$$= [\frac{h_1 \sec f \, R_1 \sin e \, dfdx}{(h_1 \sec f + R_2)(R_1 \sin e + R_2 \sin f)dfdx}]^{\frac{1}{2}} A_{APS}$$

$$= K^{\frac{1}{2}} A_{APS}$$

where

$$K = \frac{h_1 \sec f \, R_1 \sin e}{(h_1 \sec f + R_2)(R_1 \sin e + R_2 \sin f)} \qquad (2.40)$$

K = the wavefront curvature factor

By dividing numerator and denominator of equation (2.40) by sin f, we can rewrite K as

$$K = \frac{h_1 \sec f \, \frac{C_L}{C_T} R_1}{(h_1 \sec f + R_2)(\frac{C_L}{C_T} R_1 + R_2)}$$

If we write,

$$R_1' = h_1 \sec f$$

$$R_1'' = C_L/C_T \, R_1$$

then

$$K = \frac{R_1 R_1''}{(R_1' + R_2)(R_1'' + R_2)} \qquad (2.40a)$$

For a P-P wave,

$$R_1' = R_1'' = R_1$$

Therefore,

$$K = \left(\frac{R_1}{R_1 + R_2}\right)^2 \tag{2.40b}$$

It is easily seen that the curvature factor attains its maximum value when we have a direct hit (or a case of zero reflection). In that case, R^2 is zero in both equations (2.40a,b).

2.3.3 Wavefront Curvature for Multiple Reflected Rays

In the case of multiple reflected rays, the curvature factor has the same form as the equation (2.40) above with the only difference that in addition to the radial distance R_2, other distances like R_3, R_4, and so on, are present in equation (2.40) as well.

Let us examine the expression for K for a PSP wave, a case of a double reflected ray (see Fig. 2.7a). From the figure

$$K_2 = \left(\frac{O_1 A \times SA}{O_1 E \times PE}\right)\left(\frac{O_2 E \times PE}{O_2 M \times SM}\right)$$

$$= \frac{O_1 A \times SA \times O_2 E}{O_1 E \times O_2 M \times SM} = \frac{O_1 A \times O_2 E \times SA}{O_1 E \times O_2 M \times SM}$$

$$= \frac{(h_1 \sec f)(h_2 \sec e)(R_1 \sin e)}{(h_1 \sec f + R_2)(h_2 \sec e + R_3)(R_1 \sin e + R_2 \sin f + R_3 \sin e)} \tag{2.41}$$

The above equation is similar in form to equation (2.40).

Similarly, for a PSPS wave with triple reflections, the expression for the wave curvature becomes from Fig. 2.7b,

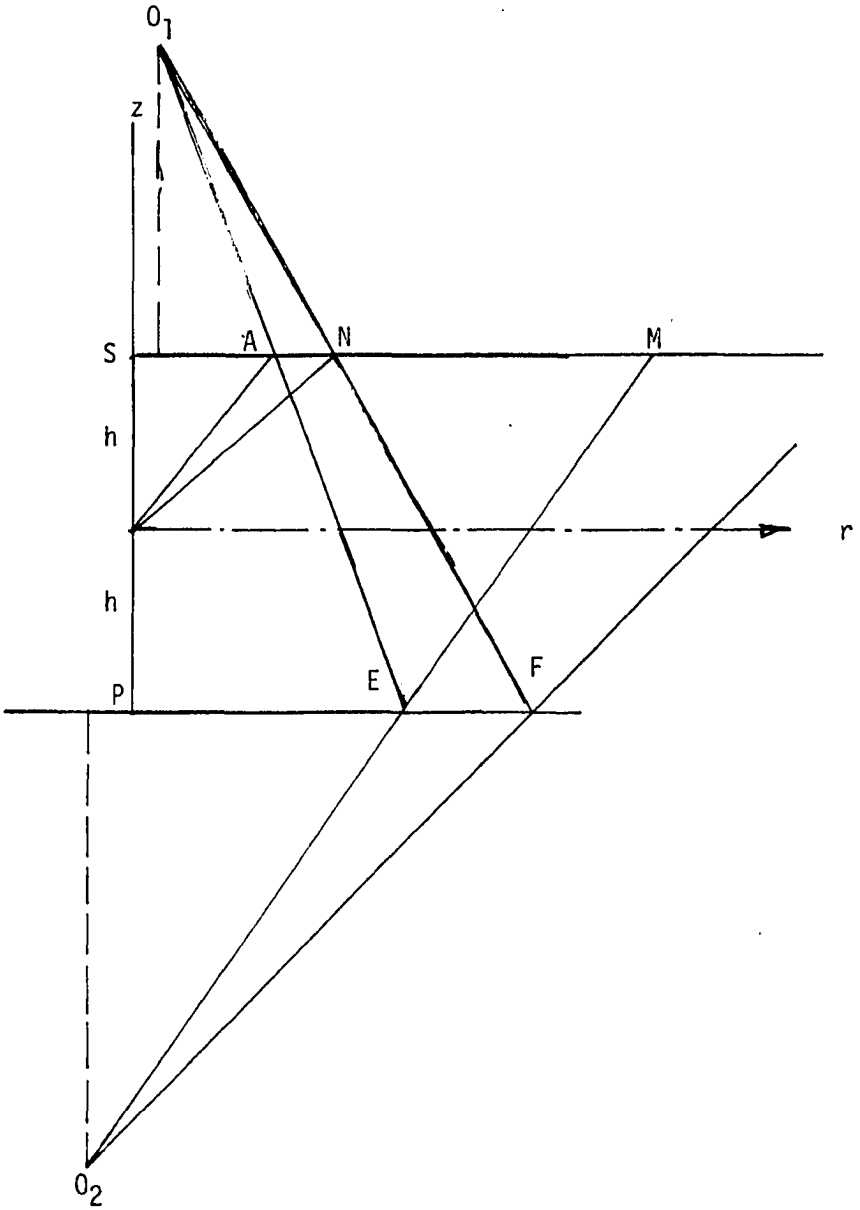

Fig. 2.7a. Mode conversion at a free surface.
(a) PSP waves

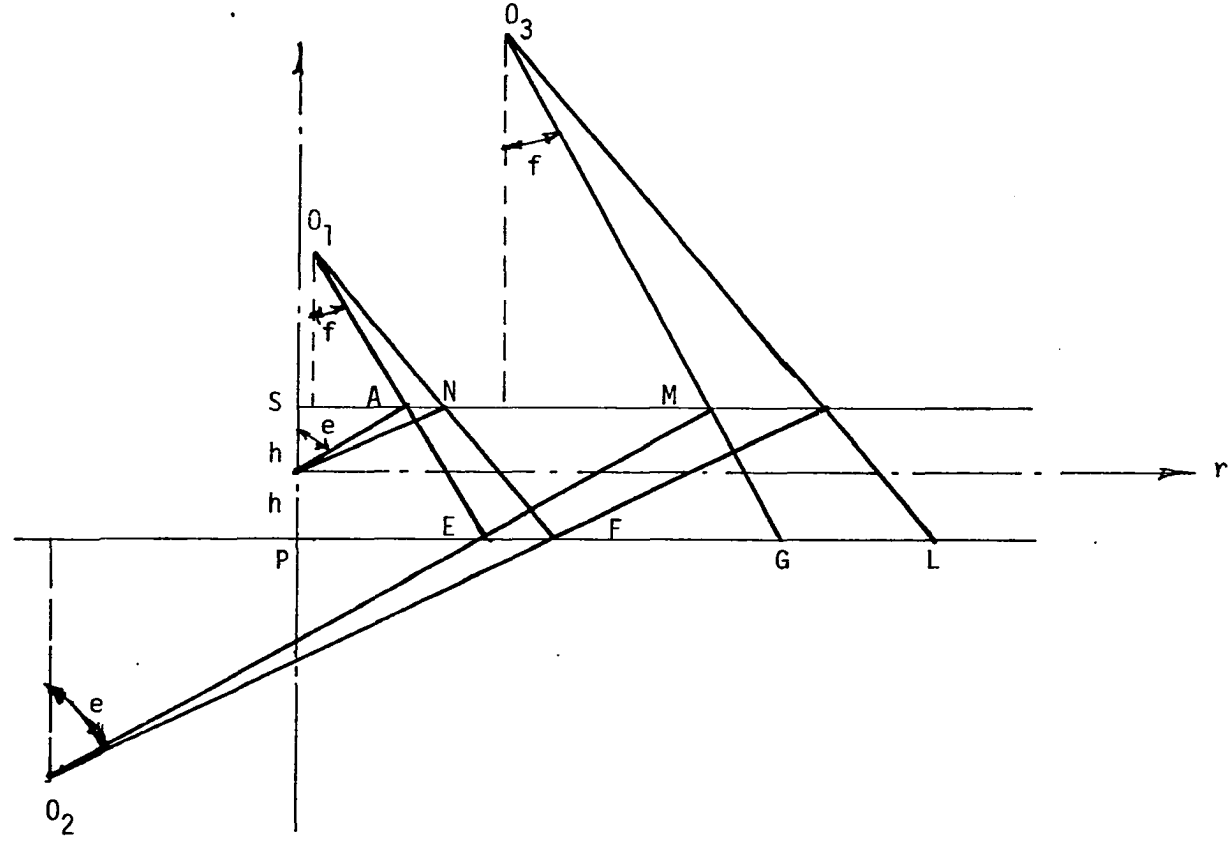

Fig. 2.7b. Mode conversion at a free surface.
(b) PSPS waves

$$K_3 = \gamma_3 \frac{h_2 \sec f \; h_2 \sec e \; h_3 \sec f}{(h_1 \sec f + R_2)(h_2 \sec e + R_3)(h_3 \sec f + R_4)} \tag{2.42}$$

where

$$\gamma_3 = \frac{R_1 \sin e}{R_1 \sin e + R_2 \sin f + R_3 \sin e + R_4 \sin f}$$

γ - the ratio of the horizontal distance of the first point of reflection from the source to the horizontal distance of the transducer (receiver) from the source (see Fig. 2.7).

In general for a two-dimensional case, the curvature factor can be written by induction as

$$K_i = \frac{\gamma_i \prod_{i=1}^{n} h_i \sec\theta_i}{\prod_{i=1}^{n} (h_i \sec\theta_i + R_{i+1})} \tag{2.43}$$

and

$$\gamma_i = \frac{R_1 \sin \omega_1}{R_1 \sin \omega_1 + \sum_{i=1}^{n} R_{i+1} \sin \theta_i}$$

θ_i - the i-th angle of reflection

$$\theta_i = \begin{cases} e - \text{if the reflected ray is a P-wave} \\ f - \text{if the reflected ray is an S-V wave} \end{cases}$$

h_i - the perpendicular distance from the i-th imaginary (apparent) source to the i-th reflecting plane

ω_1 - the incident angle at the point of first reflection

$$h_i = \frac{\sin \omega_i \cos^3\theta_i}{\sin \theta_i \cos^3\omega_i} \quad (h_{i-1} + R_i \cos \omega_i) \qquad i=2,\ldots,n$$

$$\omega_i = \begin{cases} e - \text{if the incident ray is a P-wave} \\ f - \text{if the incident ray is an SV-wave} \end{cases}$$

n = number of reflections

When there is no reflection, $h_i = 0$.

h_1 is as given in equation (2.39)

$$h_2 = \frac{\sin \omega_2 \cos^3\theta_2}{\sin \theta_2 \cos^3\omega_2} \quad (h_1 + R_2 \cos \omega_2)$$

The above expression for K is generally true for both reflection and refraction of P and S-V waves on the plate provided the successive planes of reflection are the same or parallel.

Therefore, the amplitude of displacement at a point on the plate in general becomes

$$A_i = A_{A_{i=1}} \sum^{n} K_i^{\frac{1}{2}} R_{APP_i} \qquad (2.44)$$

where

$$R_{APP_i} = R_{PP}, R_{PS}, R_{SP}, \text{ or } R_{SS}$$

depending on the waveform of the chosen ray at the i-th point of reflection.

2.3.4 Wavefront Curvature due to Reflection: A Three-Dimensional Case

It is interesting to note that the two curvatures formed as a result of the mode conversion at the reflecting surface, can be characterized by the variables: the dilatational wave speed, C_L, equivoluminal wave speed, C_T and the radial distances, R_i. When there is no mode

conversion, the radii of curvature can be determined by the radial distances (see equation (2.40b) for the P-P waves). These two curves form an orthogonal set with one directly on the plane of reflection while the other is perpendicular to it.

In order to facilitate our analysis further, let us examine in detail the two variables R_1' and R_1''. Let us consider the reflection of an incident ray of P-P waves (see Fig. 2.8). It can be easily observed that

$$R_1'' \sin f = R_1 \sin e$$

Therefore,

$$R_1'' = \frac{C_L}{C_T} R_1 \tag{2.45a}$$

i.e., $R_1'' = g_1(R_1)$. Similarly, from equation (2.40a), we see that

$$R_1' = h_1 \sec f$$

By virtue of equation (2.39)

$$R_1' = \frac{h \cos^3 f \sin e}{\sin f \cos^3 e} \sec f$$

But $h = R_1 \cos e$, therefore,

$$R_1' = R_1 \frac{\cos^2 f \sin e}{\sin f \cos^2 e}$$

$$= R_1 \frac{\cos^2 f}{\cos^2 e} \tag{2.45b}$$

where $k = C_L/C_T$. Equations (2.45a, b) show that both R_1' and R_1'' are functions of the radial distance, R_1, the incident angle e, reflected angle f, and k. In the general case where the bounding planes are inclined, a

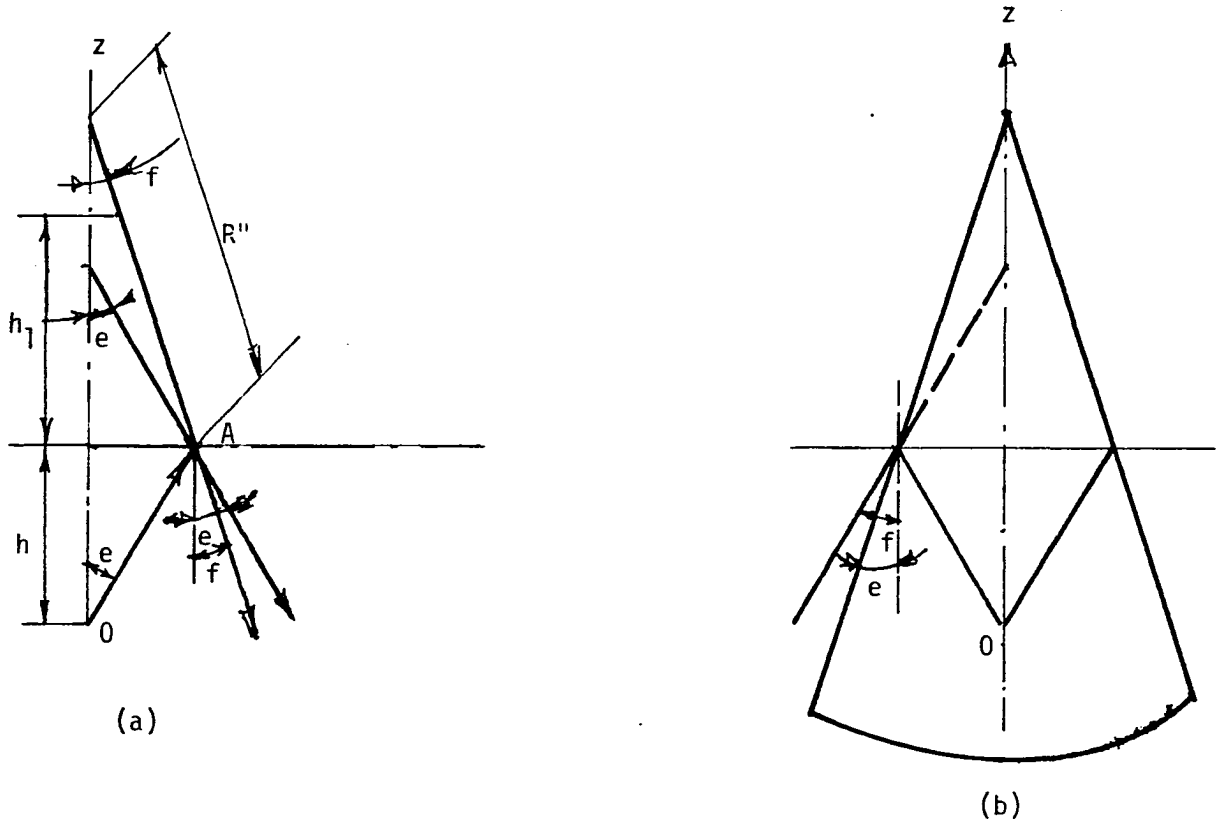

Fig. 2.8. Curvature due to reflection.
(a) Location of R_1''
(b) Rotation about z-axis

situation may arise where we have more than one reflection and the consecutive planes of reflection are also inclined. In this regard, it is essential to map the curvature into the subsequent plane of reflection before calculating the curvature factor. See for instance Fig. 2.9.

Let us assume that these lines of curvature represent parametric lines, U and V. Then, their directions at a point constitute the principal directions at that point (see [42,43] and Fig. 2.10).

Therefore, the principal curvatures at the subsequent plane of reflection which is inclined at an angle, ξ to the former can be found by using Euler's equation, as

$$\frac{1}{r_1} = \frac{\cos^2\xi}{R'_{eff}} + \frac{\sin^2\xi}{R''_{eff}} \tag{2.46a}$$

$$\frac{1}{r_2} = \frac{\cos^2(\xi+\pi/2)}{R'_{eff}} + \frac{\sin^2(\xi+\pi/2)}{R''_{eff}} \tag{2.46b}$$

where R'_{eff}, R''_{eff} are the corresponding radii of curvature.

$$R'_{eff} = k\ R_1/\gamma_j$$

$$R''_{eff} = \pi \sum_{i=1}^{n} (h \sec\theta_i + R_{i+1})$$

$$\gamma_j = \frac{R_1 \sin\omega_1}{R_1 \sin\omega_1 + \sum_{i=1}^{n} R_{i+1} \sin\theta_i}$$

From the above equations, it thus becomes apparent that the curvatures only switch positions when the consecutive planes of reflection are inclined at an angle of 90° to each other. Furthermore, when

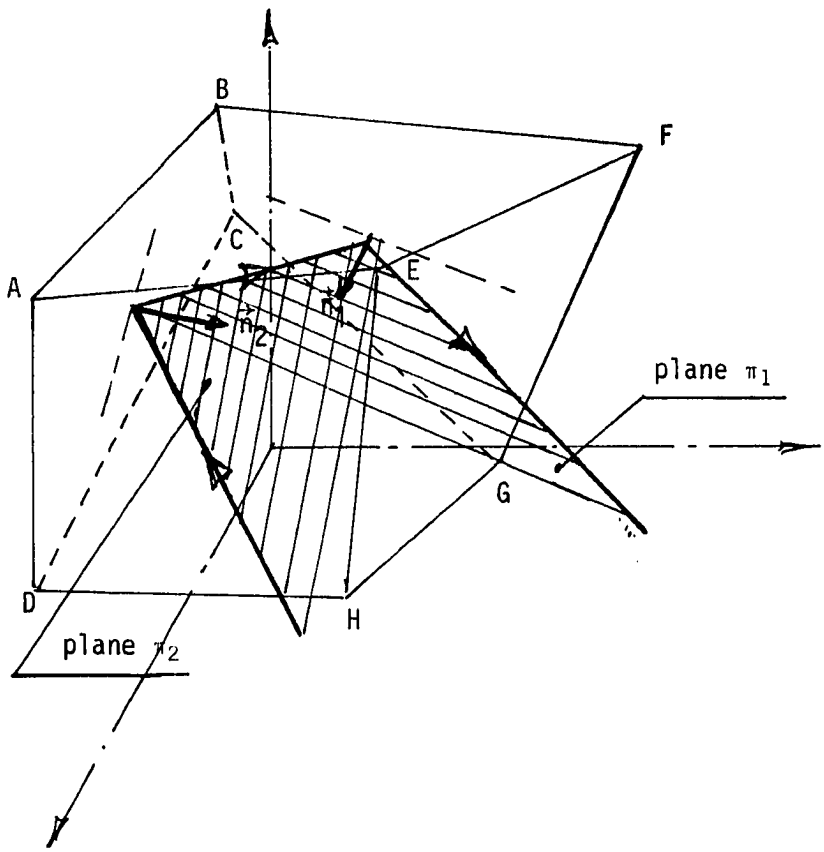

Fig. 2.9. Inclined planes of reflection.
π_1 - initial plane of reflection
π_2 - subsequent plane of reflection
$\vec{n}_1$ - the normal to the plane π_1
$\vec{n}_2$ - the normal to the plane π_2

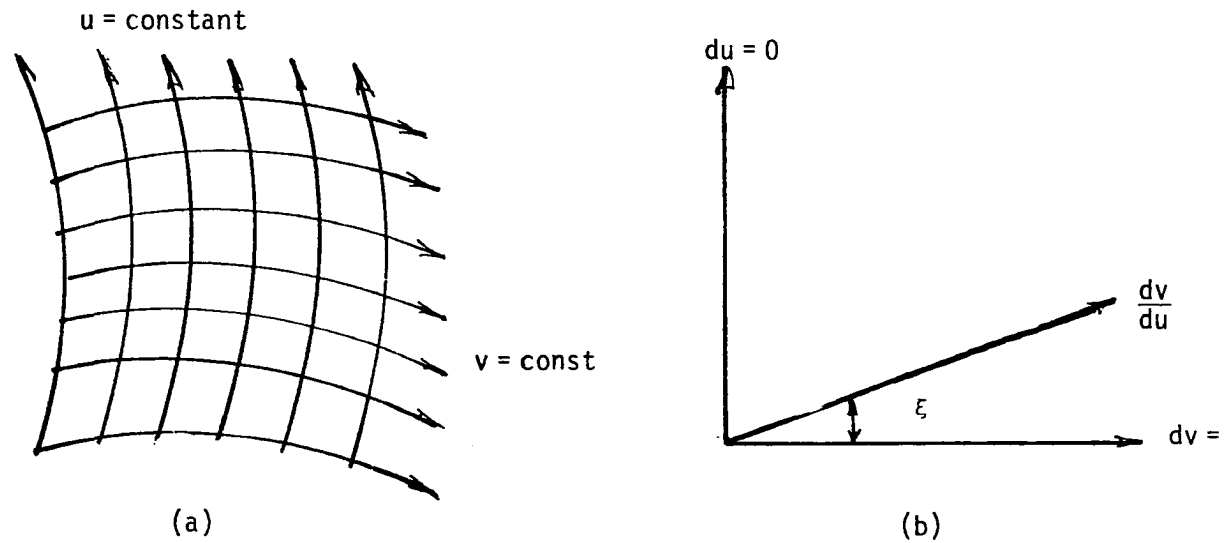

Fig. 2.10. Lines of curvature.

(a) Principal normal curvatures
(b) Normal curvature in an arbitrary direction

the planes of reflections are parallel, or coplanar

$$r_1 = R'_{eff}$$

and

$$r_2 = R''_{eff}$$

In general,

$$K_i = \frac{\gamma_i \prod_{i=1}^{n} h_i \sec\theta_i}{r_1}$$

It is easily seen that once the radial distances are calculated, the radii of curvature and hence the curvature factor are determined, we can calculate the displacement amplitude as mentioned above by "marching forward" and considering both the respective contributions at every point of reflection and the nature of the waves.

CHAPTER III

COMPUTATION ALGORITHM AND NUMERICAL EXAMPLES

In the last chapter, some theoretical cases were considered and the conditions under which they could be utilized were given. In this chapter, that discussion will be supplemented with the development of a computer algorithm for the tracing of the rays and the reflections at the boundary as well as the computation of the displacements.

Finally, numerical examples are given with specific references to the elastic waves in the plate due respectively to an impulsive point source and a point force acting normally to the free surface with a square pulse time function.

3.1 Computation Algorithm

For this work, three models were considered:

a) The first model defines a solid metal with six inclined bounding planes using the direction numbers of the bounding planes, A_i, B_i, C_i. The wave speeds and other elastic properties are taken with respect to iron [44]. The surfaces are stress free.

b) The second one defines a two-dimensional plate with stress-free boundaries using the coordinates of the edges. The force is an impulsive P-wave.

c) The third model also defines a two-dimensional plate using

the coordinates of the edges. The forces are due to a unit normal stress acting at the free surface.

For the first two cases, a ray is generated at a point (0,0) within the material, and the vector direction of the ray is determined using the Monte Carlo sampling technique having the same distributions in all directions as discussed in the earlier chapters. Because the boundaries are inclined to one another, the ray can possibly hit all the planes within or outside the solid. For our purpose, the point of impingement should occur within the specimen. The above problem is peculiar to the three-dimensional case only since in the plate problem, the two surfaces (upper and bottom surfaces) are parallel and so the ray will always hit the boundaries from within the plate.

This problem is avoided by using the parameter, r_0, expressed by equation (2.29) in the last chapter and noting that r_0 should be positive i.e., $r_0 > 0$. This parameter is calculated for each of the six possible planes (see subroutine UI in the Appendix). The smallest of all the r_0-values gives the shortest radial distance either from the origin to the first pierce point or between any two consecutive points of reflection.

The ray is then tested to determine whether it hits the transducer the base of which is defined within $\pm$ 1 mm from its location. If the ray hits the test cell, the amplitude of displacement is calculated and recorded by the subroutine AMPLCO and another ray is again generated at the point source for the next trial. Figure 3.1 shows a ray with a direct hit and a double reflected ray hitting the test cell.

But, if on the other hand no hit is recorded, the energy ratios of the reflected rays to the incident ray are calculated by the

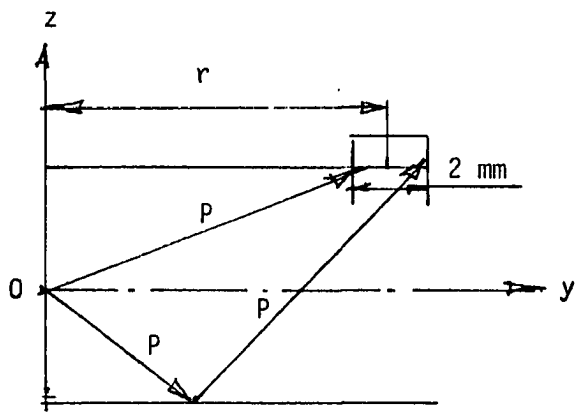

Fig. 3.1. Direct ray and a single reflected waveform.

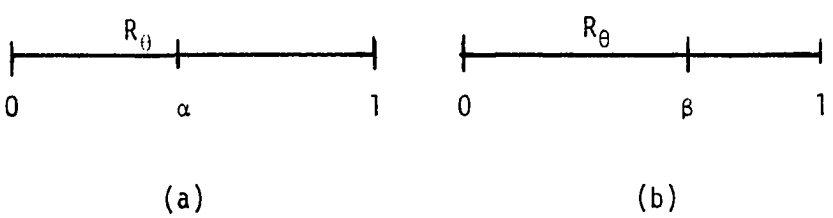

(a) (b)

Fig. 3.2 Monte Carlo decision variables.
(a) For incident P-wave
(b) For incident SV-wave

subroutine ERATIO. Then the Russian-roulette test is conducted to choose the reflected wave at the surface. As mentioned earlier, every ray incident at a free surface generates two reflected rays — the compressional wave and the shear wave. The frequency of occurrence of the reflected ray chosen depends on the mode of the incident ray and the random number generated.

For instance, if the incident ray is a P-wave (see Fig. 3.2), then the energy ratio of the reflected P-wave, α is used as a sampling parameter in the Monte Carlo operation, i.e., if

$$0 < R_\theta \leq \alpha \text{ — the reflected P-wave is chosen,}$$

but if

$$\alpha < R_\theta \leq 1, \text{ the reflected shear wave is chosen}$$

where R_θ is the random number generated. The same is true in the case of an incident shear wave where β, the energy ratio of the reflected shear wave is utilized as the sampling parameter (see the subroutine CHOREF).

Finally, once we have chosen one of the reflected rays and calculated its angle of reflection, we can then determine its direction using the transformation matrix, equation (2.27). See the subroutine REFLEC in the appendix.

Then this ray becomes the incident ray to any subsequent reflecting surface. The tracing process continues until either the maximum time for the simulation, T_{max} is reached or the ray passes the range where it no longer contributes to the response at the point of interest.

Unlike cases (a) and (b) in which only the P-waves are emitted,

both P-waves and SV-waves are emitted in case (c). Such difference in the waveform emitted is accounted for in the subroutine UI by introducing an additional Monte Carlo operation for case (c) to choose the mode of the waves to be emitted. Moreover, the initial amplitude is calculated for case (c) by an additional subroutine UTHETA.

3.2 Numerical Calculation

In this section, the above theory is used to give numerical calculations for finding the response of a plate to a point source compressional wave and the vibration of a plate due to a normal point load. For the two cases, the thickness of the plate is 2h, the wave speeds for irrotational and equipotential waves are C_L and C_T, respectively.

3.2.1 Response of a Plate to a Compressional Point Source: Numerical Calculations

For the purpose of the calculation, the following material constants are given:

C_L = 5.1 mm/μsec $\qquad$ C_T = 3.05 mm/μsec

2h = 30 mm

The plate material is iron and it is assumed to be elastic, isotropic and homogeneous.

An impulsive force is located in the plate at the point, O(0,0) and the transducer is placed at three different locations: r = 2; r = 5; r = 10 at the upper surface of the plate (see Fig. 3.3). The parameter, r is normalized with respect to 2h, the thickness of the plate; r = AY/2h; AY is the horizontal distance of the receiver.

There are many different rays which can possibly hit the

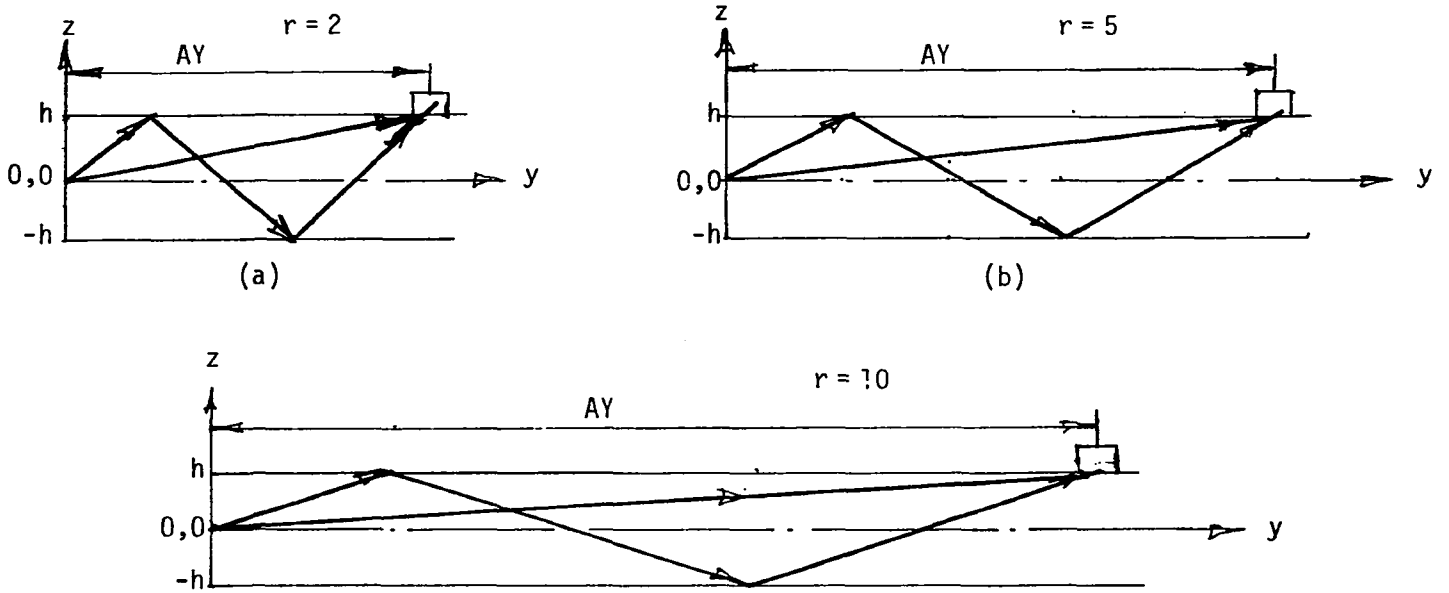

Fig. 3.3. Ray paths and the locations of the receiver. Source is at point (0,0), r = AY/2h.

receptor point; these rays range from a P-wave with a direct hit to a multiple reflected ray, like PS, PSP, PSPP, and so on. These rays do arrive at the receptor point at different times. See Tables 3.1 and 3.2 for the arrival times for the case with $r = 2$, $r = 5$, and $r = 10$.

Since the ray directions are randomly sampled with the angle θ varying within the interval $[0,2\pi]$, many rays do repeat with the same path history. To register only the first of the ray hits with the same path history and eliminating the others, the following binary expression is used:

$$IBA = N \sum_{j=1}^{n} 2^{j+1} + NN \times 2^{20} \tag{3.1}$$

where

n - the number of reflections

IBA - unique number

$$N = \begin{cases} 0, \text{if the mode of the ray is P} \\ 1, \text{if the mode is SV} \end{cases}$$

$$NN = \begin{cases} 0 \ , \text{if the mode of the ray is SV} \\ n+1, \text{if the mode of the ray is P} \end{cases}$$

The source function used in this investigation is represented by a Heaviside unit function. The displacement is then convoluted with the time function of the parabolic ramp type resulting in a saw tooth shape solution (see Pekeris et al. [18] and Fig. 3.4).

The minimum arrival times are normalized with respect to the time it takes the equivoluminal wave S, to travel across the depth of the plate, 2h, i.e.,

$$\tau = t/t_o$$

Table 3.1. Arrival Time ($\tau = tC_T/2h$)
Dilatation Point Source

r = 2		r = 2	
Waveform	Arrival Time, τ	Waveform	Arrival Time, τ
P	1.22	PS^2PS	4.2407
P^2	1.5	P^3SPSP	4.333
P^3	1.9		4.346
	2.04	PS^2PSP	4.7673
PS	2.049		4.77
	2.055	PS^2P^4	4.891
	2.061		4.901
	2.373	PS^4P	5.199
	2.376		5.201
PSP	2.381	P^{10}	5.803
	2.393	P^9S	6.2158
	2.399	P^4S^4	6.286
P^4	2.406	P^{11}	6.392
P^2SP	2.84	$P^3S^2P^5$	6.619
	2.852	PS^4P^2S	6.712
P^5	2.94	$P^3S^3P^4$	7.03
	3.292	P^2S^6	7.125
PSPS	3.30	$P^2S^2P^4S^2$	7.441
(PSSP)	3.303	P^{13}	7.571
(PPSS)	3.306		
	3.308		
P^3SP	3.363		
	3.375		
P^6	3.50		
P^2S^2P	3.795		
	3.803		
P^7	4.065		

Table 3.2. Arrival Time ($\tau = tC_T/2h$)

Dilatation Point Source

r = 5		r = 10	
Waveform	Arrival Time,	Waveform	Arrival Time,
P	2.98	P	6.0
PS	3.82	PS	6.8
PSP	3.92 3.94	PSPS	7.64 7.65 7.67
P^2S^2	4.78		
P^3S^2	5.05	PSPSP	7.79
P^3S^3	5.93		
P^4S^3	6.3 6.32		
P^4S^4	7.21		
P^5S^4	7.68		
P^7S^3	7.72		
P^9S^2	7.82		
P^4S^5	8.14		
P^5S^5	8.62		
P^7S^4	8.67		
P^8S^5	9.12		

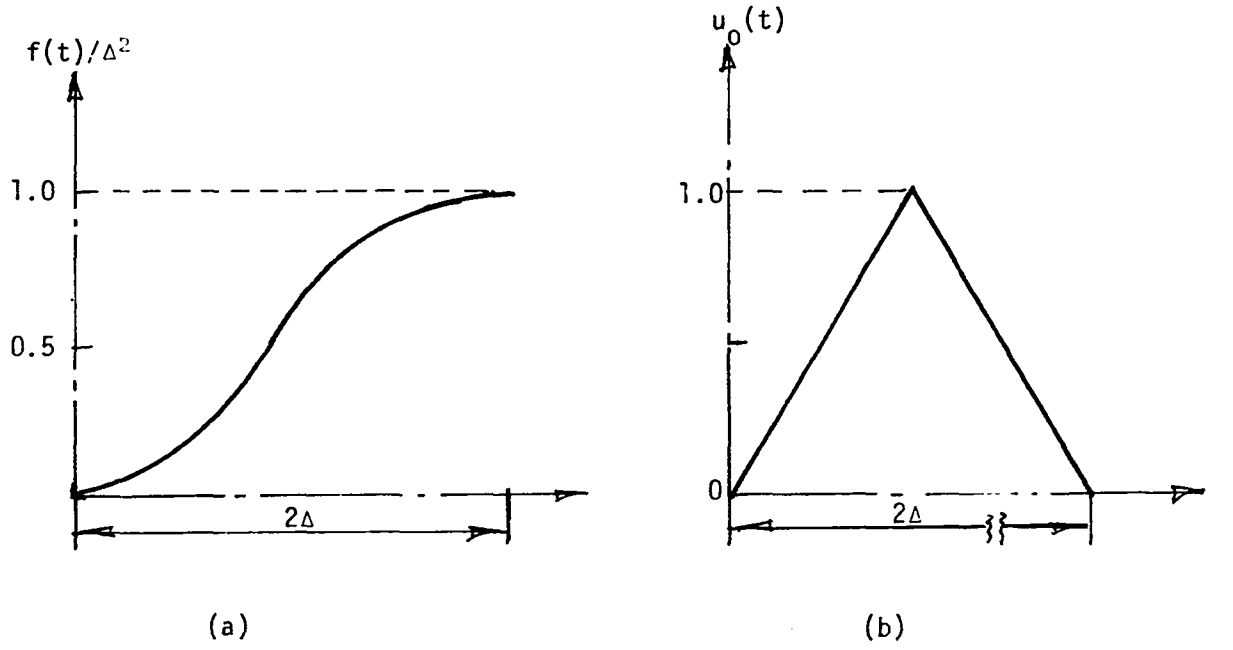

Fig. 3.4. Time function [$\Delta = f(\tau)$].
(a) Quadratic pulse
(b) Saw-tooth shape function

2Δ is the measure of the sharpness of the pulse

where

$$t_o = 2h/C_T$$

The wave field consists of many waveforms having different segments. The direct P-wave which hits the transducer directly from the point of dilatation has only one segment. PP and PS, which are reflected once, consist of two segments. When the receptor is located at the upper surface of the plate, such reflection takes place only at the lower surface. Multiple reflected waves like PSP, PPS do arrive at the transducer after two reflections: first at the upper surface and then at the lower surface of the plate. These multiple reflected waves can be grouped in accordance with the number of P and S wave modes they contain. For instance, PSP and PPS do have P and S wave modes in the ratio of 2:1 though in different combinations. They do have the same time history and they arrive at the transducer simultaneously. Contributions of such waves are summed together when computing the amplitude at the point of interest. Belonging to this class of waves are the PSPS, PSSP, and P^2S^2 which form another group.

Because of the fact that a hit is considered to occur if the ray falls within $\pm$ 1 mm of the actual location of the transducer, the arrival time of some waveforms are spread within certain ranges. Typical of these is the wavelet PSP (see Fig. 3.5 and Table 3.1). In such cases, it might be possible for the waveform close to them to arrive with them at the target almost simultaneously. Notably, the arrival time of the PSP waves from the table ranges from 2.3728τ to 2.3994τ while that of the four segmented wave P^4 is 2.406τ. In such cases, their

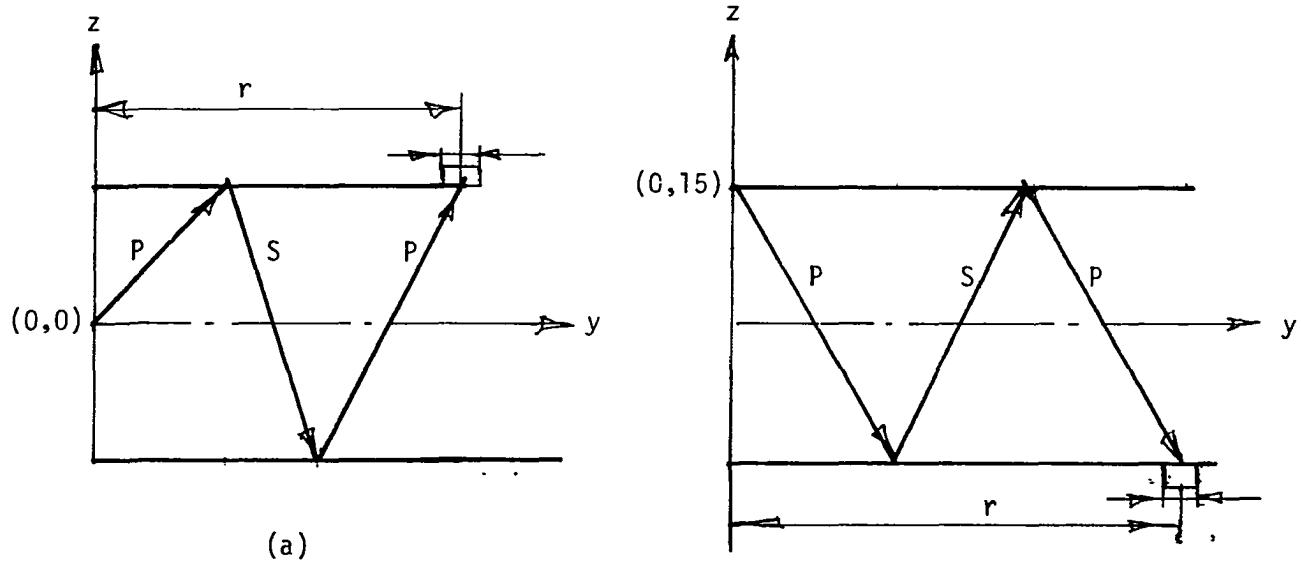

Fig. 3.5. Reflections of the PSP waves due to:

a) Dilatational force
b) Unit normal stress

Table 3.3. Peaks of the Displacement Field ($r = 2$)
Point of Dilatation (0,0)

Arrival Time, τ	Amplitude of Displacement	
	Vertical Components (mm)	Horizontal Components (mm)
1.32	0.972×10^{-2}	2.81×10^{-2}
1.58	-0.024	0.0369
2.01	0.0191	0.182
2.13	-1.68	2.65
2.48	1.51	1.3
2.95	-0.969	-0.558
3.05	0.286	0.0472
3.40	0.0202	1.82
3.47	0.804	0.708
3.59	-0.263	-0.113
3.89	0.15	-0.654
4.02	-0.644	-0.053
4.16	0.246	0.090
4.57	0.514	-0.17
4.74	-0.253	-0.024
4.86	0.199	-0.4-41
5.15	-0.433	0.0241

Table 3.4. Peaks of the Displacement Field ($r = 5$)
Point of Dilatation (0,0)

Arrival Time, τ	Amplitude of Displacement	
	Vertical Components (mm)	Horizontal Components (mm)
3.11	2.6×10^{-3}	0.849×10^{-2}
3.42	0.137	0.0287
3.91	-2.8	1.0
4.02	3.4	1.31
4.29	1.2	0.23
4.87	-6.7	0.664
5.13	4.63	1.01
5.52	-1.46	-0.20
5.71	2.33	-0.3496
5.93	1.48	0.164
6.03	-5.34	0.86
6.41	4.77	0.062
6.85	-4.38	0.16
7.31	5.54	0.4
7.81	-4.81	-0.25

Table 3.5. Peaks of the Displacement Field ($r = 10$)
Point of Dilatation (0,0)

Arrival Time, τ	Amplitude of Displacement	
	Vertical Components (mm)	Horizontal Components (mm)
6.09	0.856×10^{-3}	2.86×10^{-3}
6.95	1.37	7.24
7.76	-2.23	5.13
7.9	0.81	6.33
8.08	0.814	3.14

contributions are also added together to accurately determine the displacement at the receiver point; see Tables 3.3 - 3.5.

3.2.2 Components of Displacement at the Boundary

In resolving the radial displacement into the horizontal and vertical components, due considerations are given to the mode and direction of both the incident and the reflected rays and the location of the receiver. When the receiver is located, for example, at the bottom surface of the plate, the corresponding displacement components are given by the following equations. Assuming the incident wave is of a P mode, we have (see Fig. 3.6)

$$\begin{aligned} U_{RH} &= U_R \sin e + U_{RPP} \sin e - U_{RPS} \cos f \\ U_{RV} &= - U_R \cos e + U_{RPP} \cos e + U_{RPS} \sin f \end{aligned} \tag{3.2}$$

When the incident wave is an SV mode,

$$\begin{aligned} U_{\theta H} &= U_\theta \cos f + U_{\theta PP} \sin e - U_{\theta PS} \cos f \\ U_{\theta V} &= U_\theta \sin f + U_{\theta PP} \cos e + U_{\theta PS} \sin f \end{aligned} \tag{3.3}$$

If the transducer is located at the upper surface of the plate, the corresponding displacement components become (see Fig. 3.6):

$$\begin{aligned} U_{RH} &= U_R \sin e + U_{RPP} \sin e + U_{RPS} \cos f \\ U_{RV} &= U_R \cos e - U_{RPP} \cos e + U_{RPS} \sin f \\ U_{\theta H} &= - U_\theta \cos f + U_{\theta PP} \sin e + U_{\theta PS} \cos f \\ U_{\theta V} &= U_\theta \sin f - U_{\theta PP} \cos e + U_{\theta PS} \sin f \end{aligned} \tag{3.4}$$

where

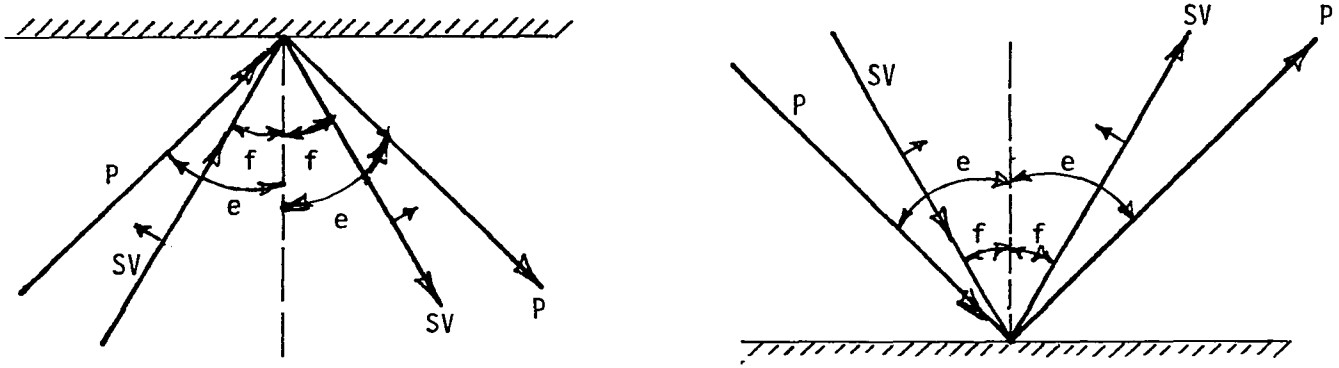

Fig. 3.6. Direction of the particle displacements.
(a) Reflection is at the upper surface
(b) Reflection is at the bottom surface

U_R, U_θ = respective radial displacements for P and SV waves

U_{RH}, U_{RV} = respective horizontal and the vertical components of displacement with a P-wave incident

$U_{\theta H}$, $U_{\theta V}$ = respectively the horizontal and the vertical components of displacement with an incident SV wave

e = incident or reflected angle for a P wave

f = incident or reflected angle for an SV wave

U_{RPP}, U_{RPS}, $U_{\theta PP}$, $U_{\theta PS}$ = corresponding displacement contributions of the reflected rays. They are functions of the corresponding radial displacements and the coefficient of reflection

$$U_{RPP} = U_R R_{PP}$$

$$U_{RPS} = U_R R_{PS}\varepsilon$$

$$U_{\theta PP} = U_\theta R_{SS}$$

$$U_{\theta PS} = U_\theta R_{SP}\varepsilon$$

$\varepsilon = \pm 1$ depending on whether or not the ray is in the $\pm$ z-direction

R_{PP}, R_{PS}, R_{SP}, and R_{SS} are the corresponding coefficients of reflection.

The complete responses due to a compressional point source are given in Figs. 3.7 - 3.12 for the three different locations of the transducers. The results obtained by Pao et al. are shown in Fig. 3.7a for the purpose of comparison.

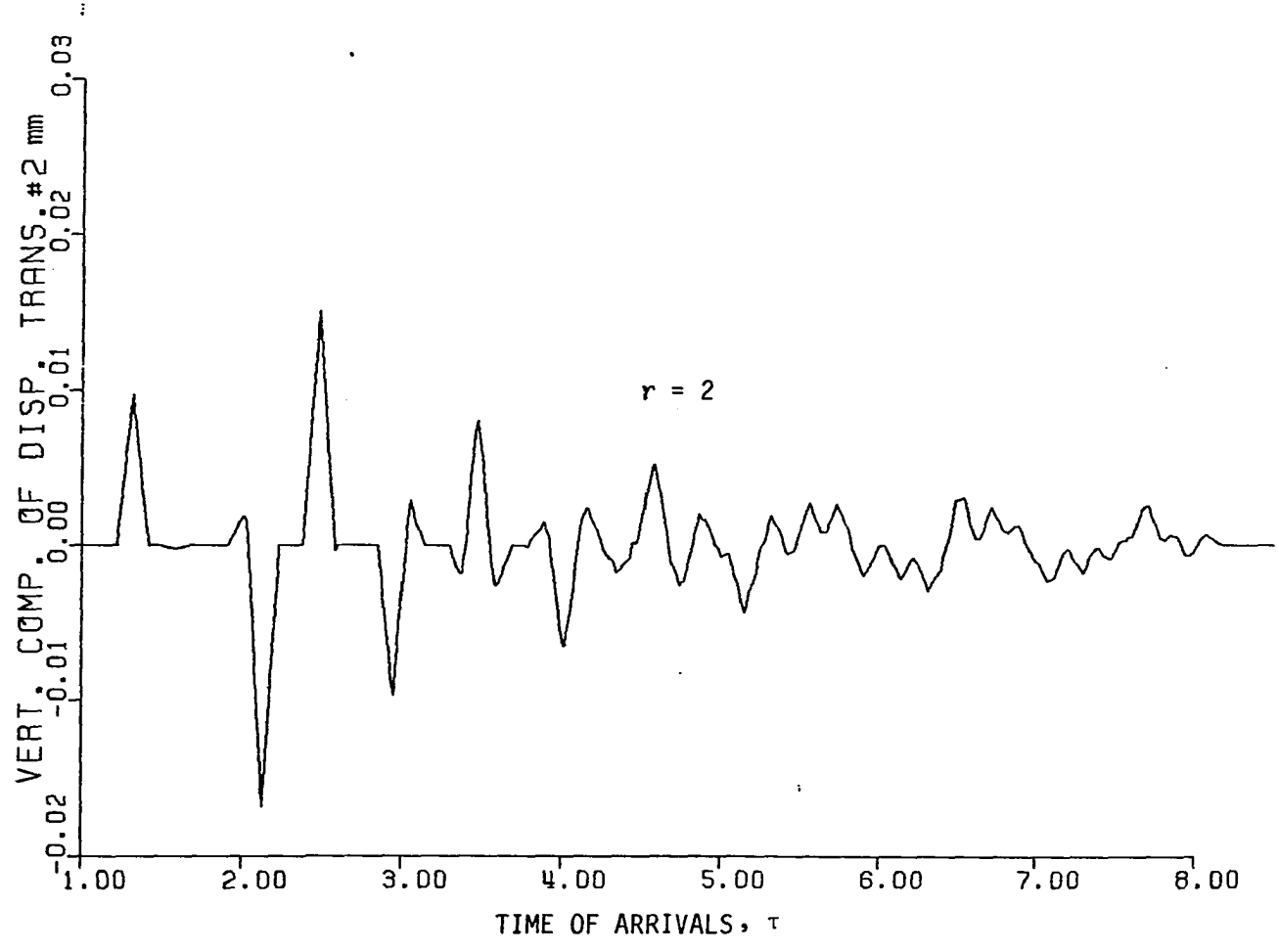

Fig. 3.7. Plates response to a unit dilatation point force. Point of dilatation (0,0) ($t_o = t/\tau$).

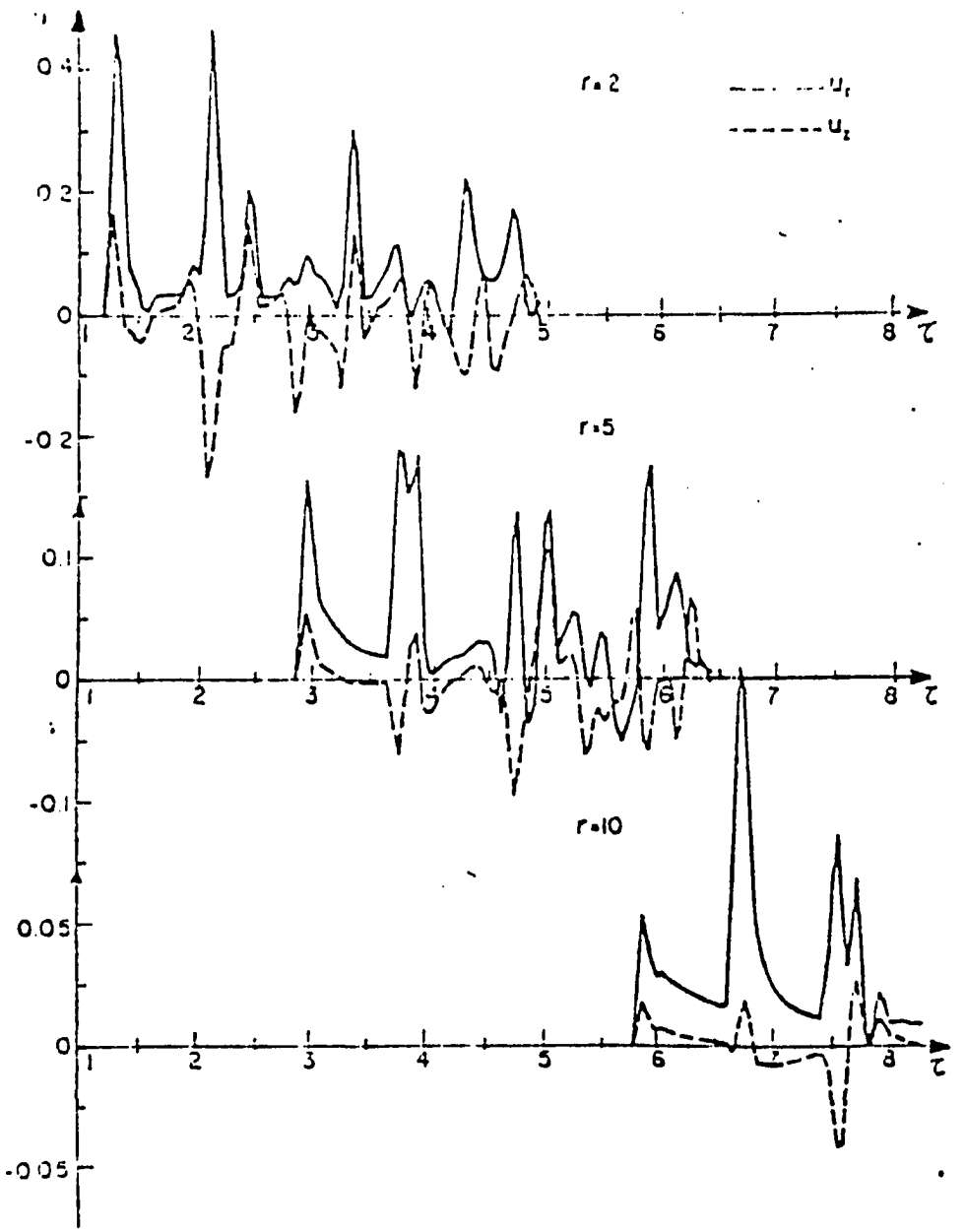

FIG. 21. Surface displacements of a plate at various ranges ($\Delta = 0.1$).

Fig. 3.7a. Responses due to dilatational point source obtained by Pao et al. [4].

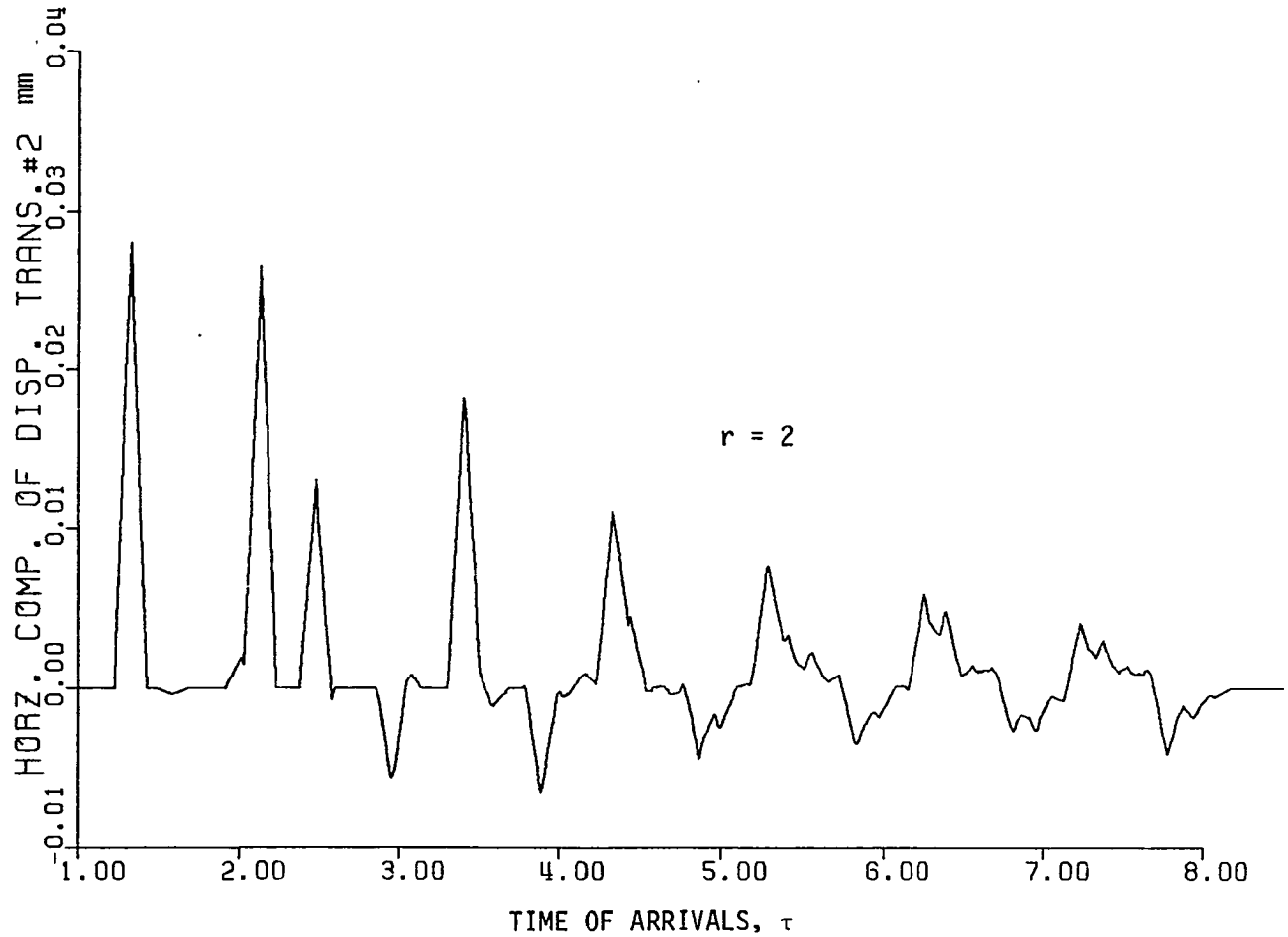

Fig. 3.8. Plates response to a unit dilatation point force. Point of dilatation (0,0) ($t_o = t/\tau$).

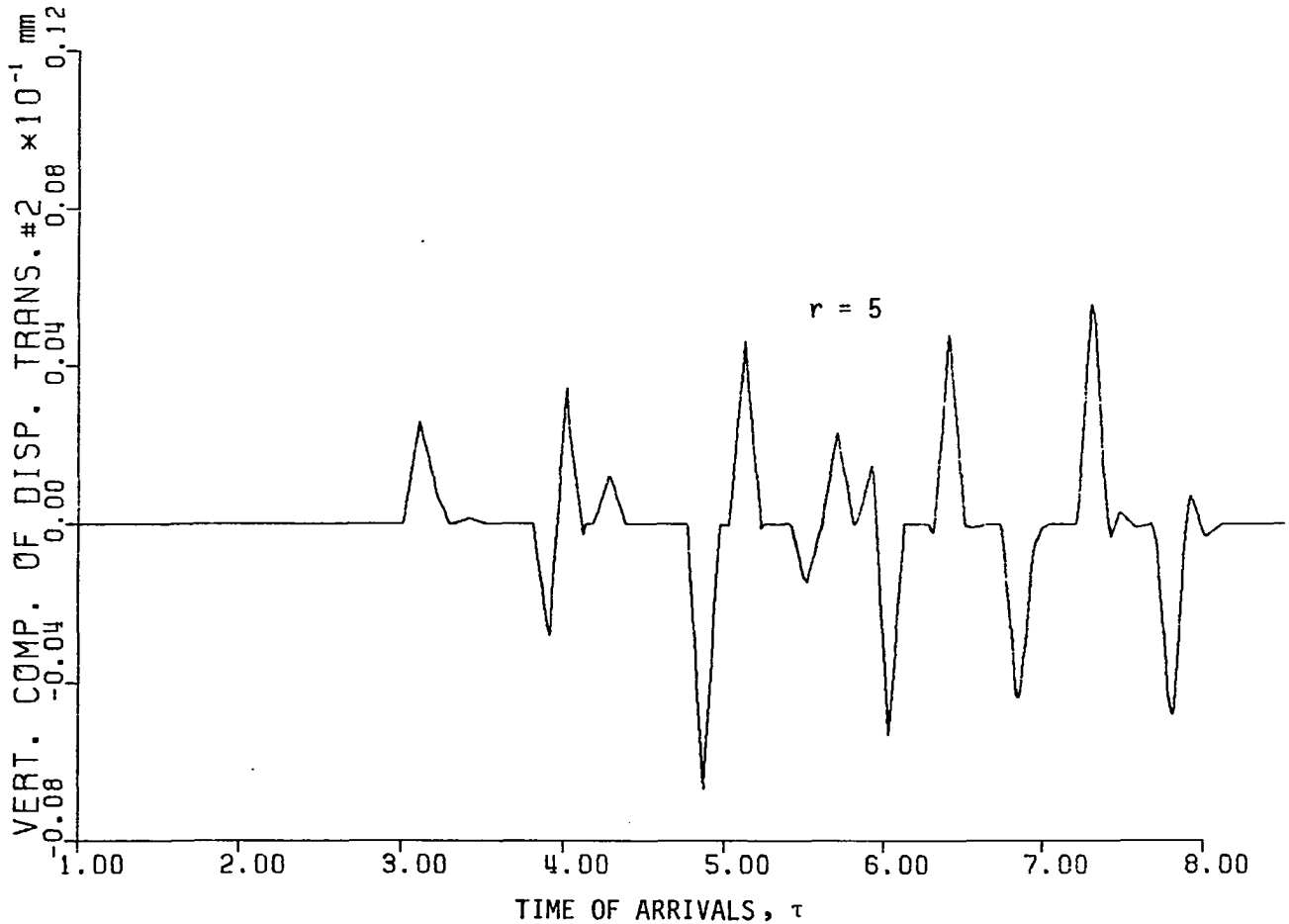

Fig. 3.9. Plates response to a unit dilatation point force. Point of dilatation (0,0) ($t_o = t/\tau$).

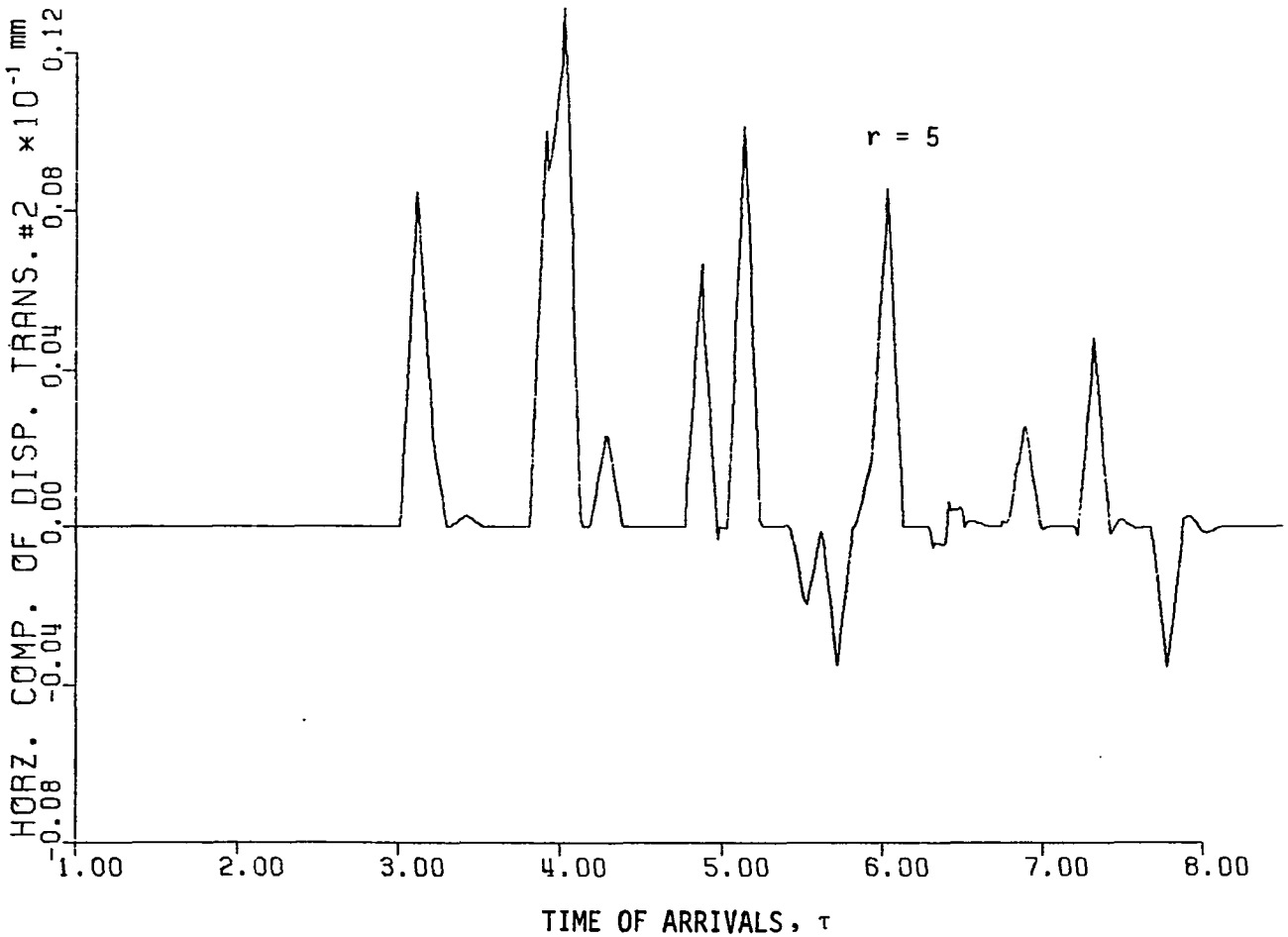

Fig. 3.10. Plates response to a unit dilatation point force. Point of dilatation (0,0) ($t_o = t/\tau$)

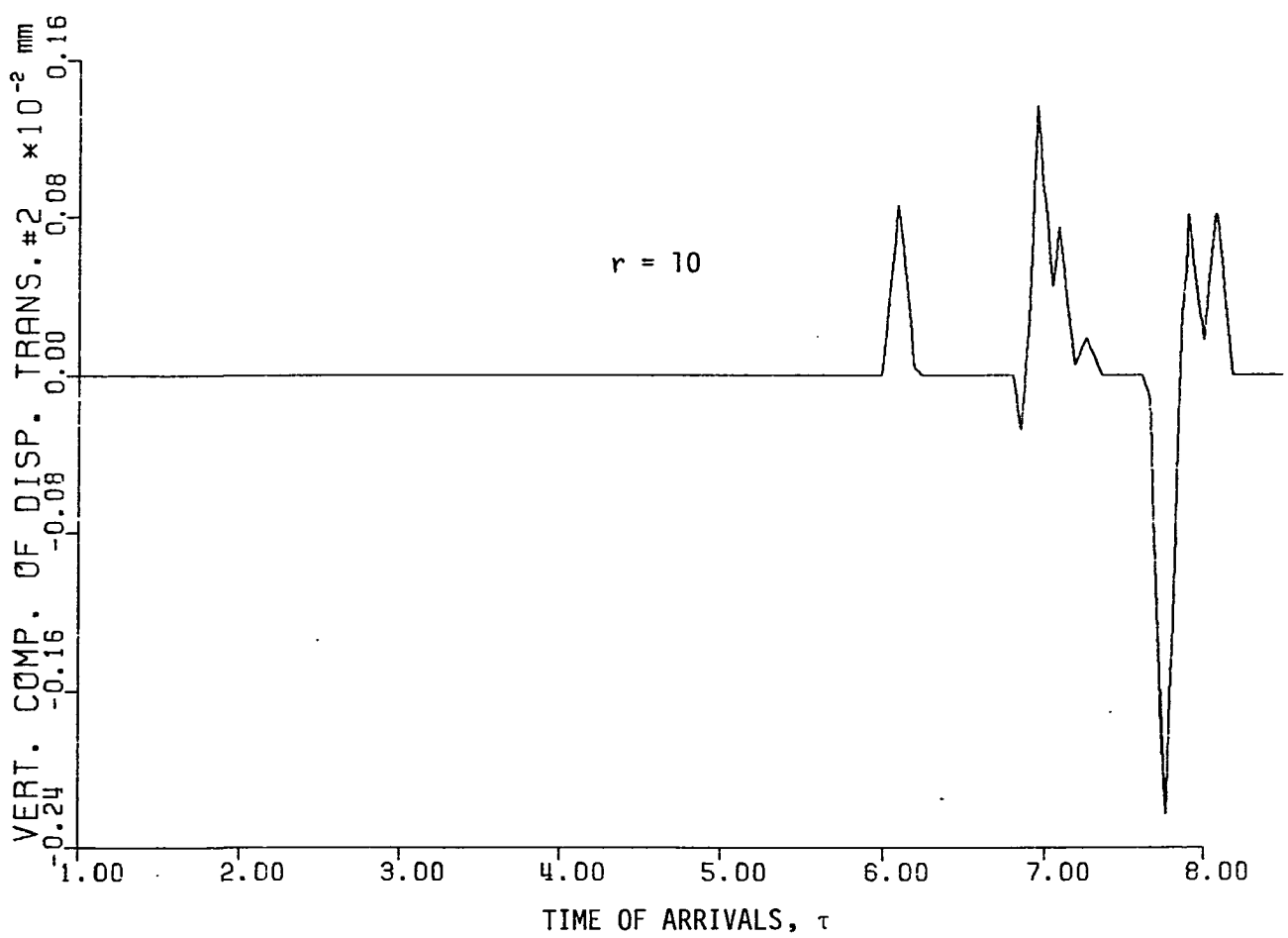

Fig. 3.11. Plates response to a unit dilatation point force. Point of dilatation (0,0) ($t_o = t/\tau$).

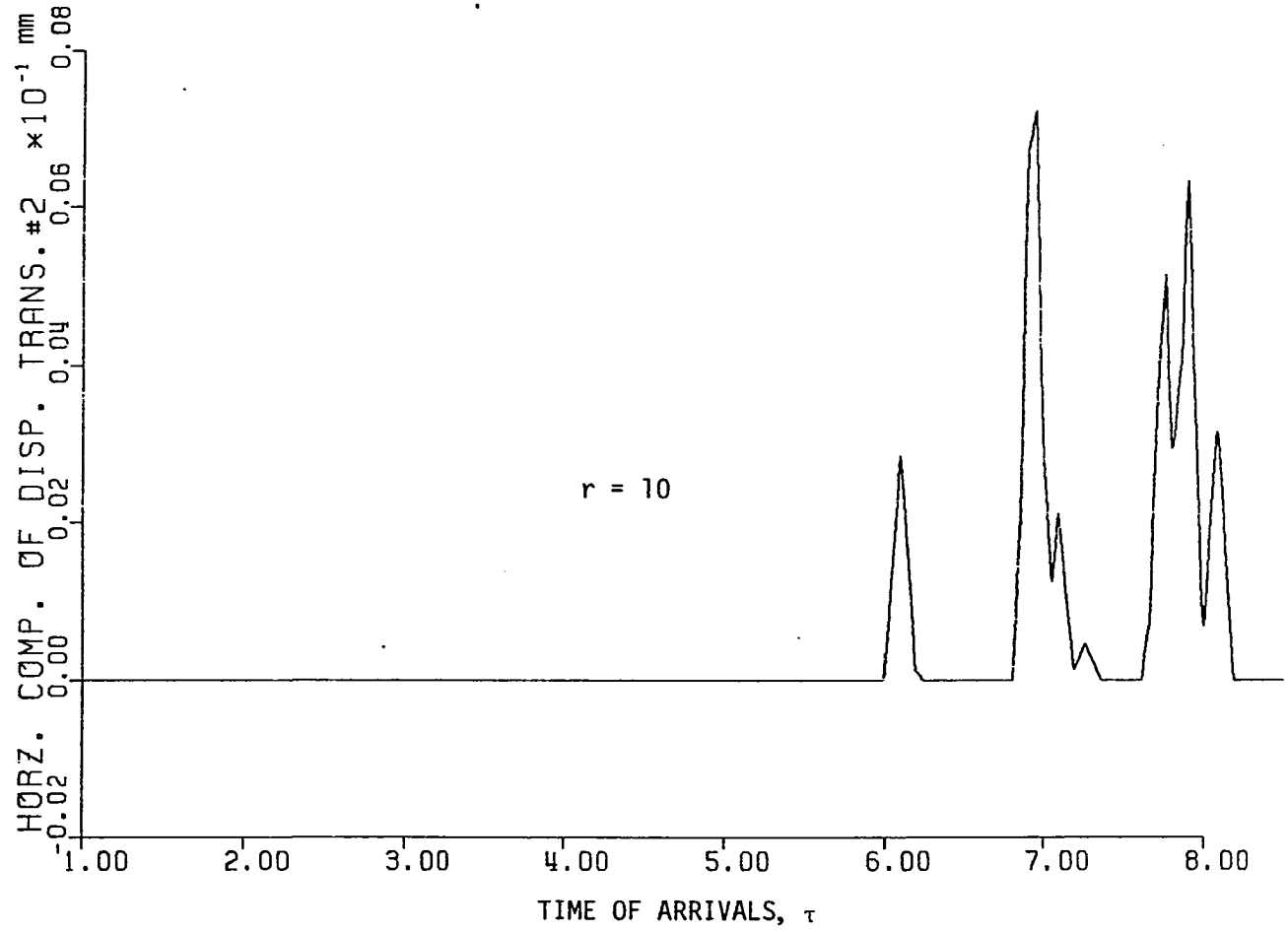

Fig. 3.12. Plates response to a unit dilatation point force. Point of dilatation (0,0) ($t_o = t/\tau$).

3.3 Response of a Plate to a Unit Stress Normal to the Surface of the Plate

The response of a plate to a circular disk vibrating normally to the surface of the plate was studied by Miller and Pursey [45,46]. In these works, they adapted Lamb's method to derive definite integrals for the displacement field in a semi-infinite isotropic solid due to a periodic normal stress. More recent investigations were conducted by Pao [4] and Pao et al. [5]. In these studies, they considered the response due to a concentrated normal load located at the surface of a plate using a square pulse time function.

In this section, the response of a plate due to a unit normal stress located at the surface of the plate is investigated using the Monte Carlo technique. The solutions of Miller and Pursey are adapted to derive a far-field impulsive response.

3.3.1 Derivation of the Far-Field Solution Compressional and Shear Waves

The far-field response to a periodic load according to Miller and Pursey [45] is given as

$$u_r = -\frac{a^2}{2C_{\psi\psi}} \frac{\cos e(k^2 - 2\sin^2 e)}{R\, F_\theta(\sin e)} e^{-iR} \tag{3.5}$$

$$u_\theta = -\frac{ia^2k^2}{2C_{\psi\psi}R} \frac{\sin 2f\sqrt{(k^2\sin^2 f - 1)}}{F_0(k \sin f)} e^{-ikR} \tag{3.6}$$

The response of a plate to a periodic force,

$$f(t) = pe^{i\omega t}$$

can be written as

$$u_r = U_R\, e^{i\omega(t-R/C_L)} \tag{3.7}$$

$$u_\theta = U_\theta\, e^{i\omega(t-R/C_T)} \tag{3.8}$$

Since

$$\delta(t) = \frac{1}{\sqrt{2\pi}} \int_{-\infty}^{\infty} e^{-i\omega t}\, d\omega$$

$$= \frac{1}{\sqrt{2\pi}} \left[\int_{-\infty}^{\infty} \cos \omega t\, d\omega - \int_{-\infty}^{\infty} i \sin \omega t\, d\omega\right]$$

But

$$\int_{-\infty}^{\infty} \sin \omega t\, d\omega = 0, \text{ being an odd function}$$

therefore,

$$\delta(t) = \frac{1}{\sqrt{2\pi}} R_e \int_{-\infty}^{\infty} e^{-\omega t}\, d\omega \tag{3.9}$$

Therefore, for an impulsive response of the plate, we are only concerned with the real part of u_r or u_θ, i.e.,

$$u_r = \frac{1}{\sqrt{2\pi}} \int_{-\infty}^{\infty} R_e[U_R\, e^{i\omega(t-R/C_L)}]d\omega \tag{3.10}$$

$$u_\theta = \frac{1}{\sqrt{2\pi}} \int_{-\infty}^{\infty} R_e[U_\theta\, e^{i\omega(t-R/C_T)}]d\omega \tag{3.11}$$

But U_r is real for all incident angles under consideration, and U_θ is complex.

Therefore,

$$R_e[U_R\, e^{i\omega(t-R/C_1)}] = U_R \cos \omega(t - R/C_L)$$

$$R_e[U_\theta\, e^{i\omega(t-R/C_2)}] = U_{\theta R} \cos \omega(t - R/C_T) - U_{\theta i} \sin \omega(t - R/C_T)$$

$$u_r = \frac{1}{\sqrt{2\pi}} U_R \int_{-\infty}^{\infty} \cos \omega(t - R/C_L) \tag{3.12}$$

$$u_\theta = \frac{1}{\sqrt{2\pi}} U_{\theta R} \int_{-\infty}^{\infty} \cos \omega(t - R/C_T)d\omega \tag{3.12}$$

$$- \frac{1}{\sqrt{2\pi}} U_{\theta i} \int_{-\infty}^{\infty} \sin \omega(t - R/C_T)d\omega$$

Since the second expression on the right hand side is an odd function,

$$u_\theta = \frac{1}{\sqrt{2\pi}} U_{\theta R} \int_{-\infty}^{\infty} \cos \omega(t - R/C_T)d\omega \tag{3.13}$$

Therefore,

$$u_r(t) = U_R \delta(t - R/C_L)$$

$$u_\theta(t) = U_{\theta R} \delta(t - R/C_T)$$

But by Miller and Pursey [45],

$$U_R = - \frac{a^2}{2\mu R} \frac{\cos e(k^2 - 2 \sin^2 e)}{F_\theta(\sin e)} \tag{3.14}$$

and

$$U_\theta = - \frac{ia^2k^2}{2\mu R} \frac{\sin 2f\sqrt{(k^2 \sin^2 f - 1)}}{F_\theta(k \sin f)} \tag{3.15}$$

where

a = radius of the circular disk

μ = shear modulus

R = radial distance

e = the incident angle for a P-wave

$k = C_L/C_T$, ratio of the wave speeds

$$F_\theta(X) = (2X^2 - k^2)^2 - 4X^2(X^2 - 1)^{\frac{1}{2}}(X^2 - k^2)^{\frac{1}{2}}$$

For a unit force, we assume $\sigma = 1$, therefore

$$P = \sigma\pi a^2 = \pi a^2$$

$$\therefore \quad a^2 = P/\pi = 1/k$$

According to Pao for a unit force, the 'i' term in the equation (3.6) should be dropped. Therefore,

$$U_R = -\frac{1}{2\pi\mu R} \frac{\cos e(k^2 - 2\sin^2 e)}{F_\theta(\sin e)}$$

$$U_\theta = -\frac{k}{2\pi\mu R} \frac{\sin f\sqrt{(k^2\sin^2 f - 1)}}{F_\theta(k \sin f)}$$

U_R, U_θ = displacement amplitudes for a P-wave and SV-wave, respectively.

For a direct P- or SV-wave, the above amplitudes are used appropriately. But in case of waves with multiple segments, the amplitudes are then multiplied by the appropriate curvature factors, K_i and the coefficients of reflection, R_{APP_i}.

3.3.2 Unit Stress Normal to the Surface of the Plate: Numerical Calculations

The material constants given are the same used in Section 3.2.1. In addition, the Lamé's constant, μ is taken as .25. The unit force is placed at the point (0,15) at the upper surface of the plate. The transducers are located at three points, r = 2, r = 4, and r = 6 where r is normalized with respect to the thickness of the plate. There are two cases considered for the location of the receiver. In the first case, the source and the receiver are located at opposite sides of the plate. In the other case, the source and the receiver are located at the upper surface of the plate. In both cases, the source function is a unit normal force and the time function is a square pulse, see [18], $f(t) = H(t) - H(t - \Delta)$ where $H(t)$ is a step function and $\Delta = 0.8\tau$.

For comparative purposes, the force is normalized with respect to $1/(2h\pi\mu)$. The time is also normalized with respect to τ, where $\tau = 2h/C_L$.

In the first case with source and receiver at the opposite side, only wavefields with odd number of segments like P, S, PSP, SPS, and PPP arrive at the receiver. On the contrary, the waves with even number of segments are recorded at the receiving post after reflection when the source and the receiver are at the upper surface (see Fig. 3.13). The times of arrival for the two cases with r = 2, r = 4, and r = 6 are shown in Tables 3.6 - 3.9 and 3.10 - 3.13. The complete responses at three locations for the first case are shown in Figs. 3.14 - 3.19. Figures 3.20 - 3.25 show the responses of the plate due to the second case — source and receiver at the same side of the plate.

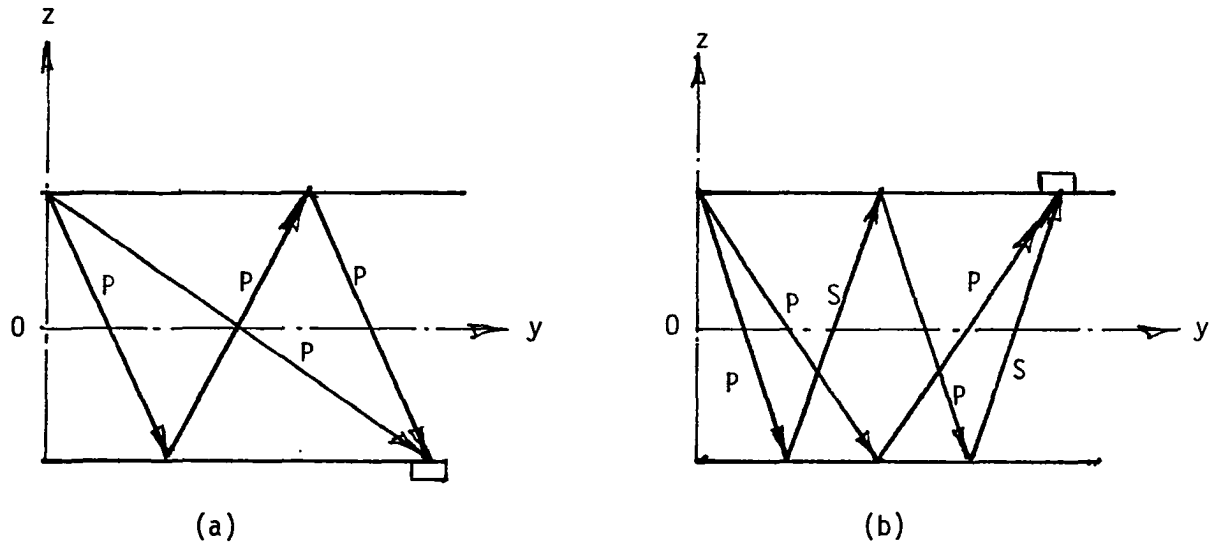

Fig. 3.13. Reflection of waves with:

(a) Odd number of segments
(b) Even number of segments

Table 3.6. Arrival Time ($\tau = tC_L/2h$)

Surface Loading - Source and Receiver on the Opposite Sides of the Plate

r = 2		r = 4		r = 6	
Waveform	Arrival Time, τ	Waveform	Arrival Time, τ	Waveform	Arrival Time, τ
P	2.21 2.22 2.26	P	4.1 4.14	P PSP (SPP)	6.11 7.68 7.73
P^3	3.62	PSP (PPS)	5.88 5.91	SPS (SSP)	8.79 8.8
S	3.7	PSS	6.85		9.54
SPP	4.34	SPS	6.87	PSPSP (PSPPS)	9.56 9.57
SPS	5.16	S	6.90 6.92		9.69
P^4	5.37	SSP	7.23	SSP	9.75
P^4S	6.07	P^2SPS	7.996	S^2P^3	9.92
P^7	7.27	SSS_c	8.17	S	10.12
PS^2PS	7.53	$S^2PS_c{}^2$	8.38	SPSPS	10.46
PSP^5	7.97	$S^2S_c{}^3$	8.53 8.61	(SSPSP)	10.51
PS^4	8.26	SPSPS	8.8 8.81	$S^2P^2S_cP^2$	11.15
PS^2P^4	9.35	P^2SPSP^2	9.55	$S^2S_c{}^2P$	11.34
PS^2PS^2P	10.06	PSPSPSP	10.29	S^2S_c	11.39
PS^3PS^2	10.75	$SPSPS^2P$	11.05	$SPSPSP^2$	11.61
P^{11}	11.17 11.18	$P^3SP^2SP^2$	11.27		
$P^3S^3P^3$	11.26	P^2SP^3SPS	11.98		
S^6P	11.45				
$P^3S^2PS^2P$	11.95				

Table 3.7. Peaks of the Displacement Field ($r = 2$) Surface Loading — Source and Receiver on Opposite Side

Arrival Time, τ	Amplitude of Displacement	
	Vertical Components	Horizontal Components
2.26	0.11×10^{-1}	0.234×10^{-1}
3.63	-0.141	-0.114
3.71	-3.94	-3.91
4.37	-4.265	-4.6
4.43	-4.12	-4.49
4.51	-0.33	-0.69
5.18	-0.04	0.07
5.38	-0.28	-0.039
6.1	-0.65	-0.61
6.18	-0.42	-0.5

Table 3.8. Peaks of the Displacement Field ($r = 4$) Surface Loading—Source and Receiver on Opposite Side

Arrival Time, τ	Amplitude of Displacement	
	Vertical Components	Horizontal Components
4.11	0.067×10^{-1}	0.195×10^{-1}
5.91	0.0268	0.04
6.85	-0.022	0.034
6.92	-1.04	-0.98
7.19	-1.073	-1.02
7.23	-2.19	-4.78
7.65	-2.17	-4.82
7.72	-1.15	-3.8
8.03	-0.068	-0.194
8.07	-0.08	-0.2
8.17	-2.07	1.09
8.87	-2.06	1.24

Table 3.9. Peaks of the Displacement Field ($r = 6$) Surface Loading — Source and Receiver on Opposite Side

Arrival Time, τ	Amplitude of Displacement	
	Vertical Components	Horizontal Components
6.12	0.035×10^{-1}	0.11×10^{-1}
6.72	0.035	0.11
6.92	0.0007	0.0016
7.75	0.05	0.0776
8.8	-0.002	0.002
9.6	0.008	0.010
9.69	-0.27	-0.93
10.12	0.7	1.42
10.51	-1.96	-2.1
10.92	-1.48	-1.62
11.31	0.268	0.98
11.39	-0.25	1.52
11.64	-0.28	1.43

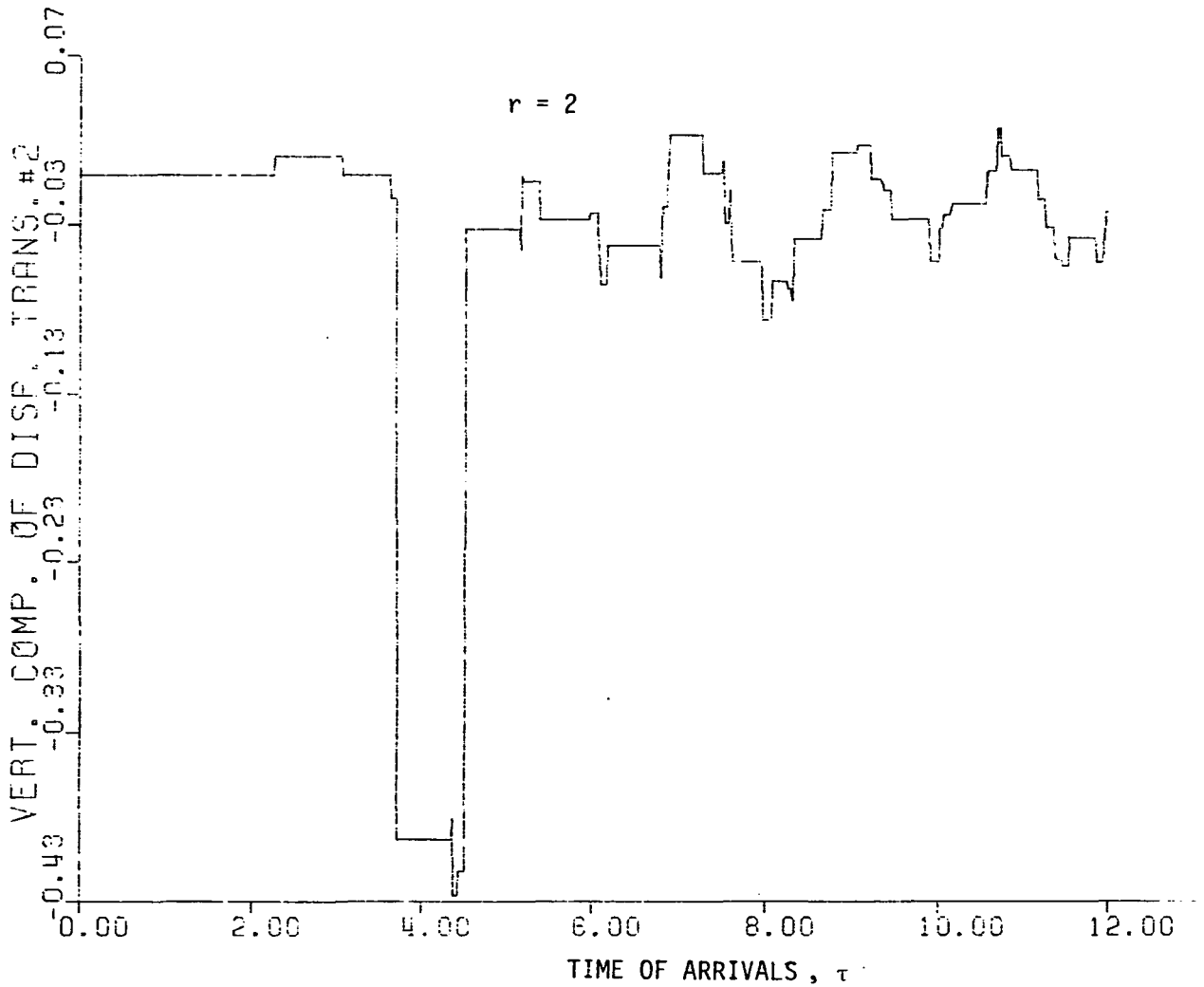

Fig. 3.14. Plate response to a unit surface force at (0,15). Receiver is located at point (60,-15).

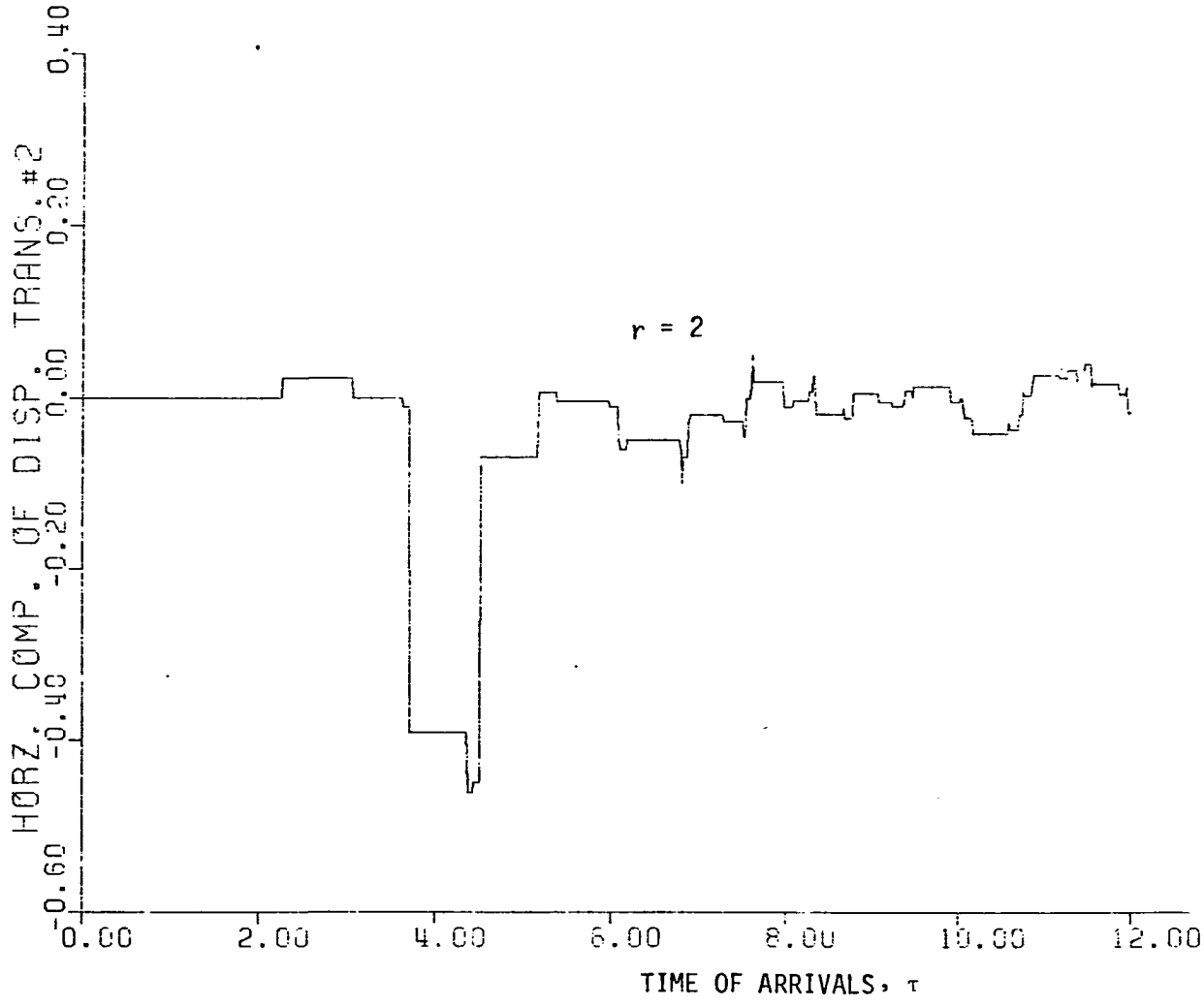

Fig. 3.15. Plate response to a unit surface force at (0,15). Receiver is located at point (60, -15).

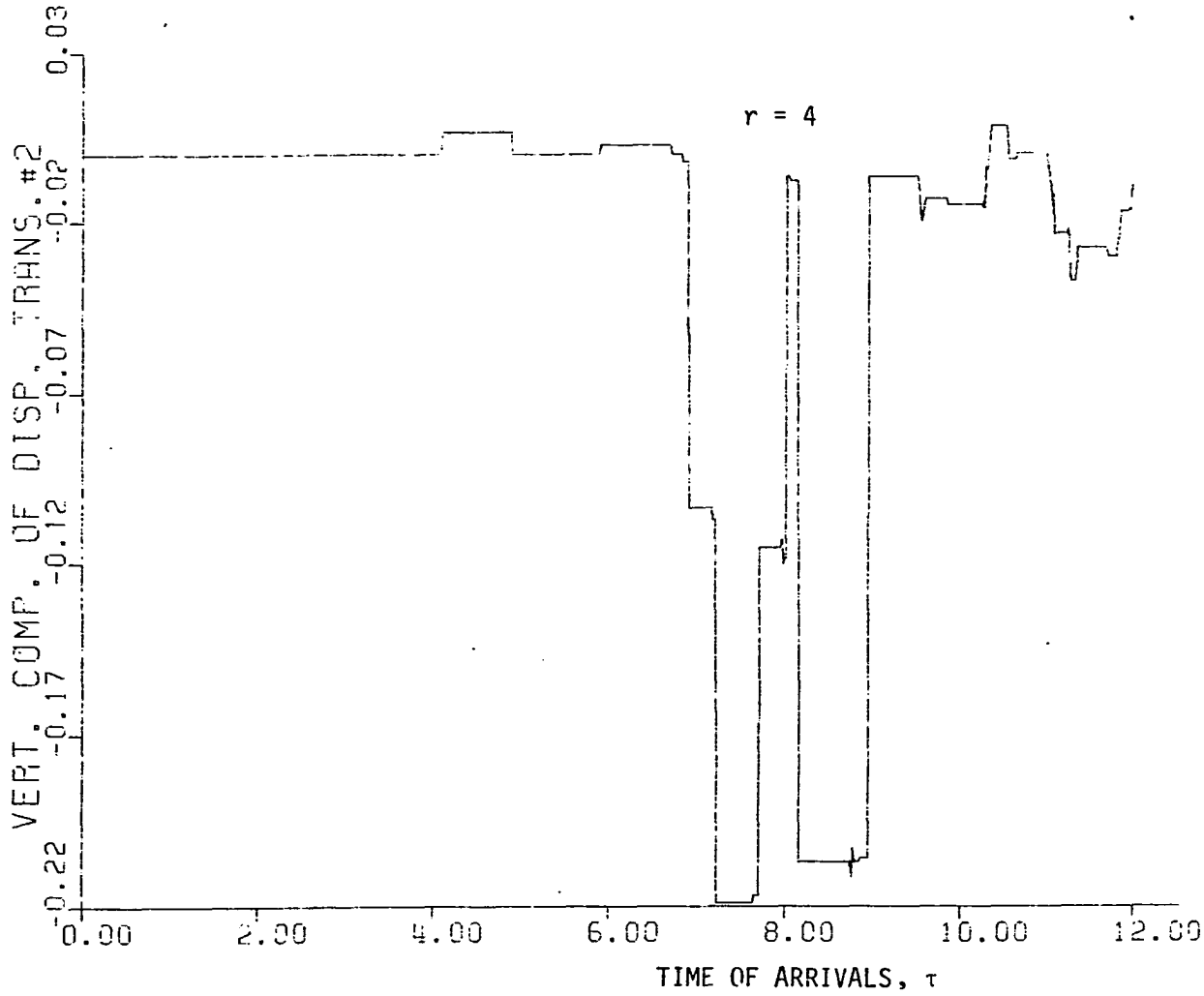

Fig. 3.16. Plate response to a unit surface force at (0,15). Receiver is located at point (120,-15).

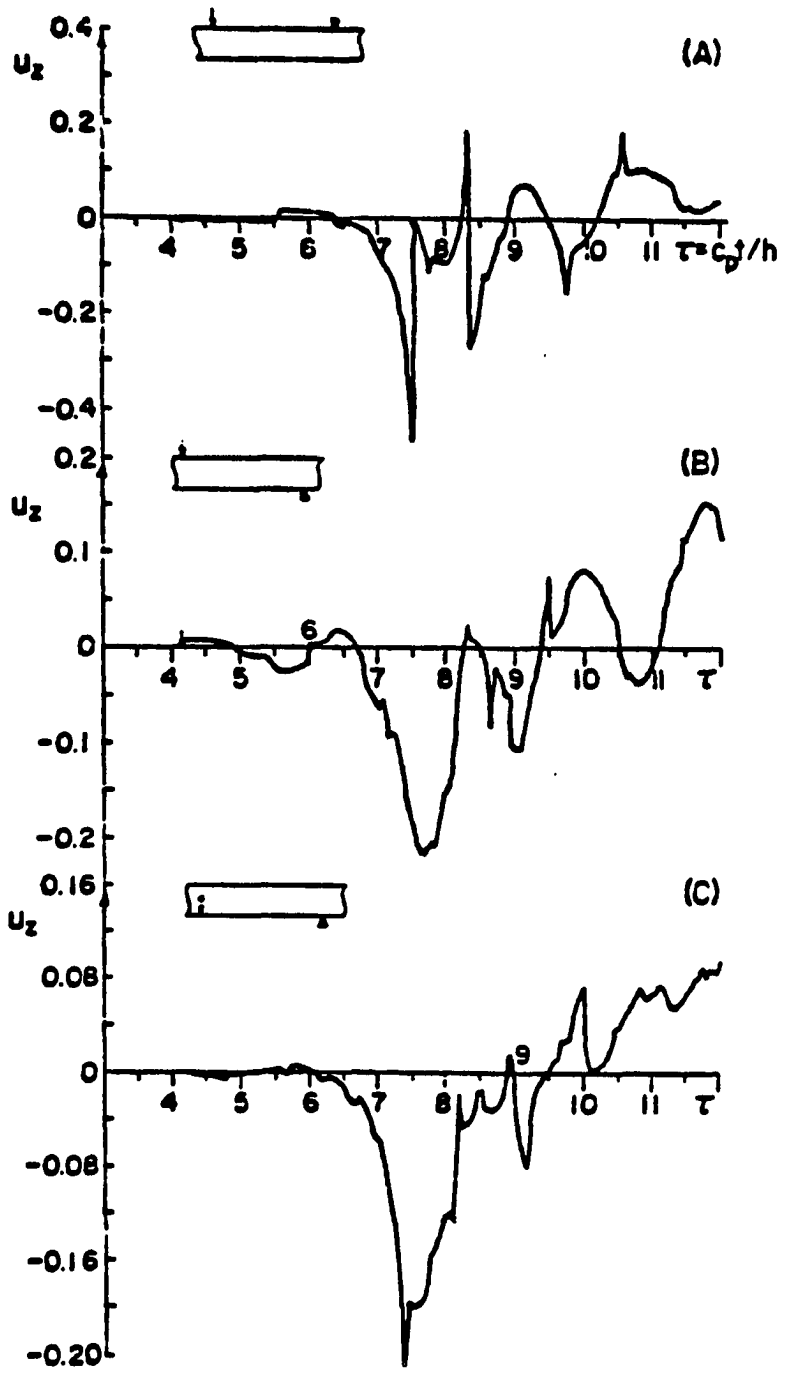

Fig. 6. Surface Response of a Plate due to a Vertical Force. (A) Source and Receiver at the Same Side, (B) Source and Receiver at the Opposite Sides, (C) A buried Vertical Force

Fig. 3.16 a. Responses due to Surface Load by Pao [5].

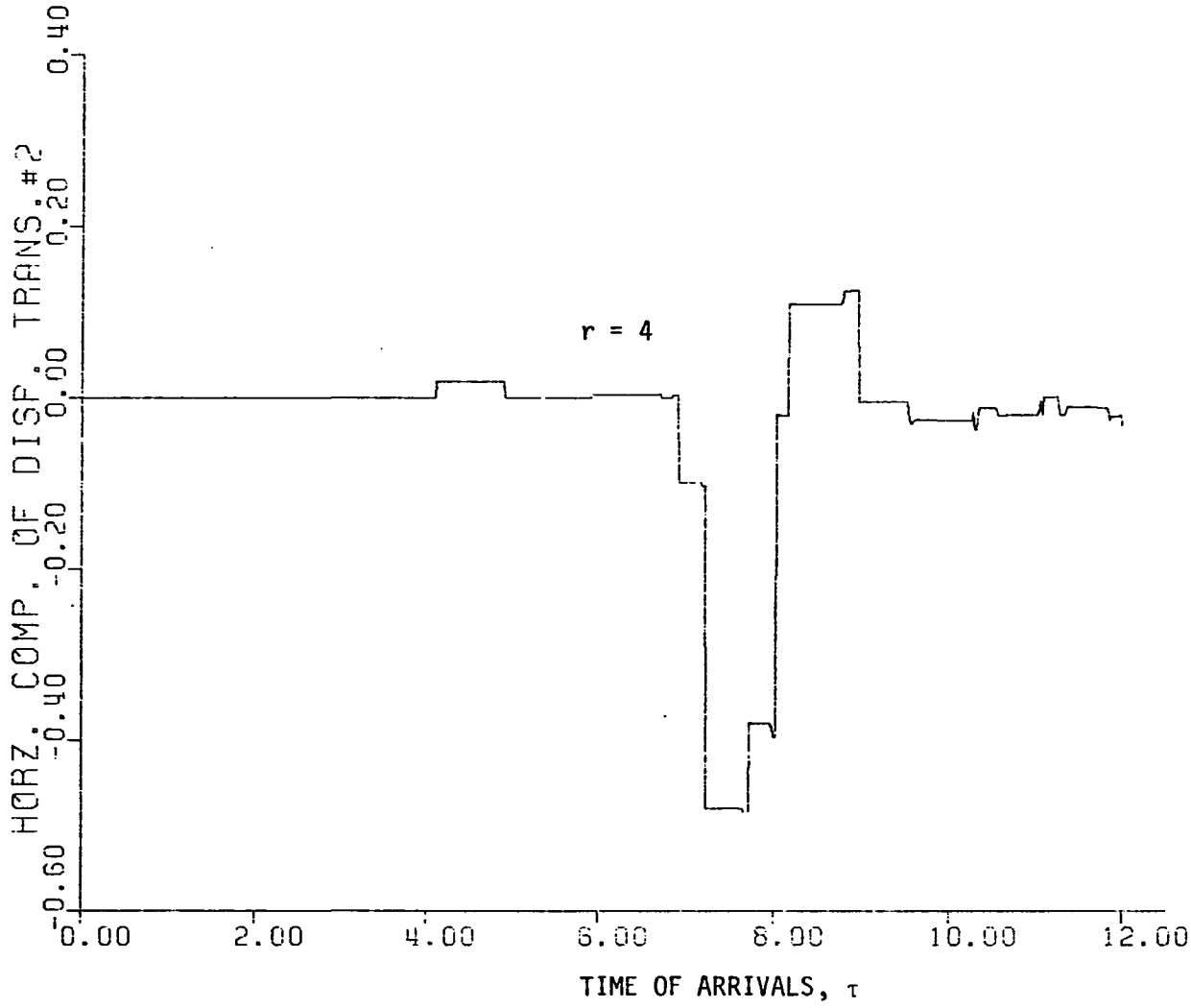

Fig. 3.17. Plate response to a unit surface force at (0,15). Receiver is located at point (120,-15).

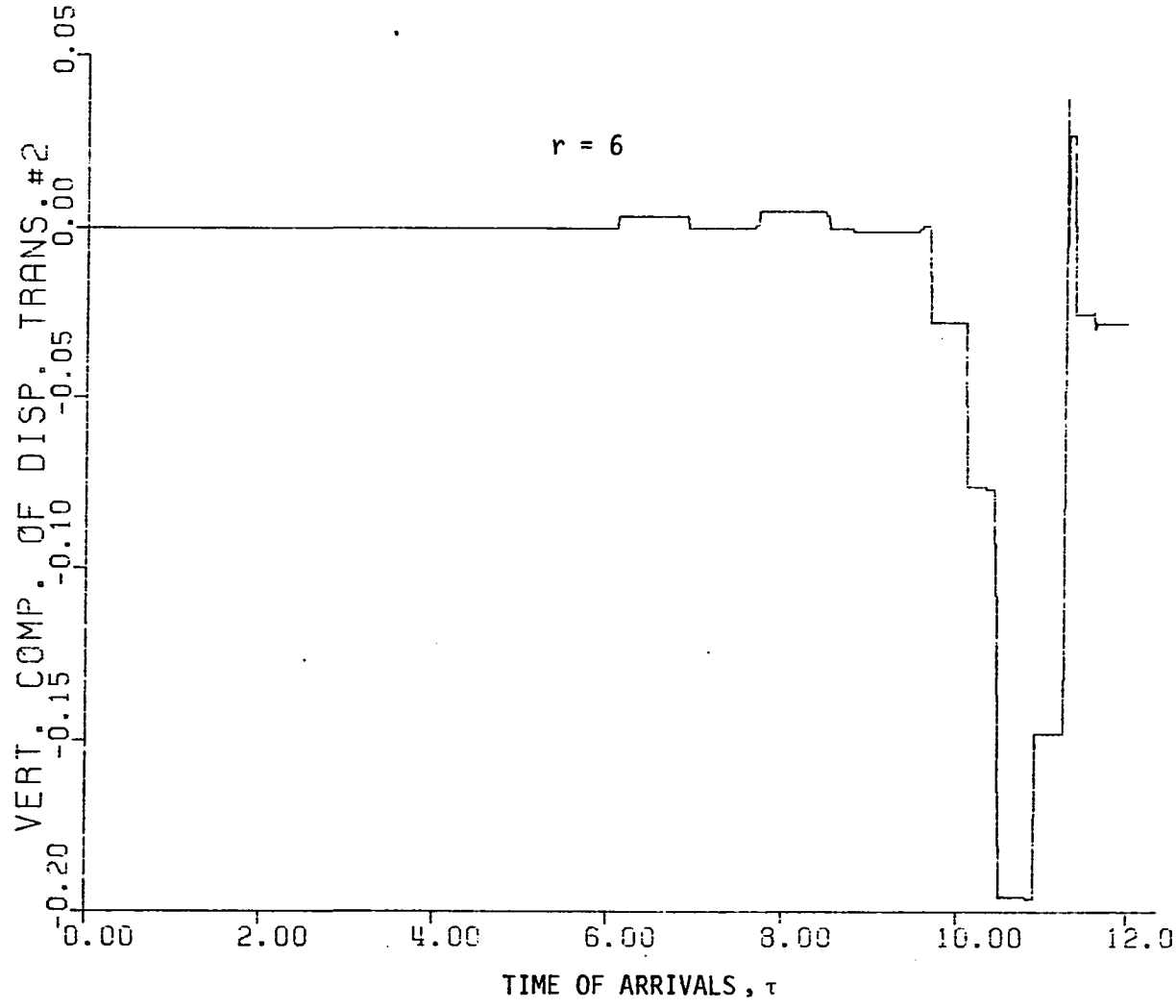

Fig. 3.18. Plate response to a unit surface force at (0,15). Receiver is located at point (180,-15).

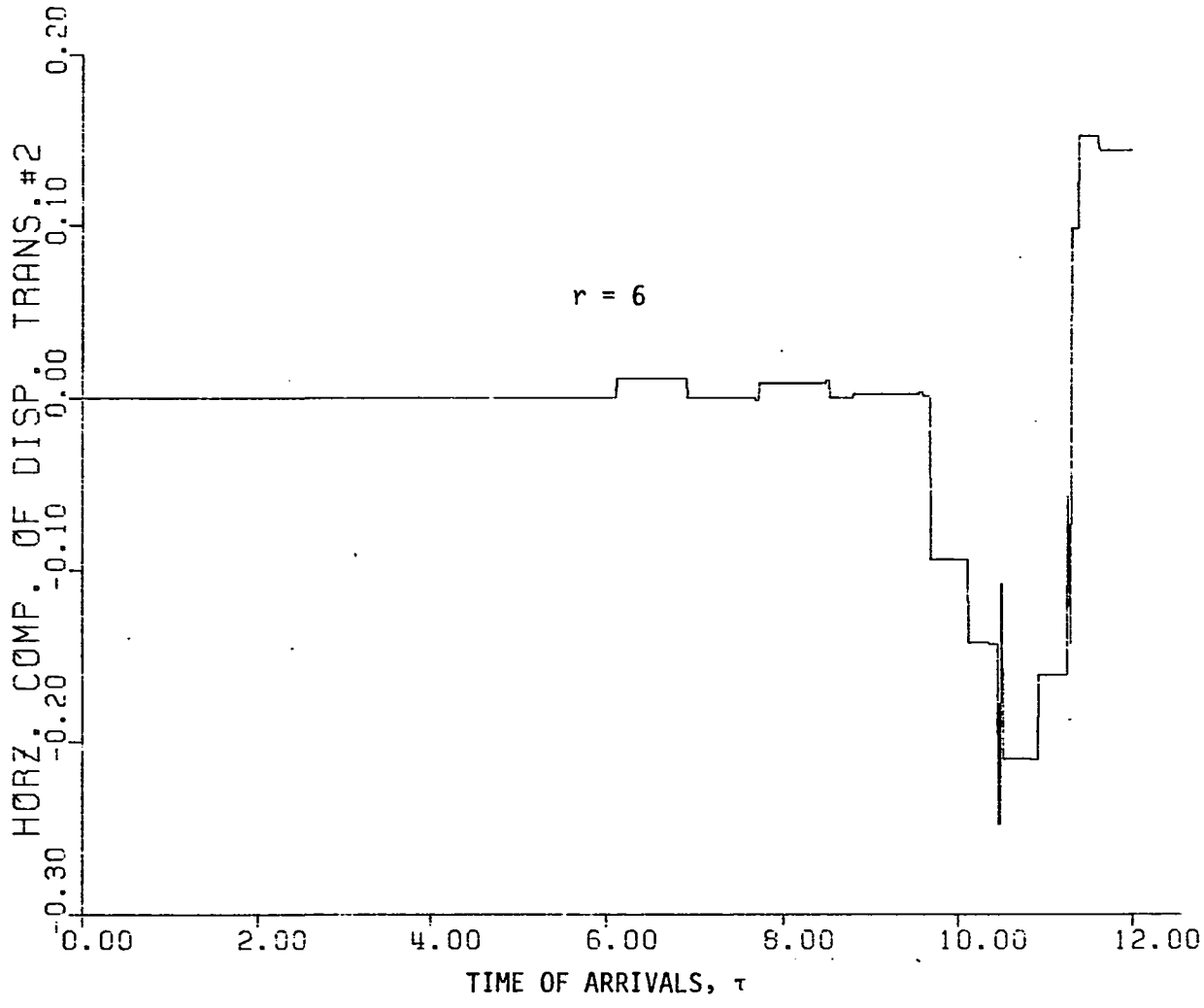

Fig. 3.19. Plate response to a unit surface force at (0,15). Receiver is located at point (180,-15).

Table 3.10. Arrival Time ($\tau = tC_L/2h$)
Surface Loading - Source and Receiver at the Upper Plate Surface

r = 2		r = 4		r = 6	
Waveform	Arrival Time, τ	Waveform	Arrival Time, τ	Waveform	Arrival Time, τ
P^2	2.84	PS	5.47	PP	6.32
PS	3.65		5.49	PS	7.45
SP	3.67		5.51		9.08
P^4	4.46	SPSP	7.33	PSPS	9.10
S^2	4.7	PSPS	7.34	S^2P^2	9.11
	4.75	PSPS	7.36		9.6
P^2SP	5.18	SS	7.5	SS	9.65
SP^3	5.2	SS	7.51	S^2PS	10.53
PPSS	5.92	SSPP	7.56	S^3P	10.56
PSPS	5.94	S^2PS_c	7.97	SS	10.57
SPPS	5.95	SSPS	8.26	S P S_c	10.6
PSSP	5.95	S^2S_c	8.64	SPSPSP	10.74
P^6	6.32	$PSPSP^2$	8.74	PSPSPS	10.99
PSSS	6.67	PSPSPS	9.5	$S^2S_cr^2P^2$	11.02
S^2PS	6.7	SPSPSP	9.51	$S^2PS_cPS_c$	11.15
P^2SP^3	7.02	SPS^2PS	10.3	S^2P^6	11.19
P^3SPS	7.71	P^3SPSP^2	10.39		11.68
P^8	8.24	PSP^2SPSP	11.12	$S^2PS_c^3$	11.71
P^3S^3	8.41	SP^2SPS^2P	11.85	S^2PSPS	11.82
PS^2P^2S	8.43	PS^2PSP^2S	11.87		11.94
P^7S	8.93				
S^2PS^2P	9.14				
P^{10}	10.19				
PSP^4S^2	10.3				
SP^9	10.88				
SP^4S^3	10.998				
$S^2P^4S^2$	11.00				
P^8S^2	11.56				
P^2S^5P	11.69				

Table 3.11. Peaks of the Displacement Field ($r = 2$) Surface Loading—Source and Receiver on the Upper Plate Surface

Arrival Time, τ	Amplitudes of Displacement	
	Vertical Components	Horizontal Components
2.85	-0.215×10^{-1}	-0.259×10^{-1}
3.7	-1.082	1.666
4.48	-1.364	1.496
4.5	-0.281	-0.169
5.19	-0.685	-0.441
5.2	-1.229	-0.301
5.24	-0.948	-0.132
5.94	-1.367	0.87
6.0	0.1348	0.997
6.34	-0.119	0.894
6.68	-0.231	1.127
6.75	-0.366	0.13
7.04	-0.946	0.147
7.14	-0.69	0.25
7.48	-0.58	0.0164
7.83	0.095	0.294
8.24	-0.138	0.225

Table 3.12. Peaks of the Displacement Field ($r = 4$) Surface Loading—Source and Receiver on the Upper Plate Surface

Arrival Time, τ	Amplitudes of Displacement	
	Vertical Components	Horizontal Components
4.5	0.0525×10^{-1}	0.111×10^{-1}
5.5	-0.3014	0.524
6.5	-0.0789	-0.1088
7.32	-0.4435	0.6866
7.49	-2.253	-5.407
7.97	-2.372	-5.51
8.12	-1.928	-6.196
8.29	-0.118	-0.103
8.61	-4.263	1.954
8.77	-4.55	1.957
8.95	-4.57	1.944
9.41	-0.427	-0.112
9.55	0.0171	0.5867

Table 3.13. Peaks of the Displacement Field (r = 6) Surface Loading—Source and Receiver on the Upper Plate Surface

Arrival Time, τ	Vertical Components	Horizontal Components
6.32	0.031×10^{-1}	0.081×10^{-1}
7.46	-0.119	0.283
8.15	-0.066	0.388
8.26	0.0533	0.105
9.11	-0.248	0.2406
9.66	-1.054	-2.52
9.93	-0.815	-2.746
10.14	-0.8565	-2.806
10.46	-0.0415	-0.06
10.58	0.0505	-5.84
10.94	0.092	-5.78
11.03	-0.165	-5.407
11.35	0.466	-3.281
11.38	-0.257	0.373
11.53	-0.2637	0.3665
11.79	-0.256	0.379
11.9	-1.458	-1.162

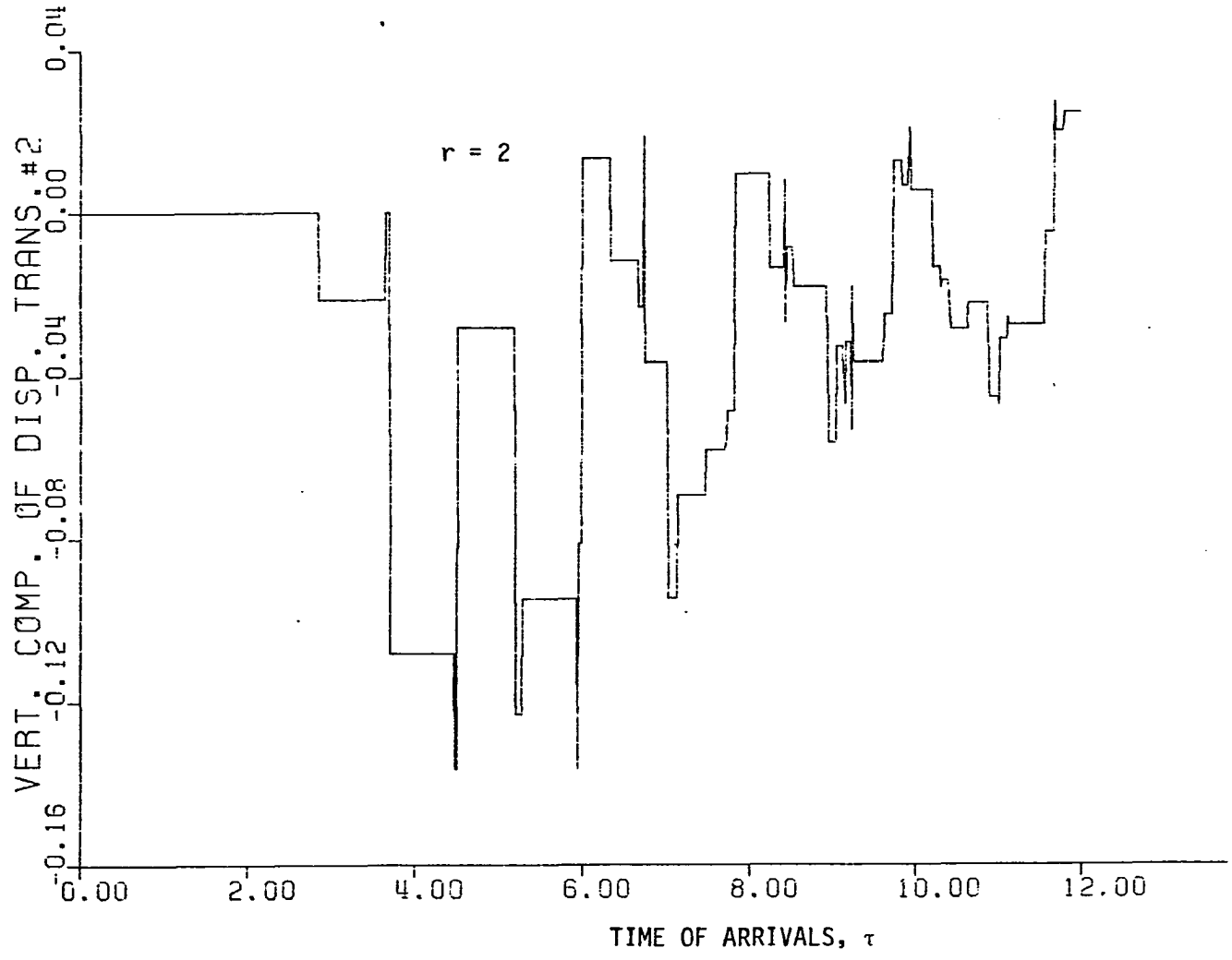

Fig. 3.20. Plate response to a unit surface force at (0,15). Receiver is located at point (60,15).

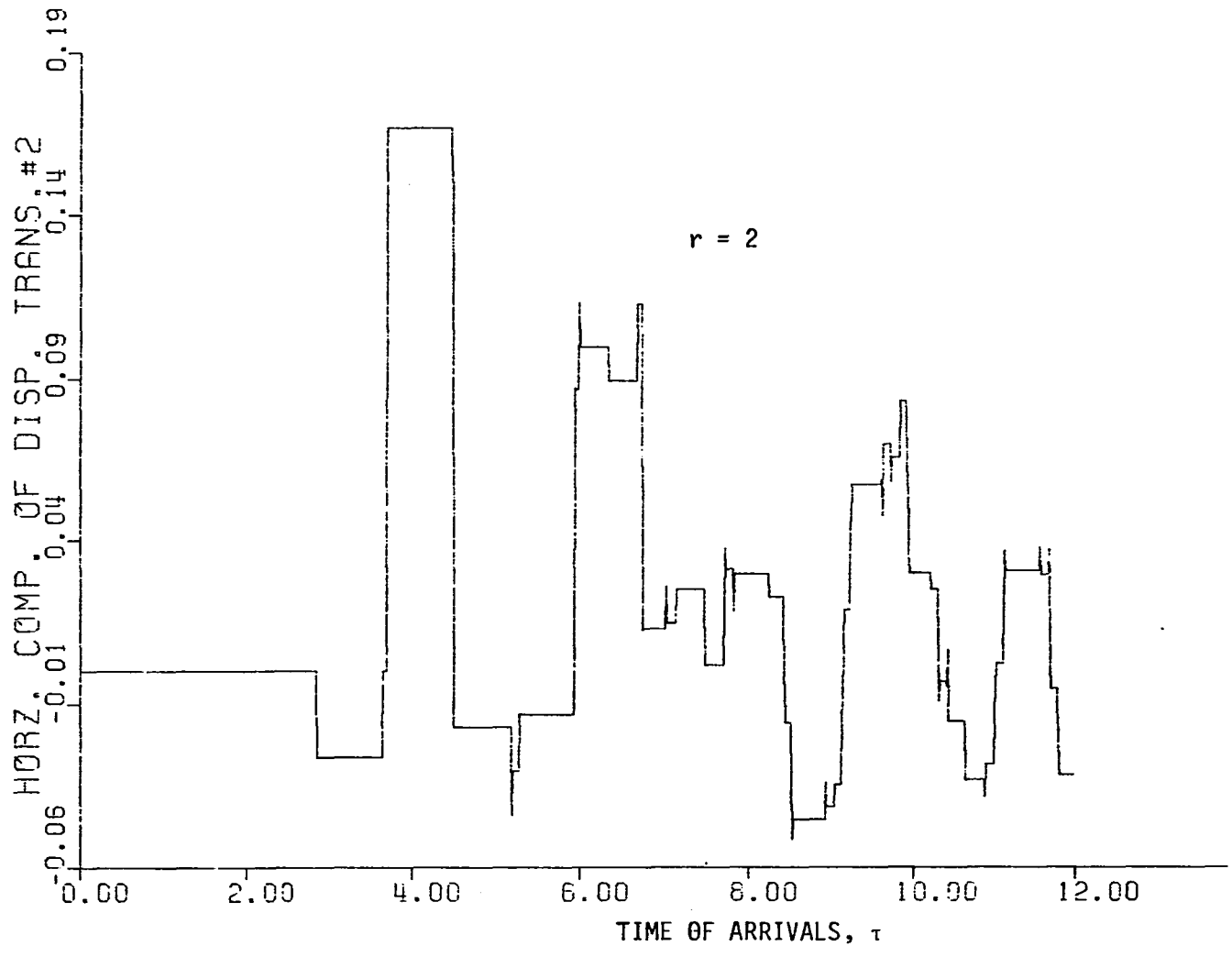

Fig. 3.21. Plate response to a unit surface force at (0,15). Receiver is located at point (60,15).

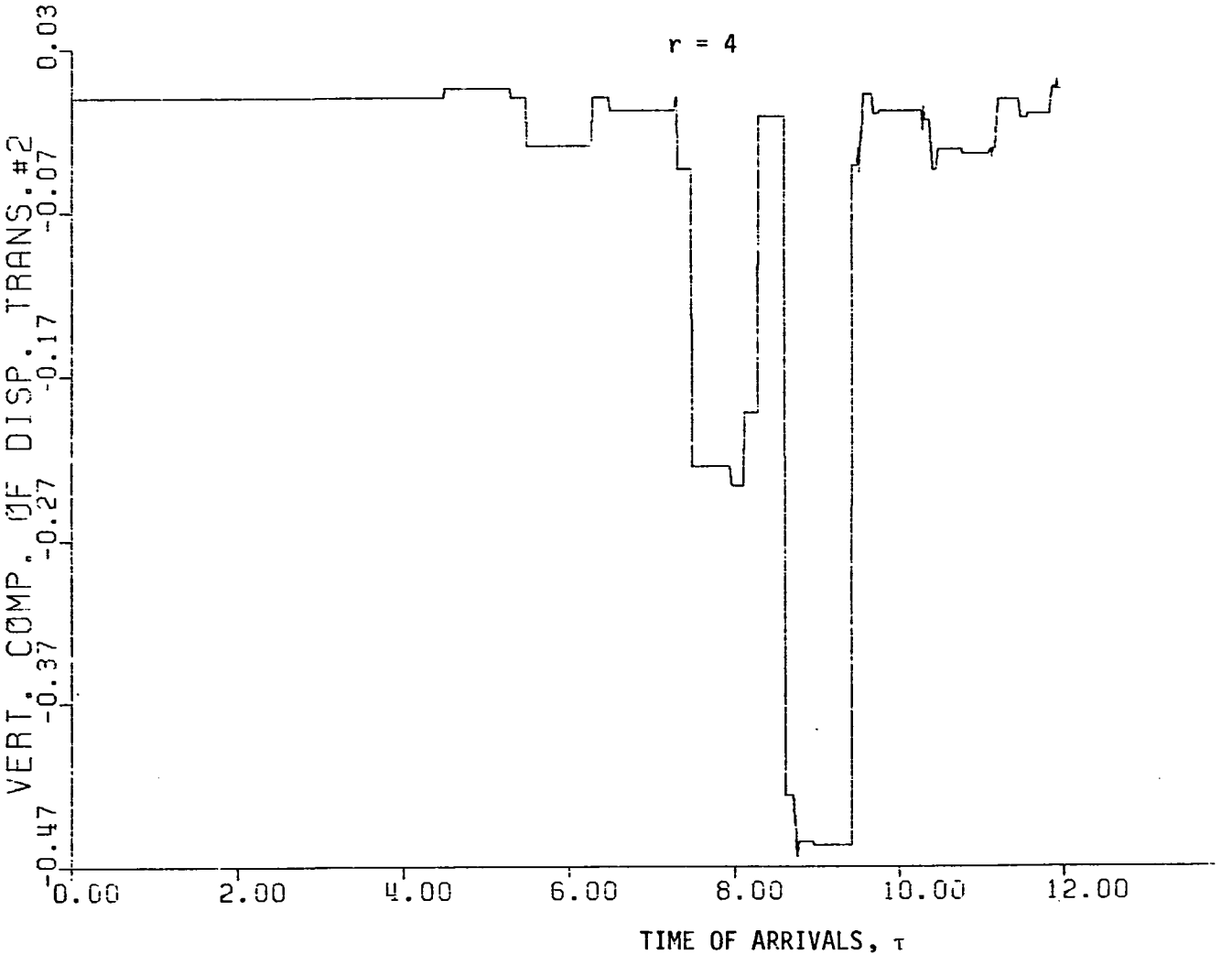

Fig. 3.22. Plate response to a unit surface force at (0,15). Receiver is located at point (120,15).

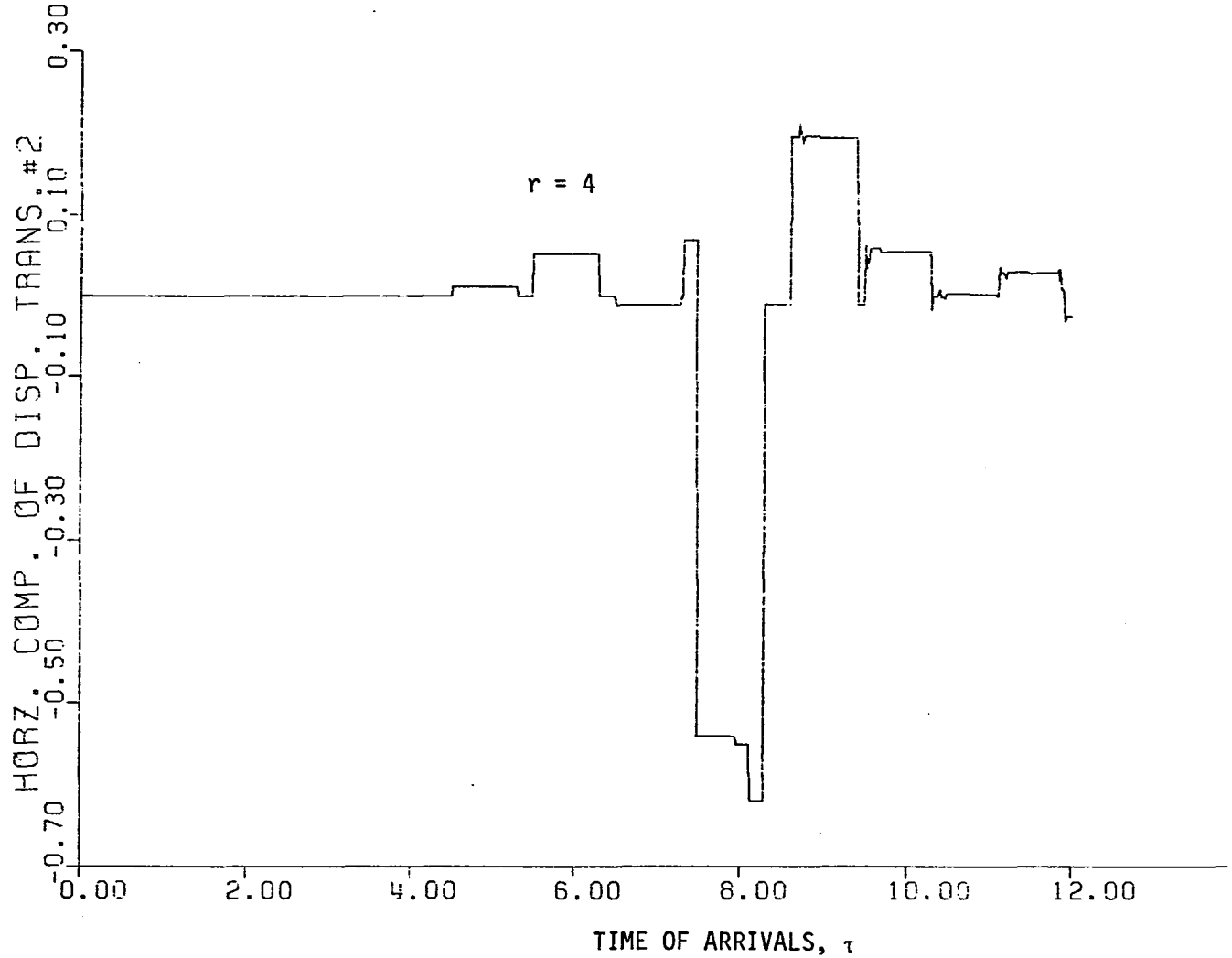

Fig. 3.23. Plate response to a unit surface force at (0,15). Receiver is located at point (120,15).

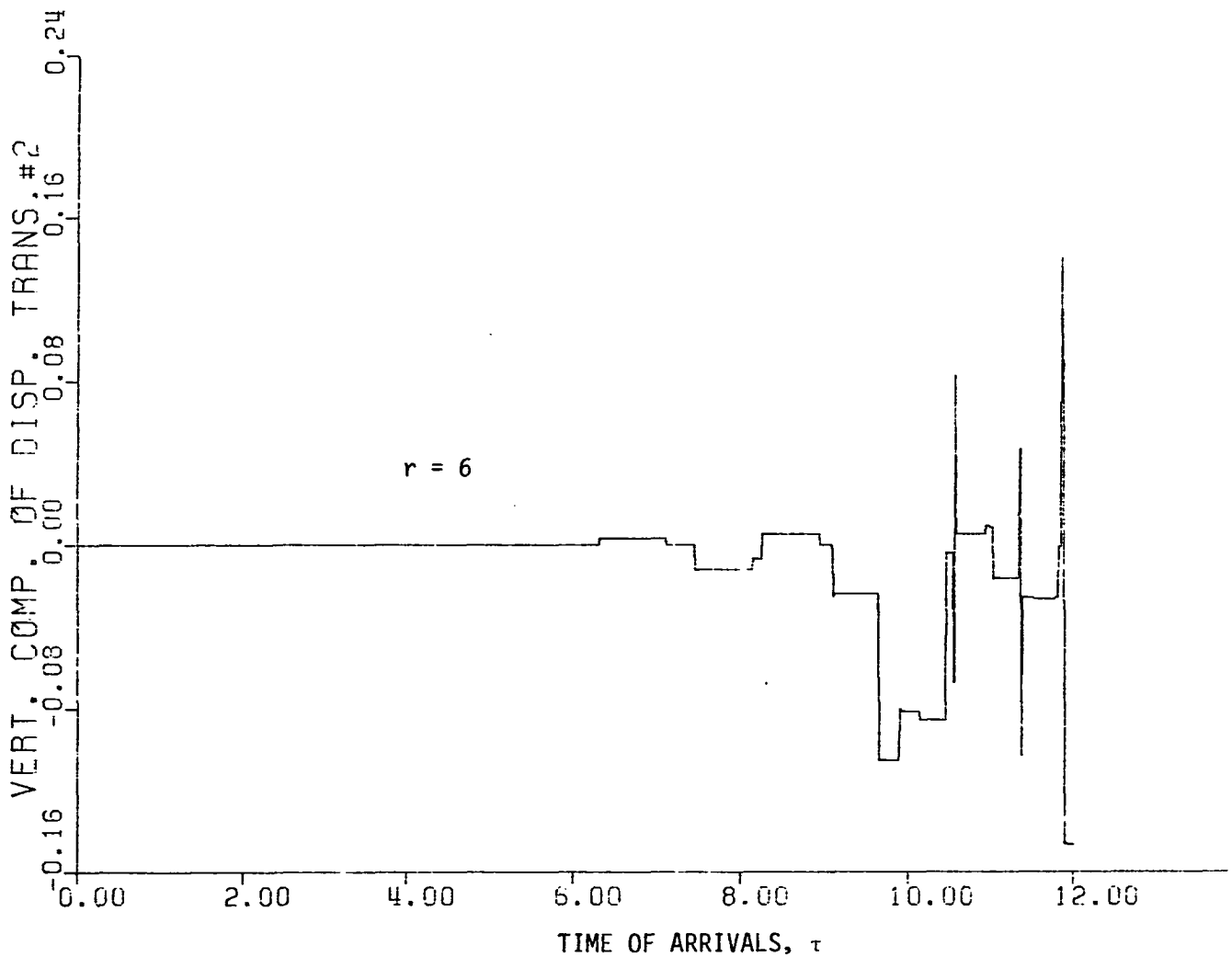

Fig. 3.24. Plate response to a unit surface force at (0,15). Receiver is located at point (180,15).

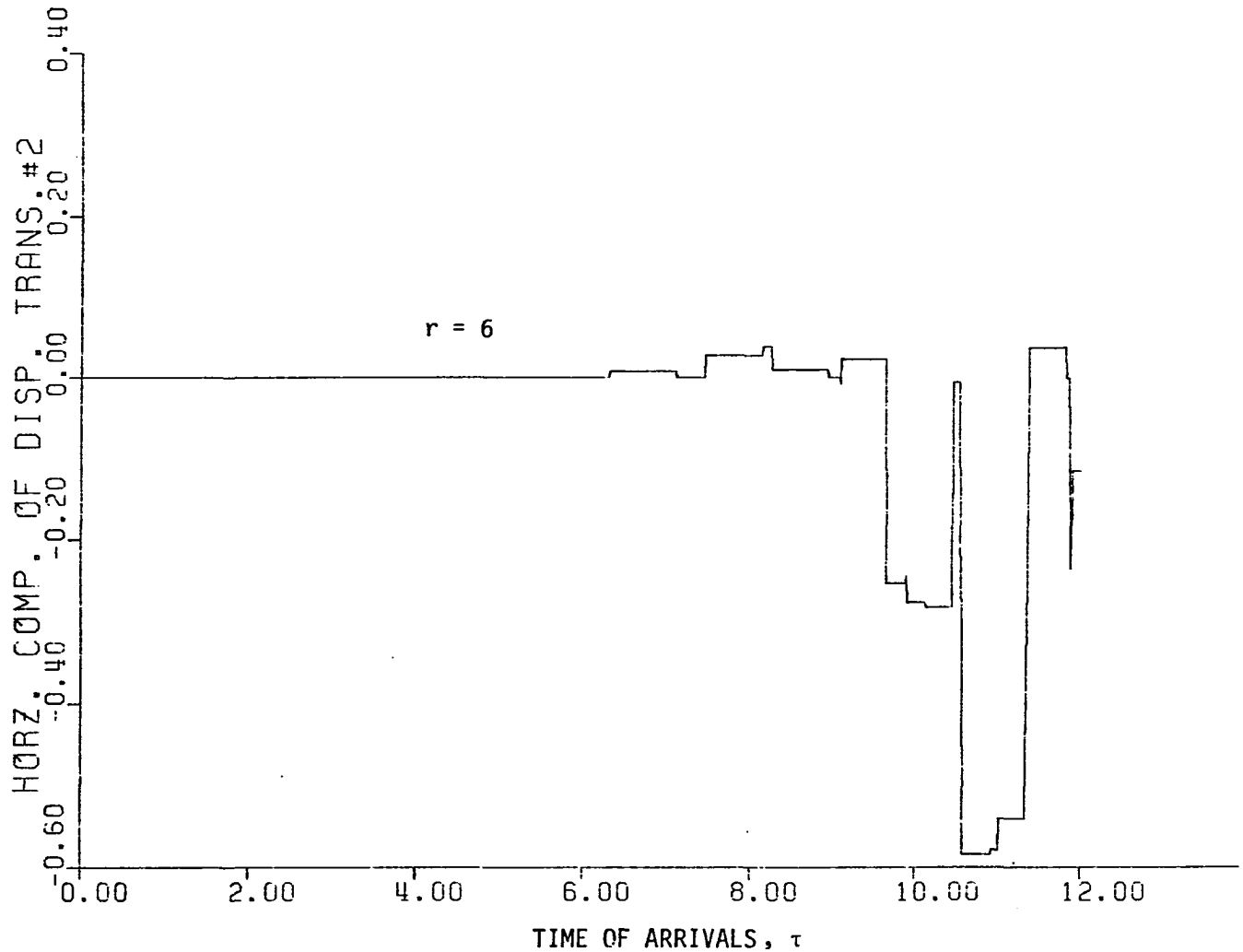

Fig. 3.25. Plate response to a unit surface force at (0,15). Receiver is located at point (180,15).

CHAPTER IV

ANALYSIS OF THE RESULTS AND CONCLUSION

In this chapter, the results are examined and analyzed. Comparisons are made with the previous investigation by Pao [4] and Pao et al. [5]. Finally, recommendations are made for future research.

4.1 Results and Analysis

In this section, analyses are made for the following results:

(i) The displacement field due to a dilatational point source.

(ii) The response of the plate due to a unit normal stress, with the source and the receiver on opposite sides of the plate.

(iii) The response of the plate due to a unit normal stress, with the source and the receiver at the upper surface of the plate.

4.1.1 Case (i) Dilatation Point Source

It can be observed from Figs. 3.7 and 3.8 that the first arrival observed at the receiving point (when $r = 2$) is the source ray, P at time $\tau = 1.22$ followed by the PP, PPP, PS, PSP, and subsequently by multiple reflected rays. The parameter, r, and the variable, τ, are dimensionless.

Featuring prominently with the vertical components of displacement of -1.68×10^{-2} mm, 1.51×10^{-2} mm, and 0.97×10^{-2} mm are PS, PSP, and P, respectively. Their corresponding horizontal peaks are 2.65×10^{-2} mm, 1.3×10^{-2} mm, and 2.8×10^{-2} mm. This shows that at $r = 2$, the source ray gives the largest contribution to the displacement field in the horizontal direction, strongly followed by PS rays. However, as the distance of the receiver from the source point increases, the contribution of multiple reflected rays with multiple mode conversions, P^2S^2 predominates in the vertical direction. This is evident in Fig. 3.9 when $r = 5$ and Fig. 3.11 with $r = 10$. It is interesting to note that the peak of the displacement for the source ray, P, decreases approximately by a factor of 0.66 for all the three locations. The contributions from the rays without mode conversion like PP, P^3, and others are very gible.

4.1.2 Case (ii) - Response Due to Surface Force (Source and Receiver on the Opposite Sides of the Plate)

From Table 3.6, it is easily seen that the early arrivals at the receiving point with $r = 2$ are P-waves at 2.21τ, P^3-waves at 3.62τ, and S-waves at 3.7τ followed by other multiple reflected waves like SPP ($\tau = 4.34$), SPS ($\tau = 5.16$), and the others. It is interesting to note that for all the three locations of the transducer, the waves with the source ray in an SV mode predominate. See Tables 3.7 - 3.9. This fact can be utilized to identify the dominant of the source rays for the case in which both P- and S-waves are emitted from the source point. Typical of these are the SPP and S at $r = 2$ with the peak amplitudes of

-4.265×10^{-1} and -3.93×10^{-1}, respectively in the vertical direction and -4.6×10^{-1} and -3.91×10^{-1} in the horizontal direction. The displacement amplitude due to the rays, P, P^3 are negligible. As the distance of the transducer increases to r = 4 and r = 6, the contributions from the multiple reflected waves with odd number of segments become predominant.

4.1.3 Case (iii) - Response Due to Surface Force
(Source and Receiver at the Upper Plate Surface)

From Table 3.10, we can see that the PP, PS, P^4, S^2 waves arrive in succession at the receiver followed by some complex multiple reflected ways. Since the source ray can either be a P or S mode, the multiple waves formed thus possess the appropriate mode of the emitted ray. For example, the P^2S^2 and P^2SP waves show that the source rays are of a P mode while SP, SS, and SPPS indicate that their source rays are of an S mode.

When r = 2, P^2S^2, P^4, P^3S, and PS arrive at the receiver at the time $\tau = 5.94$, $\tau = 4.48$, $\tau = 5.2$, and $\tau = 3.7$, respectively with very strong peaks of -1.367×10^{-1}, -1.364×10^{-1}, -1.229×10^{-1}, and -1.082×10^{-1} in the vertical direction. A major contribution to the displacement in the horizontal direction comes from the PS-waves (1.666×10^{-1}) followed by P^4 with 1.496×10^{-1}. As the distance of the receiver from the source increases to r = 5, the contribution from the P^2S^2 waves in the horizontal direction significantly increases to -2.25×10^{-1} but returns to -1.054×10^{-1} at r = 10.

At r = 4, the major contributions come from P^4S^2 and $S^2S_c^2$ at

τ = 8.77 and τ = 8.61, respectively (see Table 3.12). At r = 6, major contributions to the horizontal displacement come from S^3P (-5.84×10^{-1}) at τ = 10.58, S^3P^3 (-5.78×10^{-1}) at τ = 10.94, and P^3S^3 (-5.407×10^{-1}) at τ = 11.05 (see Table 3.13).

4.2 Comparison of Results and Conclusions

In this work, the propagation of the elastic waves in a plate due to a dilatational point source and two types of surface point force, have been investigated using the proposed Monte Carlo/ray tracing technique.

The theoretical formulations are given for both the two- and three-dimensional cases. In the plate case, numerical calculations are made for determining the horizontal and vertical components of displacement field for the three cases mentioned above.

In case (i), the dilatational point source, comparison with the generalized ray analysis of Pao [4] for similar geometry and the same load condition shows a very strong agreement in spite of the difference in the basis of normalization and in the wave speeds used (see Fig. 3.7a) In case (ii), the surface load with a source and receiver on opposite sides, an interesting result comes to light. For the case with r = 4 which is used for comparison purposes, the strongest motion with an amplitude of -0.219 arrives at the time, τ = 7.23 followed by another strong wave of less magnitude (of amplitude, -0.217) at τ = 7.65 as compared to the waves with the peak of -0.21 and -0.12, respectively reported by Pao [5]. Similarly, in case (iii), with the force and receiver on the same surface of the plate, a good agreement has been found (see Fig. 3.16a).

In essence, the results shown in Figs. 3.7-3.12, Figs. 3.14-3.19, and Figs. 3.20-3.25 have demonstrated the effectiveness of the Monte Carlo/ray tracing technique in determining the displacement fields of a plate due to different loading conditions. Moreover, unlike the generalized ray method, it is effective for investigating long-term responses as well.

4.3 Recommendations for Future Research

As mentioned earlier, in order to characterize accurately the structural integrity of a material using acoustic emission as a non-destructuve testing technique, it is essential to be able to identify the mode of the dominant wave emitted and locate the source of the mechanism (defects, voids). Although it has been shown that the Monte Carlo ray-tracing technique can be used to answer some of these questions, nonetheless, further investigations need to be conducted.

As a result, the following recommendations are made for future research:

a) The study of the wave motion in a plate having wedge-shaped surfaces and with the assumption that after the wave passes the receiver location, it can still possibly contribute to the displacement field after reflecting at the farther end of the plate.

b) Wave motion in a multilayered isotropic medium
This could be extended to a case where scattering effects are assumed to occur. Such investigations will undoubtedly be useful in studying solids with welded joints.

c) Numerical solution for the three-dimensional case already developed.

d) Finally, experimental investigations should be conducted to justify the applicability of these theoretical results.

REFERENCES

1. Hsu, N.H., 1978. "Experiments in Acoustic Emission Waveform Analysis for Characterization of AE Sources, Sensors and Structures." Elastic Waves and Nondestructive Testing of Materials. Applied Mechanics Division, ASME, Vol. 29, pp. 85-106.

2. Egle, D.M., 1979. "A Stochastic Model for Transient Acoustic Emission Signals." Journal of Acoustical Society of America, Vol. 65, No. 5, pp. 1198-1203.

3. Egle, D.M. and Ewumi, J.O., 1983. "A Monte-Carlo/Geometric Ray Technique for Wave Propagation in Plates." Paper to be presented at the 20th Annual Meeting of the Society for Engineering Science, University of Delaware, August 1983.

4. Pao, Y. and Gajewski, R.R., 1977. "The Generalized Ray Theory and Transient Responses of Layered Elastic Solids." Physical Acoustics, Vol. 13, pp. 183-265.

5. Pao, Y., 1978. "Theory of Acoustic Emission." Elastic Waves and Nondestructive Testing of Materials. Applied Mechanics Division, ASME, Vol. 29, pp. 107-128.

6. Pao, Y., Gajewski, R.R., and Ceranoglu, A.N., 1979. "Acoustic Emission and Transient Waves in an Elastic Plate." Journal of Acoustical Society of America, Vol. 65, No. 1, pp. 96-105.

7. Lamb, H., 1904. "On the Propagation of Tremors over the Surface of an Elastic Solid." Philosophical Transactions of the Royal Society (London), Series A, Vol. 203, pp. 1-42.

8. Lamb, H., 1916. "On Wave Patterns Due to a Travelling Disturbance." Philosophical Magazine, Series 6, Vol. 31, pp. 539-548.

9. Ewing, W.M., Jardetzky, W.S., and Press, F., 1957. Elastic Waves in Layered Media. New York: McGraw-Hill Book Company, Inc.

10. Bromwich, T.J.Ia., 1916. "Normal Coordinates in Dynamical Systems." Proceedings, London Mathematical Society, Series 2, Vol. 15, pp. 401-448.

11. Pekeris, C.L. and Lifson, H., 1957. "Motion of the Surface of a Uniform Elastic Half-Space Produced by Buried Pulse." Journal of Acoustical Society of America, Vol. 29, pp. 1233-1238.

12. Pekeris, C.L. and Longman, I.M., 1958. "The Motion of the Surface of a Uniform Elastic Half-Space Produced by a Buried Torque-Pulse." Geophysical Journal, Vol. 1, pp. 146-153.

13. Pekeris, C.L., Alterman, Z., and Abramovici, F., 1963. "Propagation of an SH- Torque Pulse in a Layered Solid." Bulletin of the Seismological Society of America, Vol. 53, pp. 39-57.

14. Weyl, H., 1919. "Ausbreitung Electromagnetischer Wellen Über Einen Ebenen Leiter," Annalen der Physik, Vol. 60, pp. 481-500.

15. Poritsky, H., 1951. "Extension of Weyl's Integral for Harmonic Spherical Waves to Arbitrary Wave Shapes." Symposium on the Theory of Electromagnetic Waves, p. 97. Interscience Inc., New York.

16. Cagniard, L., 1962. Reflection and Refraction of Progressive Seismic Waves. Translated by Flinn, E.A. and Dix, C.H. McGraw-Hill Book Company, Inc., New York.

17. Lapwood, E.R., 1949. "The Disturbance Due to a Line Source in a Semi-Infinite Elastic Medium." Philosophical Transactions of the Royal Society (London), Series A, Vol. 242, pp. 63-100.

18. Pekeris, C.L., Alterman, Z., Abramovici, F., and Jarosch, H., 1965. "Propagation of Compressional Pulse in a Layered Solid." Review of Geophysics, Vol. 3, No. 1, pp. 25-47.

19. Pinney, E., 1951. "A Theory of Use in Wave Theory." Journal of Mathematics and Physics, Vol. 30, pp. 1-10.

20. Pinney, E., 1954. "Surface Motion Due to a Point Source in a Semi-Infinite Elastic Medium." Bulletin of the Seismological Society of America, Vol. 44, pp. 571-596.

21. Knopoff, L., Gilbert, F., and Pilant, W.L., 1960. "Wave Propagation in a Medium with a Single Layer." Journal of Geophysical Research, Vol. 65, No. 1, pp. 265-278.

22. Chopra, S.D., 1958. "On the Equivalence of Saddle Point Approximations and Ray Theory in Elastic Wave Problems." Geophysical Journal, Royal Astronomical Society, Vol. 1, pp. 164-179.

23. Newlands, M., 1952. "The Disturbance Due to a Line Source in a Semi-Infinite Elastic Medium with a Single Layer." Philosophical Transactions of the Royal Society (London), Series A, Vol. 245, pp. 213-308.

24. Hong, T.-L. and Helmberger, D.V., 1977. "Generalized Ray Theory for Dipping Structures." Bulletin of the Seismological Society of America, Vol. 67, No. 4, pp. 995-1008.

25. Hong, T.-L. and Helmberger, D.V., 1978. "Glorified Optics and Wave Propagation in Nonplanar Structure," Bulletin of the Seismological Society of America, Vol. 68, No. 5, pp. 1313-1330.

26. Buslenko, N.P., Golenko, D.I., Shrieder, Yu.A. Sobol', and Sragovich, V.G., 1966. The Monte Carlo Method. Translated from Russian. New York: Pergamon Press.

27. Dunens, E.K. and Lambert, R.F., 1977. "Impulsive Sound-Level Response Statistics in a Reverberant Enclosure." Journal of Acoustical Society of America, Vol. 61, No. 6, pp. 1524-1532.

28. Haviland, J.K. and Thanedar, B.D., 1973. "Monte Carlo Applications to Acoustical Field Solution." Journal of Acoustical Society of America, Vol. 54, No. 6, pp. 1442-1448.

29. Stockham, L.W., 1967. "Radiative Heat Transfer from a Finite Cylindrical Particle Cloud." Unpublished Ph.D. dissertation. University of Oklahoma.

30. Turner, W.D. 1969. "Directional Emittance of Emitting, Absorbing and Scattering Media." Unpublished Ph.D. dissertation. University of Oklahoma.

31. Lindgren, B.W., 1965. Statistical Theory. The Macmillan Company, New York.

32. Shooman, M.L., 1968. Probabilistic Reliability: An Engineering Approach. New York: McGraw-Hill Book Company, Inc.

33. Achenbach, J.D., 1973. Wave Propagation in Elastic Solids. North-Holland, Amsterdam.

34. Achenbach, J.D., Gautesen, A.K., 1977. "Geometrical Theory of Diffraction for Three-D Elastodynamics." Journal of Acoustical Society of America, Vol. 61, pp. 413-421.

35. Achenbach, J.D., Gautesen, A.K., and McMaken, H., 1982. Ray Methods for Waves in Elastic Solids. Pitman Advanced Publishing Program, Boston, London, Melbourne.

36. Graff, K.F., 1975. Wave Motion in Elastic Solids. Ohio State University Press, Columbus, Ohio.

37. Bath, J., 1968. Developments in Solid Earth Geophysics 4 — Mathematical Aspects of Seismology. Amsterdam, England, and New York. Elsevier Publishing Company.

38. van der Pol, B. and Bremmer, H., 1937. "Diffraction of Electromagnetic Waves from an Electrical Point Source." Philosophical Magazine, Series 7, Vol. 24, pp. 825-864.

39. Bremmer, H., 1949. Terrestial Radio Waves. Elsevier Publishing Company, New York.

40. Ewumi, J.O., 1980. "The Study of Wave Motion in a Bounded Elastic Medium Using Monte Carlo Tracing Approach." A doctoral proposal for research, submitted to the Graduate Faculty, School of Aerospace, Mechanical and Nuclear Engineering, University of Oklahoma, Norman, OK.

41. Ewumi, J.O., 1982. "Wave Motion in a Bounded Elastic Medium Using Monte Carlo Tracing Approach." Proceedings, Thirteenth Southwestern Graduate Research Conference in Applied Mechanics, Norman, Oklahoma, pp. 79-96.

42. Granstein, W.C., 1935. Differential Geometry. The Macmillan Company, New York.

43. Struik, D.J., 1961. Lectures on Classical Differential Geometry. Addison-Wesley Publishing Company, Inc., Reading, MA, USA, London, England.

44. Bolz, R.E. and Tuve, G.L., 1976. Handbook of Tables for Applied Engineering Science. CRC Press, Cleveland, OH.

45. Miller, G.F. and Pursey, H., 1954. "The Field and Radiation Impedance of Mechanical Radiators on the Free Surface of a Semi-Infinite Isotropic Solid." Proceedings, Royal Society (London), Series A, Vol. 223, pp. 521-541.

46. Miller, G.F. and Pursey, H., 1955. "On the Partition of Energy Between Elastic Waves in a Semi-Infinite Solid." Proceedings, Royal Society (London), Series A, Vol. 233, pp. 55-69.

APPENDIX: COMPUTER PROGRAMS

The two programs which are used for this Monte Carlo ray-tracing investigation and included in this appendix are as follows:

a) The INCPLATE which is used for the dilatational case where the source ray emitted from the source point is a P-wave.

b) The INCPLATE which is used for calculating the response due to the surface loading. In this case, the emitted waves are dilatational and equivoluminal waves from the same point source.

Since there are two rays emitted in case (b) and the Monte Carlo ray-tracing technique can only account for a single ray at a time, an additional Monte Carlo decision is taken in the UI Subroutine to choose one of those rays to pursue. Moreover, Subroutine UTHETA is also added to calculate the amplitude at the first pierce point. When calculating the horizontal and the vertical components, it is essential to use the appropriate expression to account for the fact that the receiver is either at the upper or the bottom surface.

The programs are written in FORTRAN IV G1 language (FORTGCLG) compatible with the IBM system 3081 having 24 million bytes of main storage. The plots are implemented on the electrostatic Versatec V80 plotter having 200 dots/inch resolution.

The generation of the random number was obtained from the

IBM scientific subroutine using the 'DSEED' of 731540.DD for double precision on the random number generator of the multiplicative congruent type. Any number generated was found not to repeat in 2^{39} generations, see Turner [30] for details.

The computer time has been large, though not as large as other cases where Monte Carlo have just been utilized. Table A.1 shows the computer time (CPU) for the dilatational case for the three locations of the transducer and the surface case for some locations of the transducer.

Table A.1. Computer Time (CPU)

Type of Force	Location/ Receiver	No. of Trials	Max. No./ Reflections	CPU Time
Dilatational	2	100,000	18	2 min, 30.92 sec
		300,000	18	29 min, 38.98 sec
		500,000	18	77 min, 39.22 sec
	5	100,000	18	2 min, 28.30 sec
		300,000	18	9 min, 36.41 sec
		500,000	18	19 min, 51.32 sec
	10	100,000	18	2 min, 26.51 sec
		300,000	18	7 min, 5.71 sec
		500,000	18	11 min, 53.39 sec
Surface force	2	300,000	18	6 min, 14.91 sec
(Force &	4	300,000	18	4 min, 56.90 sec
Receiver on Opposite Sides)	6	300,000	18	4 min, 21.61 sec
	4	10,000	18	10.72 sec
		100,000	18	1 min, 22.40 sec
		300,000	18	4 min, 56.90 sec

The number of the trials required in using the Monte Carlo technique to solve a problem cannot be easily determined. Although it is a well-known fact that where the conventional techqniues are very difficult to apply or cannot be applied to solve a problem as in this case, the use of Monte Carlo is unquestionable, see Buslenko [26]. In this investigation, the number of trials is dictated by the appearance of all the necessary waveforms and the stability of their amplitudes.

A list of the symbols used for the dilatational case is as follows:

ISUMT1 - number of hits

TIME1(ISUMT1) - time of arrival (normalized)

M - number of reflections minus one

VCDAT1(ISUMT1) - vertical component of displacement recorded

HCDAT1(ISUMT1) - horizontal component of displacement recorded

R1(M), R2(M-1) - two consecutive radial distances

AY - horizontal distance of the receiver from the z-axis

YTB1,YTB2 - limit of $\pm$ 1 mm determining the base of the transducer

ZT,YT - coordinates of the transudcer

NL - number of trials (emissions)

NT - maximum number of reflections

CL,CT - speeds of the P- and SV-waves, respectively

TMAX - maximum time of ending the calculation

IBA - a number which makes a ray-path history unique, Eq. (3.1)

GAM1,TET - incident angles (for either P- or SV-wave)

GAML - reflected angle for P-wave

GAMT - reflected angle for SV-waves

ET - reflected angle (for either P- or SV-wave)

GCO - γ-value in Eq. (2.43)

ZI,YI - coordinates of the points of reflection starting with the source point

TIME - time a ray takes to travel between two reflection points

SUM(M) - cummulative time between reflections

N1 - number of hits

AR1(M) - variable R_1'

RC(M) - coefficients of reflection

UM,UN - direction cosines of the incident ray

VM,VN - direction cosines of the reflected ray

AKT11 - amplitude at the point of hit (location of the transducer)

ARPP - displacement contribution of the P-wave

ARPS - displacement contribution of the SV-wave

PHI - angle of emission

P1 - 3.1415927

RPHI,RPHA,RAND - random numbers generated

Z - the upper or the lower surface of the plate

RM,RN - direction cosines of the normal to the planes of the plate

AT - parameter, r_0

TET1 - incident or reflected angle for P-wave

TETT1 - reflected angle for SV-wave

TET2 - incident or reflected angle for SV-wave

TETL - reflected angle for P-wave

ENRLLI,ENRTLI - energy ratio of the reflected P-wave and SV-wave to the incident P-wave, respectively

ENRLTI,ENRTTI - energy ratio of the reflected P- and SV-waves to the incident SV-wave, respectively

ADENR - summation of the energy ratios

RPSD,RPPD,RSSD,RSPD - coefficients of reflection of P-SV, P-P, SV-P, and SV-SV waves, respectively

WFN - weighting function (taken = one in this calculation)

AH1 - distance of the imaginary source from the reflecting plane

K - ratio of the wave speeds, C_L/C_T

AK(I) - wave front curvature factor

AI(I) - radial amplitude at the receiving point

DI - time interval

X1(I) - the vertical components of displacement

Y2(I) - the horizontal components of displacement

X(I) - the arrival time

SUBROUTINE UI - subroutine for choosing the direction of emission

SUBROUTINE HITPLN - subroutine which determines the point of reflection

SUBROUTINE REFLEC - subroutine which determines the direction of the reflected ray

SUBROUTINE ERATIO - subroutine which calculates the coefficient of reflection and the energy ratio

SUBROUTINE CHOREF - subroutine which chooses the reflected ray and the reflected angles

SUBROUTINE AMPLCO - subroutine which calculates the radial amplitude at the receiving point

SUBROUTINE UTHETA - subroutine which calculates the amplitude at the initial point of reflection (for the case with the surface force)

SUBROUTINE PP - the plotting subroutine

The following pages contain the list of the programs used.

COMPUTER PROGRAM LIST FOR

DILATATIONAL CASE

```
//INCPLATE JOB ********,'   ENUMI              ',CLASS=K,TYPRUN=COPY,     JOB 2049
// REGION=2048K
/*JOBPARM P=PROC01,LINES=10,F=9002,UCS=TN,FCB=6006
// EXEC FORTGCLG,PARM.LKED='SIZE=(2048)'
//FORT.SYSIN DD *
      REAL PI,K,KAY
      DOUBLE PRECISION DSEED
      DIMENSION TIME1(30000),VCDAT1(30000),HCDAT1(30000)
      DIMENSION R1(100),AK(100),RC(100),AI(100),AR1(100),AR2(100)
      DIMENSION R2(150),AKD(150),AKN(150),SUM(150),I(150)
      DIMENSION X(1500),X1(1500),Y2(1500)
      DIMENSION GCO(100)
      INTEGER P(30000),Q(30000),PE,ARA
      COMMON/COM1/UM,UN,ZI,YI,Z,ZZ,N2,N3,L
      COMMON/COM2/AT,AH,ATET2,APP,APS,AR
      COMMON/COM3/VK,VM,TET,N1,COI,ADELR,COSIN,COSR
      COMMON/COM4/WFN,ENFITI,ENRLTI,ENRLLI,ENRILI,R,OS,CT,CL,IETI1,TETL
      COMMON/COM5/E1,GAM1,GAMI,GAML,AH1,CCA,AR1,RTPD,RPSD,RSSD,
     1RSPD,RCC
      COMMON/COM6/R1,AK,RC,AI,AR2,I
      COMMON/COM7/DSEED
      COMMON/COM8/X1,Y2,P
      COMMON/COM9/TIME1,TIME2,VCDAT1,HCDAT1,VCDAT2,HCDAT2
      COMMON/COM10/MMM,TAT,BAT,TII,KAY,ZDIR,ARA
      COMMON/COM11/GCO
      CALL CPUTIM
      DSEED=731549.D0
      CL=5.1
CC AY=HORIZONTAL DISTANCE OF TRANSDUCERS FROM POINT OF ORIGIN
      AY=300.
      YTB1=AY-1.
      YTB2=AY+1.
      YT=AY
      ZT=15.
      YTB3=ZT-1.
```

```
      ISUM11=0
      JJ=0.
      NT=18
      DO300L=1,500000
      DO1IJK=1,NT
      R1(IJK)=0.
      AR1(IJK)=0.
    1 CONTINUE
      AH1=0.
      YI=0.
      ZI=0.
      SUM(1)=0.
      IBA=0
      CT=3.05
      TMAX=8.*2.*ZT/CT
      CS=CL
      CALL UI
      IF(MMM.EQ.1)GOTO300
      DO400M=1,NT
      IF(CS.EQ.CL)GOTO26
      N=1
      PE=N*(2**M)
      GOTO27
   26 N=0
      PE=M*(2**20)
   27 IBA=IBA+PE
      IF(M.EQ.1)GOTO221
      GOTO122
  221 ET=TET
      GAM1=0.
      IF(UN.EQ.0.)GOTO300
  122 CONTINUE
      GN1=YI
      CALL HITPLN
      IF(UN.LT.0)GOTO10
      IF(YI.GE.YTB1.AND.YI.LE.YTB2)GOTO126
```

```
 10 IF(YI.GT.YTB2)GOTO300
126 R1(M)=AT
    TIME=R1(M)/CS
    IF(M.EQ.1)GOTO251
     SUM(M)= SUM(M-1)+TIME
    GD=YI
    GCO(M)=GN1/GD
    GOTO253
251 CONTINUE
    SUM(M)=TIME
253 CONTINUE
    IF(SUM(M).GE.TMAX)GOTO300
    IF(UN.LT.0)GOTO233
    IF(YI.GE.YTB1.AND.YI.LE.YTB2)GOTO234
    GOTO233
234 ISUMT1=ISUMT1+1
    P(ISUMT1)=IBA
    BAT=1.
    TIME1(ISUMT1)=SUM(M)*CI/(2.*ZT)
    NN=M
    N1=NN
    GOTO235
233 BAT=0.
235 CALL ERATIO
    CALL CHOREF
    I(M)=TAT
    RC(M)=RCC
    AR1(M)=AR
263 CONTINUE
    IF(UN.LT.0)GOTO264
    IF(YI.GE.YTB1.AND.YI.LE.YTB2)GOTO600
264 CONTINUE
    CALL REFLEC
    IF(VN.LT.0.)GOTO29
    UM=SIN(ET)
    UN=COS(ET)
```

```
      GOTO311
   29 ER=ARCOS(VN)
      ETER=(TET-ET)+ER
      UM=SIN(ETER)
      UN=COS(ETER)
  311 TET=ET
      IF( SUM(M).GT.TMAX) GOTO300
  400 CONTINUE
      GOTO300
  600 CONTINUE
CC CALCULATION OF AMPLITUDE COEF.,AK
      IF(N1.EQ.1) GOTO4
      CALL AMPLCO
      AKT11=AI(N1)
      ARPP=APP*AKT11
      ARPS=APS*AKT11
      GOTO7
    4 AKT11=1./R1(1)
      ARPP=APP*AKT11
      ARPS=APS*AKT11
    7 CONTINUE
      IF(CS.EQ.CT) GOTO8
      HCDAT1(ISUMT1)=AKT11*SIN(GAM1)+ARPP*SIN(GAML)+ARPS*COS(GAMT)
      VCDAT1(ISUMT1)=AKT11*COS(GAM1)-ARPP*COS(GAML)+ARPS*SIN(GAMT)
      GOTO300
    8 HCDAT1(ISUMT1)=-AKT11*COS(GAM1)+ARPP*SIN(GAML)+ARPS*COS(GAMT)
      VCDAT1(ISUMT1)=+AKT11*SIN(GAM1)-ARPP*COS(GAML)+ARPS*SIN(GAMT)
  300 CONTINUE
      N2=JJ
      N3=ISUMT1
      WRITE(6,9000) ISUMT1
 9000 FORMAT(4X,I10)
      CALL PP
      STOP
      END
      SUBROUTINE  UI
```

```
CC UI CALCULATES DIRECTION COSINE OF INCIDENT RAY
CC UM,UN ¬DIRECTION COSINES
      REALPI,PHI
      DOUBLE PRECISION DSEED
      DIMENSION R1(100),AK(100),RC(100),AI(100),AR1(100),AR2(100)
      DIMENSION R2(150),AKD(150),AKN(150),SUM(150),T(150)
      INTEGER P(30000),Q(30000),PE,ARA
      COMMON/COM1/UM,UN,ZI,YI,Z,Z2,N2,N3,L
      COMMON/COM2/AT,AH,ATET2,APP,APS,AR
      COMMON/COM3/VN,VM,TET,N1,COI,ADENR,COSIN,COSR
      COMMON/COM4/WPN,ENRTII,ENRLTI,ENRLLI,ENRTLI,K,CS,CI,CL,TETT1,TETL
      COMMON/COM5/ET,GAM1,GAMT,GAML,AH1,CCA,AR1,RPPD,RPSD,RSSD,
     1RSPD,RCC
      COMMON/COM6/R1,AK,RC,AI,AR2,T
      COMMON/COM7/DSEED
      COMMON/COM10/MMM,TAT,BAT,TIT,KAY,ZDIR,ARA
      PI=3.1415927
  141 RPHI=GGUBFS(DSEED)
      IF(RPHI.GT.0 .AND. RPHI.LT.1.)GOTO271
      MMM=1
      GOTO142
  271 CONTINUE
      MMM=0
      PHI=PI*RPHI
      IF(PHI.GT.PI/2.)GOTO143
      TET=PHI
      GOTO144
  143 TET=PI-PHI
  144 CONTINUE
      UN=COS(PHI)
      UM=SIN(PHI)
  142 CONTINUE
      RETURN
      END
      SUBROUTINE HITPLN
CC AT¬PARAMETER=DISTANCE FROM ORIGIN OFFIRST PIERCE POINT TOTHE NEXT
```

```
      DIMENSION R1(100),AK(100),RC(100),AI(100),AR1(100),AR2(100)
      DIMENSION R2(150),AKD(150),AKN(150),SUM(150),T(150)
      DOUBLE PRECISION DSEED
      COMMON/COM1/UM,UN,ZI,YI,Z,Z2,N2,N3,L
      COMMON/COM2/AT,AH,ATET2,APP,APS,AK
      COMMON/COM3/VN,VM,TET,N1,COI,ADENR,COSIN,COSR
      COMMON/COM4/WPN,ENRTI,ENRLTI,ENRLLI,ENRTLI,K,CS,CI,CL,IETT1,IETL
      COMMON/COM5/ET,GAM1,GAMT,GAML,AH1,CCA,AR1,RPPD,RPSD,RSSD,
     1RSPD,RCC
      COMMON/COM6/R1,AK,RC,AI,AR2,I
      COMMON/COM7/DSEED
      COMMON/COM10/MMM,TAT,BAT,TIT,KAY,ZDIR,ARA
      AH=15.
      IF(UN)7,11,9
    7 Z=-AH
      ZDIR=1.
      GOTO10
    9 Z=AH
      ZDIR=0.
   10 AT=(Z-ZI)/UN
      ZI=ZI+UN*AT
      YI=YI+UM*AT
   11 CONTINUE
      RETURN
      END
      SUBROUTINE REFLEC
CC CALCULATION OF REFLECTED RAY, VI
      REALPI,PHI
      DIMENSION R1(100),AK(100),RC(100),AI(100),AR1(100),AR2(100)
      DIMENSION R2(150),AKD(150),AKN(150),SUM(150),T(150)
      DOUBLE PRECISION DSEED
      COMMON/COM1/UM,UN,ZI,YI,Z,Z2,N2,N3,L
       COMMON/COM2/AT,AH,ATET2,APP,APS,AK
      COMMON/COM3/VN,VM,TET,N1,COI,ADENR,COSIN,COSR
      COMMON/COM4/WPN,ENRTI,ENRLTI,ENRLLI,ENRTLI,K,CS,CI,CL,IETT1,IETL
      COMMON/COM5/ET,GAM1,GAMT,GAML,AH1,CCA,AR1,RPPD,RPSD,RSSD,
     1RSPD,RCC
```

```
      COMMON/COM6/R1,AK,RC,AI,AR2,T
      COMMON/COM7/DSEED
      COMMON/COM10/MMM,TAT,BAT,TIT,KAY,ZDIR,ARA
      IF(Z.EQ.AH)GOTO281
      RM=0
      RN=1.
      GOTO283
  281 CONTINUE
      RM=0.
      RN=-1.
  283 CONTINUE
      VM=-UM*RM*RM+UM
      VN=-UN*RN*RN
      RETURN
      END
      SUBROUTINE ESATIO
CC CALCULATION OF THE ENERGY RATIOS
      DIMENSION R1(100),AK(100),RC(100),AI(100),AR1(100),AR2(100)
      DIMENSION R2(150),AKD(150),AKN(150),SUM(150),T(150)
      DOUBLE PRECISION DSEED
      REAL PI,K,KAY
      COMMON/COM1/UM,UN,Z1,YI,Z,Z2,N2,N3,L
      COMMON/COM2/AI,AH,ATET2,APP,APS,AR
      COMMON/COM3/VN,VM,TET,N1,COI,ADENR,COSIN,COSn
      COMMON/COM4/WFN,ENRTI,ENRLI,ENRLLI,ENRTLI,K,CS,CT,CL,TETT1,TETL
      COMMON/COM5/ET,GAM1,GAMI,GAML,AH1,CCA,AR1,RPPD,RPSD,RSSD,
     1RSPD,RCC
      COMMON/COM6/R1,AK,RC,AI,AR2,T
      COMMON/COM7/DSEED
      COMMON/COM10/MMM,TAT,BAT,TIT,KAY,ZDIR,ARA
      K=CL/CT
      IF(CS.EQ.CT)GOTO110
CC    CALCULATE ENERGY RATIOS TO LONGITUDINAL INCIDENCE
      TET1=TET
      CCA=0.
```

```
      ATET1=SIN(TET1)
      TETT=ATET1/K
      TETT1=ARSIN(TETT)
      COSR=COS(TETT1)
      COSIN=COS(TET1)
      UMSQ=ATET1*ATET1
      AUMSQ=(ATET1/K)**2
      ACC=1.-2.*AUMSQ
      AC1=1.-AUMSQ
      ACCT=(4.*UMSQ*COSIN)/(K*K*K)
      RPS=+(4.*ATET1*COSIN*ACC)/K
      RPP=-(ACC*ACC-ACCT*SQRT(AC1))
      DELTA=ACC*ACC+ACCT*SQRT(AC1)
      RPSD=RPS/DELTA
      RPPD=RPP/DELTA
      ENRTLI=COSR*RPSD*RPSD/(K*COSIN)
      ENRLLI=RPPD*RPPD
      ADENR=ENRTLI+ENRLLI
      GOTO111
  110 TET2=TET
      ATET2=SIN(TET2)
      CCA=ATET2*K
      IF(CCA .GT. 1.)GOTO291
      TETL=ARSIN(CCA)
      COSIN=COS(TET2)
      COSR=COS(TETL)
      UMSQ=ATET2*ATET2
      AUMSQS=(1.-CCA**2)/(K*K)
      ACCS=1.-2.*UMSQ
      RSP=-(4.*ATET2*COSIN*ACCS/K)
      RSS=-(ACCS*ACCS-4.*UMSQ*COSIN*SQRT(AUMSQS))
      DELTAS=ACCS*ACCS+4.*UMSQ*COSIN*SQRT(AUMSQS)
      RSPD=RSP/DELTAS
      RSSD=RSS/DELTAS
      ENRTTI=RSSD*RSSD
      ENRLTI=RSPD*RSPD*COSR*K/COSIN
```

```
      ADENR=ENRLTI+ENRTTI
      GOTO111
  291 CONTINUE
      ENRTTI=1.
      ENRLTI=0.
      RSSD=1.
      RSPD=0.
  111 CONTINUE
      RETURN
      END
      SUBROUTINE CHOREF
CC CHOREF CHOOSES DIRECTION OF REFLECTED RAY
      DIMENSION R1(100),AK(100),RC(100),AI(100),AR1(100),AR2(100)
      DIMENSION R2(150),AKD(150),AKN(150),SUM(150),T(150)
      REAL PI,K,KAY
      DOUBLE PRECISION DSEED
      COMMON/COM1/UM,UN,ZI,YI,Z,Z2,N2,N3,L
       COMMON/COM2/AT,AH,ATET2,APP,APS,AR
      COMMON/COM3/VN,VM,TET,N1,COI,ADENR,COSIN,COSR
      COMMON/COM4/WFN,ENRTTI,ENRLTI,ENRLLI,ENRTLI,K,CS,CT,CL,TETT1,TETL
      COMMON/COM5/ET,GAM1,GAMT,GAML,AH1,CCA,AR1,RPPD,RPSD,RSSD,
     1RSPD,RCC
      COMMON/COM6/R1,AK,RC,AI,AR2,T
      COMMON/COM7/DSEED
      COMMON/COM10/MMM,TAT,BAT,TIT,KAY,ZDIF,ARA
      PI=3.1415927
      RAND=GGUBFS(DSEED)
      COET=COS(ET)
      COCUBR=COET*COET*COET
      COSQRI=COS(GAM1)*COS(GAM1)*COS(GAM1)
      AH1N=COCUBR*SIN(GAM1)
      AH1D=COSQRI*SIN(ET)
      IF(AH1D.EQ.0.)GOTO113
      AH1=AH1N*(AH1+ABS(ZI))/AH1D
      AR=AH1/COET
      GOTO118
```

```
113 AR=0.
118 CONTINUE
    IF(CS.EQ.CT)GOTO 114
    BETA=ENRLLI
    BET=1./BETA
    IF((1.-BETA).LT.0.00001)GOTO222
    BETT=1./(1.-BEIA)
    IF(BAT.EQ.1.)GOTO224
    IF(RAND.LE.BETA)GOTO222
    IAT=1.
    WFN=BETI
    CS=CT
    KAY=K
    RCC=RPSD
    ET=TETI1
    IF(ZDIR.EQ.0.)GOTO224
     RCC=-RCC
    GOTO224
222 CONTINUE
    TAI=0.
    WFN=BEI
    CS=CL
    RCC=RPPD
    ET=TET
224 CONTINUE
    GAM1=TET
    GAMI=TETI1
    GAML=TET
    APP=RPPD
    APS=RPSD
    GOTO120
114 ALFA=ENRTTI
    ALF=1./ALFA
    IF(ALFA.EQ.1.)GOTO232
    ALFL=1./(1.-ALFA)
    GOTO234
```

```
232 CONTINUE
    ALFL=0.
    API=PI*.5
    TETL=API
234 CONTINUE
    IF(BAT.EQ.1.)GOTO244
    IF(RAND.LE.ALFA)GOTO242
    TAT=1.
    KAY=1./K
    WFN=ALFL
    CS=CL
    RCC=RSPD
    ET=TETL
    IF(ZDIR.EQ.0.)GOTO244
    RCC=-RCC
    GOTO244
242 CONTINUE
    TAT=0.
    WFN=ALF
    CS=CT
    RCC=RSSD
    ET=TET
244 CONTINUE
    GAM1=TET
    GAML=TETL
    GAMT=TET
    APP=RSPD
    APS=RSSD
120 CONTINUE
    IF(CCA.GT.1.)GOTO252
    GOTO129
252 CONTINUE
    CCT=CT/AIET2
    CT=CCT
129 CONTINUE
    RETURN
```

```
      END
      SUBROUTINE AMPLCO
      DIMENSION R1(100),AK(100),RC(100),AI(100),AR1(100),AR2(100)
      DIMENSION R2(150),AKD(150),AKN(150),SUM(150),T(150)
      DIMENSION GCO(100)
      DOUBLE PRECISION DSEED
      COMMON/COM1/UM,UN,ZI,YI,Z,Z2,N2,N3,L
      COMMON/COM2/AT,AH,ATEI2,APP,APS,AR
      COMMON/COM3/VN,VM,TET,N1,COI,ADENR,COSIN,COSR
      COMMON/COM4/WFN,ENRTTI,ENRLTI,ENRLLI,ENRTLI,K,CS,CI,CL,TETI1,TETL
      COMMON/COM5/ET,GAM1,GAMT,GAML,AH1,CCA,AR1,RPPD,RPSD,RSSD,
     1RSPD,RCC
      COMMON/COM6/R1,AK,RC,AI,AR2,T
      COMMON/COM7/DSEED
      COMMON/COM10/MMM,TAT,BAT,TIT,KAY,ZDIR,ARA
      COMMON/COM11/GCO
      NIT=N1-1
      DO551IK=1,NIT
      R2(IK)=R1(IK+1)
551   CONTINUE
      DO555I=1,N1
      IF(I.EQ.1)GOTO262
      AR2(I)=AR1(I)+R2(I-1)
      ARR=AR1(I)/AR2(I)
      AK(I)=ARR*GCO(I)
      AI(I)=SQRT(AK(I))*AI(I-1)*RC(I-1)
      GOTO555
262   CONTINUE
      AI(1)=1./R1(I)
555   CONTINUE
      RETURN
      END
      SUBROUTINE  PE
      DIMENSION TIME1(30000),VCDAT1(30000),HCDAT1(30000)
      DIMENSION X(1500),X1(1500),Y2(1500)
      INTEGER P(30000),Q(30000),PE,ARA
```

```
      DOUBLE PRECISION DSEED
      COMMON/COM1/UM,UN,ZI,Y1,Z,Z2,N2,N3,L
      COMMON/COM2/AT,AH,ATET2,APP,APS,AR
      COMMON/COM3/VN,VM,TET,N1,COI,ADENR,COSIN,COSE
      COMMON/COM4/WFN,ENRTTI,ENRLII,ENELLI,ENRTLI,K,CS,CT,CL,TETT1,TETL
      COMMON/COM7/DSEED
      COMMON/COM8/X1,Y2,P
      COMMON/COM9/TIME1,TIME2,VCDAT1,HCDAT1,VCDAT2,HCDAT2
      N=840
      N=850
      DO10I=1,N
      X1(I)=0.
      Y2(I)=0.
   10 CONTINUE
      DI=.01
      IW=20
      KJ=0
      DO15I=1,N3
      Q(I)=P(I)
   15 CONTINUE
      DO41K=1,N3
      DO40J=1,N3
      IF(P(K).EQ.Q(J))GOTO44
      GOTO40
   44 IF(K.EQ.J)GOTO42
      Q(J)=0.
      GOTO40
   42 Q(K)=0.
      KJ=KJ+1
      TIME1(KJ)=TIME1(K)
      VCDAT1(KJ)=VCDAT1(K)
      HCDAT1(KJ)=HCDAT1(K)
   40 CONTINUE
   41 CONTINUE
      DO100K=1,KJ
      II=INT(TIME1(K)/DI)
```

```
      DO100I=1,20
      IF(I.LE.10)GOTO11
      W=(IW-I)/10.
      GOTO13
   11 W=I/10.
   13 JJ=I+II
      X1(JJ)=VCDAT1(K)*W+X1(JJ)
      Y2(JJ)=HCDAT1(K)*W+Y2(JJ)
  100 CONTINUE
      I=0
      DO200K=100,N
      I=I+1
      X(I)=K*.01
      X1(I)=X1(K)
      Y2(I)=Y2(K)
      WRITE(6,27)X(I),X1(I),Y2(I)
   27 FORMAT(4X,3F15.6)
  200 CONTINUE
      N4=I
      F=36./40.
      CALL PLOT(0.0,2.0,-3)
      CALL FACTOR(F)
      X(N4+1)=1.
      X(N4+2)=1.
      X1(N4+1)=-.0024
      X1(N4+2)=.0008
      Y2(N4+1)=-.002
      Y2(N4+2)=.002
      CALL AXIS(0.,0.,'TIME OF HITS',-12,7.,0.,X(N4+1),X(N4+2))
      CALL AXIS(0.,0.,'VERT. COMP. OF DISP. TRANS.#2',29,5.,90.,
     5X1(N4+1),X1(N4+2))
      CALL LINE(X,X1,N4,1,0,0)
      CALL PLOT(12.,0.,-3)
      CALL AXIS(0.,0.,'TIME OF HITS',-12,7.,0.,X(N4+1),X(N4+2))
      CALL AXIS(0.,0.,'HORZ. COMP. OF DISP. TRANS.#2',29,5.,90.,
     6Y2(N4+1),Y2(N4+2))
```

```
      CALL LINE(X,Y2,N4,1,0,0)
      CALL PLOT(6.,-3.,999)
      RETURN
      DEBUG SUBCHK
      END

------ JES2 JOB STATISTICS ------

       508 CARDS READ

         0 SYSOUT PRINT RECORDS

         0 SYSOUT PUNCH RECORDS

      0.00 MINUTES EXECUTION TIME
```

COMPUTER PROGRAM LIST FOR

SURFACE LOAD

```
//INCPLATE JOB ########,'   ENUMI              ',CLASS=N,TYPRUN=COPY,     JOB 2652
// REGION=2048K
/*JOBPARM P=PROC01,LINES=10,F=9002,UCS=TN,FCB=6Ooc
// EXEC FORTGCLG,PARM.LKED='SIZE=(2048)',PARM.GO='DEVICE=PLOTV80'
//FORT.SYSIN DD *
      REAL PI,K,KAY
      DOUBLE PRECISION DSEED
      DIMENSION TIME1(30000),VCDAT1(30000),HCDAT1(30000)
      DIMENSION R1(100),AK(100),RC(100),AI(100),AR1(100),AR2(100)
      DIMENSION R2(150),AKD(150),AKN(150),SUM(150),I(150)
      DIMENSION X(2240),X1(2240),Y2(2240)
      DIMENSION GCO(100)
      INTEGER P(30000),Q(30000),PE,ARA
      COMMON/COM1/UM,UN,ZI,YI,Z,Z2,N2,N3,L
      COMMON/COM2/AT,AH,ATET2,APP,APS,AR
      COMMON/COM3/VN,VM,TET,N1,COI,ADENR,COSIN,COSR
      COMMON/COM4/WFR,ENRTTI,ENRLII,ENRLLI,ENRTLI,K,CS,CT,CL,TETT1,TETL
      COMMON/COM5/ET,GAM1,GAMT,GAML,AM1,CCA,AR1,RPPD,RPSD,RSSD,
     1RSPD,RCC
      COMMON/COM6/R1,AK,RC,AI,AR2,I
      COMMON/COM7/DSEED
      COMMON/COM8/X1,Y2,P
      COMMON/COM9/TIME1,TIME2,VCDAT1,HCDAT1,VCDAT2,HCDAT2
      COMMON/COM10/MMM,TAT,BAT,TIT,KAY,ZDIR,ARA,ICS
      COMMON/COM11/GCO
      COMMON/COM12/TETTA
      CALL CPUTIM
      DSEED=731549.DO
      CL=5.1
CC AY-HORIZONTAL DISTANCE OF TRANSDUCERS FROM POINT OF ORIGIN
      AY=120.
      YTB1=AY-1.
      YTB2=AY+1.
```

```
      YT=AY
      ZI=15.
      ZIT=-ZI
      YIB3=ZT-1.
      ISUMI1=0
      JJ=0.
      NT=18
      NL=500000
      DO300L=1,NL
      YI=0.
      ZI=15.
      DO1IJK=1,NI
      R1(IJK)=0.
      AR1(IJK)=0.
    1 CONTINUE
      AR1=0.
      SUM(1)=0.
      IBA=0
      CT=3.05
      TMAX=12.*2.*ZT/CL
      CALL UI
      IF(MMM.EQ.1)GOTO300
      DO400M=1,NI
      IF(CS.EQ.CL)GOTO26
      N=1
      PE=N*(2**M)
      GOTO27
   26 N=0
      PE=M*(2**20)
   27 IBA=IBA+PE
      IF(M.EQ.1)GOTO221
      GOTO122
  221 ET=TET
      TETTA=TET
      GAM1=0.
  122 CONTINUE
      GN1=YI
```

```
      CALL HITPLN
      IF(YI.GE.YTB1.AND.YI.LE.YTB2)GOTO126
   10 IF(YI.GT.YTB2)GOTO300
  126 R1(M)=AT
      TIME=R1(M)/CS
      IF(M.EQ.1)GOTO251
       SUM(M)= SUM(M-1)+TIME
      GD=YI
      GCO(M)=GN1/GD
      GOTO253
  251 CONTINUE
      SUM(M)=TIME
  253 CONTINUE
      IF(SUM(M).GE.TMAX)GOTO300
      IF(YI.GE.YTB1.AND.YI.LE.YTB2)GOTO236
      GOTO233
  236 IF(ABS(ZI-ZII).LE..01)GOTO234
      GOTO233
  234 ISUMT1=ISUMT1+1
      P(ISUMT1)=IBA
      BAT=1.
      TIME1(ISUMT1)=SUM(M)*CL/(2.*ZT)
      NN=M
      N1=NN
      GOTO235
  233 BAT=0.
  235 CALL ERATIO
      CALL CHOREF
      T(M)=TAT
      RC(M)=RCC
      AR1(M)=AR
  263 CONTINUE
      IF(UN.EQ.0.)GOTO300
      IF(UN.GT.0.)GOTO264
      IF(YI.GE.YTB1.AND.YI.LE.YTB2)GOTO600
  264 CONTINUE
```

```
      CALL REFLEC
      IF(VN.LT.0.)GOTO29
      UM=SIN(ET)
      UN=COS(ET)
      GOTO311
   29 ER=ARCOS(VN)
      ETER=(TET-ET)+ER
      UM=SIN(ETER)
      UN=COS(ETER)
  311 TET=ET
      IF( SUM(M).GT.TMAX)GOTO300
  400 CONTINUE
      GOTO300
  600 CONTINUE
CC CALCULATION OF AMPLITUDE COEF.,AK
      CALL UTHETA
      IF(AI(1).EQ.0.)GOTO300
      IF(N1.EQ.1)GOTO4
      CALL AMPLCO
    4 AKT11=AI(N1)
      ARPP=APP*AKT11
      ARPS=APS*AKT11
      IF(CS.EQ.CT)GOTO8
      HCDAT1(ISUMT1)=AKT11*SIN(GAM1)+ARPP*SIN(GAML)-ARPS*COS(GAMI)
      VCDAT1(ISUMT1)=-AKT11*COS(GAM1)+ARPP*COS(GAML)+ARPS*SIN(GAMI)
      GOTO300
    8 HCDAT1(ISUMT1)=+AKT11*COS(GAM1)+ARPP*SIN(GAML)-ARPS*COS(GAMI)
      VCDAT1(ISUMT1)=+AKT11*SIN(GAM1)+ARPP*COS(GAML)+ARPS*SIN(GAMI)
  300 CONTINUE
      N2=JJ
      N3=ISUMT1
      WRITE(6,9000)ISUMI1
 9000 FORMAT(4X,I10)
      CALL PP
      STOP
      DEBUG SUBCHK
```

```
      END
      SUBROUTINE  UI
CC UI CALCULATES DIRECTION COSINE OF INCIDENT RAY
CC UM,UN -DIRECTION COSINES
      REALPI,PHI
      DOUBLE PRECISION DSEED
      DIMENSION R1(100),AK(100),RC(100),AI(100),AR1(100),AR2(100)
      DIMENSION R2(150),AKD(150),AKN(150),SUM(150),T(150)
      INTEGER P(30000),Q(30000),PE,ARA
      COMMON/COM1/UM,UN,Z1,YI,Z,Z2,N2,N3,L
      COMMON/COM2/AT,AH,AIET2,APP,APS,AR
      COMMON/COM3/VN,VM,TET,N1,CO1,ADENR,COSIN,COSR
      COMMON/COM4/WPN,ENRTTI,ENRLTI,ENRLLI,ENRTLI,K,CS,CT,CL,TETI1,TETL
      COMMON/COM5/ET,GAM1,GAMI,GAML,AH1,CCA,AR1,RPPD,RPSD,RSSD,
     1RSPD,RCC
      COMMON/COM6/R1,AK,RC,AI,AR2,T
      COMMON/COM7/DSEED
      COMMON/COM10/MMM,IAI,BAT,TIT,KAY,ZDIR,ARA,ICS
      PI=3.1415927
  141 RPHI=GGUBFS(DSEED)
      IF(RPHI.GT.0 .AND. RPHI.LE.1.)GOTO271
      MMM=1
      GOTO142
  271 CONTINUE
      PHI=PI*RPHI
      IF(PHI.GT.PI/2.)GOTO143
      MMM=1
      GOTO142
  143 TET=PI-PHI
      MMM=0
      UN=COS(PHI)
      UM=SIN(PHI)
      RPHA=GGUBFS(DSEED)
      IF(RPHA.LE..5)GOTO144
      CS=C1
      ICS=0
```

```
      GOTO142
  144 CS=CL
      ICS=1
  142 CONTINUE
      RETURN
      DEBUG SUBCHK
      END
      SUBROUTINE HITPLN
CC AT=PARAMETER=DISTANCE FROM ORIGIN OFFIRST PIERCE POINT TOTHE NEAT
      DIMENSION R1(100),AK(100),RC(100),AI(100),AR1(100),AR2(100)
      DIMENSION R2(150),AKD(150),AKN(150),SUM(150),T(150)
      DOUBLE PRECISION DSEED
      COMMON/COM1/UM,UN,ZI,YI,Z,ZZ,N2,N3,L
      COMMON/COM2/AT,AH,ATET2,APP,APS,AR
      COMMON/COM3/VN,VM,TET,N1,COI,ADENR,COSIN,COSR
      COMMON/COM4/WFN,ENRITI,ENRLTI,ENRLLI,ENRILI,K,CS,CI,CL,TETT1,TETL
      COMMON/COM5/ET,GAM1,GAMI,GAML,AH1,CCA,AR1,RPPD,RPSD,RSSD,
     1RSPD,RCC
      COMMON/COM6/R1,AK,RC,AI,AR2,T
      COMMON/COM7/DSEED
      COMMON/COM10/MMM,TAT,BAT,TIT,KAY,ZDIR,ARA,ICS
      AH=15.
      IF(UN)7,11,9
    7 Z=-AH
      ZDIR=1.
      GOTO10
    9 Z=AH
      ZDIR=0.
   10 AT=(Z-ZI)/UN
      ZI=ZI+UN*AT
      YI=YI+UM*AT
   11 CONTINUE
      RETURN
      DEBUG SUBCHK
      END
      SUBROUTINE REFLEC
```

```
CC CALCULATION OF REFLECTED RAY, VI
      REALPI,PHI
      DIMENSION R1(100),AK(100),RC(100),AI(100),AR1(100),AR2(100)
      DIMENSION R2(150),AKD(150),AKN(150),SUM(150),I(150)
      DOUBLE PRECISION DSEED
      COMMON/COM1/UM,UN,ZI,YI,Z,Z2,N2,N3,L
       COMMON/COM2/AT,AH,AIET2,APP,APS,AR
      COMMON/COM3/VN,VM,TET,N1,COI,ADENR,COSIN,COSR
      COMMON/COM4/WFN,ENRIII,ENRLTI,ENRLLI,ENRTLI,K,CS,CT,CL,TETT1,TETL
      COMMON/COM5/ET,GAM1,GAMT,GAML,AH1,CCA,AR1,RPPD,RPSD,RSSD,
     1RSPD,RCC
      COMMON/COM6/R1,AK,RC,AI,AR2,I
      COMMON/COM7/DSEED
      COMMON/COM10/MMM,TAT,BAT,III,KAY,ZDIR,ARA,ICS
      IF(Z.EQ.AH) GOTO281
      RM=0
      RN=1.
      GOTO283
  281 CONTINUE
      RM=0.
      RN=-1.
  283 CONTINUE
      VM=-UM*RM*RM+UM
      VN=-UN*RN*RN
      RETURN
      DEBUG SUBCHK
      END
      SUBROUTINE ERATIO
CC CALCULATION OF THE ENERGY RATIOS
      DIMENSION R1(100),AK(100),RC(100),AI(100),AR1(100),AR2(100)
      DIMENSION R2(150),AKD(150),AKN(150),SUM(150),I(150)
      DOUBLE PRECISION DSEED
      REAL PI,K,KAY
      COMMON/COM1/UM,UN,ZI,YI,Z,Z2,N2,N3,L
       COMMON/COM2/AI,AH,AIET2,APP,APS,AR
      COMMON/COM3/VN,VM,TET,N1,COI,ADENR,COSIN,COSR
```

```
      COMMON/COM4/WFN,ENRTTI,ENRLT1,ENRLLI,ENRTLI,K,CS,CT,CL,TET1,TETL
      COMMON/COM5/ET,GAM1,GAMT,GAML,AH1,CCA,AR1,RPPD,RPSD,RSSD,
     1RSPD,RCC
      COMMON/COM6/R1,AR,RC,AI,AR2,I
      COMMON/COM7/DSEED
      COMMON/COM10/HMM,IAI,BAT,TIT,KAY,ZDIR,ARA,ICS
      K=CL/CT
      IF(CS.EQ.CT)GOTO110
CC    CALCULATE ENERGY RATIOS TO LONGITUDINAL INCIDENCE
      TET1=TET
      CCA=0.
      ATET1=SIN(TET1)
      TETT=ATET1/K
      TETT1=ARSIN(TETT)
      COSR=COS(TETT1)
      COSIN=COS(TET1)
      UMSQ=ATET1*ATET1
      AUMSQ=(ATET1/K)**2
      ACC=1.-2.*AUMSQ
      AC1=1.-AUMSQ
      ACCT=(4.*UMSQ*COSIN)/(K*K*K)
      RPS=+(4.*ATET1*COSIN*ACC)/K
      RPP=-(ACC*ACC-ACCT*SQRT(AC1))
      DELTA=ACC*ACC+ACCT*SQRT(AC1)
      RPSD=RPS/DELTA
      RPPD=RPP/DELTA
      ENRTLI=COSR*RPSD*RPSD/(K*COSIN)
      ENRLLI=RPPD*RPPD
      ADENR=ENRTLI+ENRLLI
      GOTO111
  110 TET2=TET
      ATET2=SIN(TET2)
      CCA=ATET2*K
      IF(CCA .GT. 1.)GOTO291
      TETL=ARSIN(CCA)
      COSIN=COS(TET2)
```

```
      COSR=COS(TETL)
      UMSQ=ATET2*ATET2
      AUMSQS=(1.-CCA**2)/(K*K)
      ACCS=1.-2.*UMSQ
      RSP=-(4.*ATET2*COSIN*ACCS/K)
      RSS=-(ACCS*ACCS-4.*UMSQ*COSIN*SQRT(AUMSQS))
      DELTAS=ACCS*ACCS+4.*UMSQ*COSIN*SQRT(AUMSQS)
      RSPD=RSP/DELTAS
      RSSD=RSS/DELTAS
      ENRTTI=RSSD*RSSD
      ENRLTI=RSPD*RSPD*COSR*K/COSIN
      ADENR=ENRLTI+ENRTTI
      GOTO111
  291 CONTINUE
      ENRTTI=1.
      ENRLTI=0.
      RSSD=1.
      RSPD=0.
  111 CONTINUE
      RETURN
      DEBUG SUBCHK
      END
      SUBROUTINE CHOREF
CC CHOREF CHOOSES DIRECTION OF REFLECTED RAY
      DIMENSION R1(100),AK(100),RC(100),AI(100),AR1(100),AR2(100)
      DIMENSION R2(150),AKD(150),AKN(150),SUM(150),T(150)
      REAL PI,K,KAY
      DOUBLE PRECISION DSEED
      COMMON/COM1/UM,UN,ZI,Y1,Z,Z2,N2,N3,L
       COMMON/COM2/AI,AH,ATET2,APP,APS,AR
      COMMON/COM3/VN,VM,TET,N1,COI,ADENR,COSIN,COSR
      COMMON/COM4/WFN,ENRTTI,ENRLTI,ENRLLI,ENRTLI,K,CS,CI,CL,TETT1,TETL
      COMMON/COM5/ET,GAM1,GAMT,GAML,AH1,CCA,AR1,RPPD,RPSD,RSSD,
     1RSPD,RCC
      COMMON/COM6/R1,AK,RC,AI,AR2,T
      COMMON/COM7/DSEED
```

```
      COMMON/COM10/MMM,TAT,BAT,TIT,KAY,ZDIR,ARA,ICS
      PI=3.1415927
      RAND=GGUBFS(DSEED)
      COET=COS(ET)
      COCUBR=COET*COET*COET
      COSQRI=COS(GAM1)*COS(GAM1)*COS(GAM1)
      AH1N=COCUBR*SIN(GAM1)
      AH1D=COSQRI*SIN(ET)
      IF(AH1D.EQ.0.)GOTO113
      AH1=AH1N*(AH1+ABS(ZI))/AH1D
      AR=AH1/COET
      GOTO118
  113 AR=0.
  118 IF(CS.EQ.CT)GOTO 114
      BETA=ENRLLI
      BET=1./BETA
      IF((1.-BETA).LT.0.00001)GOTO222
      BETT=1./(1.-BETA)
      IF(BAT.EQ.1.)GOTO224
      IF(RAND.LE.BETA)GOTO222
      TAT=1.
      WFN=BETT
      CS=CT
      KAY=K
      RCC=RPSD
      ET=TETT1
      IF(ZDIR.EQ.0.)GOTO224
       RCC=-RCC
      GOTO224
  222 CONTINUE
      TAT=0.
      WFN=BET
      CS=CL
      RCC=RPPD
      ET=TET
  224 CONTINUE
```

```
      GAM1=TEI
      GAMT=TETI1
      GAML=TET
      APP=RPPD
      APS=RPSD
      GOTO120
  114 ALFA=ENRTTI
      ALF=1./ALFA
      IF(ALFA.EQ.1.)GOTO232
      ALFL=1./(1.-ALFA)
      GOTO234
  232 CONTINUE
      ALFL=0.
      API=PI*.5
      TETL=API
  234 CONTINUE
      IF(BAT.EQ.1.)GOTO244
      IF(RAND.LE.ALFA)GOTO242
      TAT=1.
      KAY=1./K
      WFN=ALFL
      CS=CL
      RCC=RSPD
      ET=TETL
      IF(ZDIR.EQ.0.)GOTO244
      RCC=-RCC
      GOTO244
  242 CONTINUE
      TAT=0.
      WFN=ALF
      CS=CT
      RCC=RSSD
      ET=TET
  244 CONTINUE
```

```
      GAM1=TET
      GAML=TETL
      GAMT=TET
      APP=RSPD
      APS=RSSD
  120 CONTINUE
      IF(CCA.GT.1.)GOTO252
      GOTO129
  252 CONTINUE
      CCI=CT/ATET2
      CT=CCI
  129 CONTINUE
      RETURN
      DEBUG SUBCHK
      END
      SUBROUTINE AMPLCO
      DIMENSION R1(100),AK(100),RC(100),AI(100),AR1(100),AR2(100)
      DIMENSION R2(150),AKD(150),AKN(150),SUM(150),T(150)
      DIMENSION GCO(100)
      DOUBLE PRECISION DSEED
      COMMON/COM1/UM,UN,ZI,YI,Z,Z2,N2,N3,L
      COMMON/COM2/AT,AH,ATET2,APP,APS,AR
      COMMON/COM3/VN,VM,TET,N1,COI,ADENR,COSIN,COSA
      COMMON/COM4/WFN,ENRTII,ENRLTI,ENRLLI,ENRTLI,K,CS,CI,CL,TETI1,TETL
      COMMON/COM5/ET,GAM1,GAMT,GAML,AH1,CCA,AR1,RPPD,RPSD,RSSD,
     1RSPD,RCC
      COMMON/COM6/R1,AK,RC,AI,AR2,T
      COMMON/COM7/DSEED
      COMMON/COM10/MMM,TAT,BAT,TIT,KAY,ZDIR,ARA,ICS
      COMMON/COM11/GCO
      NIT=N1-1
      DO551IK=1,NIT
      R2(IK)=R1(IK+1)
  551 CONTINUE
      DO555I=1,N1
      IF(I.EQ.1)GOTO555
```

```
      AR2(I)=AR1(I)+R2(I-1)
      ARR=AR1(I)/AR2(I)
      AK(I)=ARR*GCO(I)
      AI(I)=SQRT(AK(I))*AI(I-1)*RC(I-1)
  555 CONTINUE
      RETURN
      DEBUG SUBCHK
      END
      SUBROUTINE UTHETA
      REAL PI,K,K2,K3
      COMPLEX UTTA
      DOUBLE PRECISION DSEED
      DIMENSION R1(100),AK(100),RC(100),AI(100),AR1(100),AR2(100)
      COMMON/COM1/UM,UN,ZI,YI,Z,Z2,N2,N3,L
      COMMON/COM3/VN,VM,TET,N1,COI,ADENR,COSIN,COSE
      COMMON/COM4/WFN,ENRITI,ENRLTI,ENRLLI,ENRTLI,K,CS,CT,CL,IETI1,IETL
      COMMON/COM6/R1,AK,RC,AI,AR2
      COMMON/COM7/DSEED
      COMMON/COM10/MMM,TAT,BAT,TIT,KAY,ZDIR,ARA,ICS
      COMMON/COM12/TETTA
      C44=.25
      PI=3.1415927
      A=K
      K2=A*A
      K3=A*A*A
      AP2=R1(1)*C44*SQRT(2.*PI)/(C44*PI*30.)
      IF(ICS.EQ.1)GOTO121
      X=A*SIN(TETTA)
      X2=2.*TETTA
      AB=X*X
      SX2=SIN(X2)
      XQ=2.*AB-K2
      XSQ=XQ*XQ
      XS=(AB-1.)*(AB-K2)
      IF(AB.LT.1.)GOTO123
      XKSQR=SQRT(AB-1.)
```

```
      XSR=K3*SX2*XKSQR
      IF(AB.GE.1..AND.AB.LT.K2) GOTO124
      XSQR=SQRT(XS)
      FTHETA=XSQ-4.*AB*XSQR
      UITETA=-XSR/(AP2*FTHETA)
      GOTO125
  124 XSQR=CMPLX(0.,SQRT(-XS))*CMPLX(4.,0.)*CMPLX(AB,0.)
      FTHETA=CMPLX(XSQ,0.)-XSQR
      UITA=CMPLX(XSR,0.)*CMPLX(-1.,0.)/(FTHETA*CMPLX(AP2,0.))
      UITETA=REAL(UITA)
      GOTO125
  123 XKSQR=SQRT(ABS(AB-1.))
      XSQR=SQRT(XS)
      FTHETA=XSQ+4.*AB*XSQR
       XR=(-K3*SX2)
      UITA=CMPLX(XR,0.)*CMPLX(0.,XKSQR)/(CMPLX(AP2,0.)*CMPLX(FTHETA,0.))
      UITETA=REAL(UITA)
  125 AI(1)=UITETA
      GOTO122
  121 X=SIN(TETTA)
      AB=X*X
      Y=COS(TETTA)
      XS=(AB-1.)*(AB-K2)
      XSQR=SQRT(XS)
      XQ=(2.*AB-K2)
      XSQ=XQ*XQ
      FTHETA=XSQ+4.*AB*XSQR
      UR=+(Y*(-XQ))/(AP2*FTHETA)
      AI(1)=UR
  122 CONTINUE
      RETURN
      DEBUG SUBCHK
      END
      SUBROUTINE  PP
      DIMENSION TIME1(30000),VCDAT1(30000),HCDAT1(30000)
      DIMENSION X(2240),X1(2240),Y2(2240)
```

```
      INTEGER P(30000),Q(30000),PE,ARA
      DOUBLE PRECISION DSEED
      COMMON/COM1/UM,UN,ZI,Y1,Z,Z2,N2,N3,L
      COMMON/COM2/AT,AH,ATET2,APP,APS,AR
      COMMON/COM3/VN,VM,IET,N1,COI,ADENB,COSIN,COSR
      COMMON/COM4/WFN,ENRTII,ENRLTI,ENRLLI,ENRTLI,K,CS,CT,CL,IETI1,IETL
      COMMON/COM7/DSEED
      COMMON/COM8/X1,Y2,P
      COMMON/COM9/TIME1,TIME2,VCDAT1,HCDAT1,VCDAT2,HCDAT2
      N=1200
      DO10I=1,N
      X1(I)=0.
      Y2(I)=0.
10    CONTINUE
      DI=.01
      IW=80
      KJ=0
      DO15I=1,N3
      Q(I)=P(I)
15    CONTINUE
      DO41K=1,N3
      DO40J=1,N3
      IF(P(K).EQ.Q(J))GOTO44
      GOTO40
44    IF(K.EQ.J)GOTO42
      Q(J)=0.
      GOTO40
42    Q(K)=0.
      KJ=KJ+1
      TIME1(KJ)=TIME1(K)
      VCDAT1(KJ)=VCDAT1(K)
      HCDAT1(KJ)=HCDAT1(K)
40    CONTINUE
41    CONTINUE
      DO100K=1,KJ
      II=INT(TIME1(K)/DI)
```

```
      DO100I=1,IW
      IF(I.GE.1.AND.I.LE.IW)GOTO11
      W=0.
      GOTO13
   11 W=1.
   13 JJ=I+II
      X1(JJ)=VCDAT1(K)*W+X1(JJ)
      Y2(JJ)=HCDAT1(K)*W+Y2(JJ)
  100 CONTINUE
      DO200I=1,N
      X(I)=I*DI
      X1(I)=X1(I)
      Y2(I)=Y2(I)
      WRITE(6,27)X(I),X1(I),Y2(I)
   27 FORMAT(4X,3F15.6)
  200 CONTINUE
      N4=N
      CALL PLOT(0.0,2.0,-3)
      CALL SCALE(X,8.,N4,1)
      CALL AXIS(0.,0.,'TIME OF HITS',-12,8.,0.,X(N4+1),X(N4+2))
      CALL SCALE(X1,5.,N4,1)
      CALL AXIS(0.,0.,'VERT. COMP. OF DISP. TRANS.#2',29,5.,90.,
     5X1(N4+1),X1(N4+2))
      CALL LINE(X,X1,N4,1,0,0)
      CALL PLOT(12.,0.,-3)
      CALL SCALE(X,8.,N4,1)
      CALL AXIS(0.,0.,'TIME OF HITS',-12,8.,0.,X(N4+1),X(N4+2))
      CALL SCALE(Y2,5.,N4,1)
      CALL AXIS(0.,0.,'HORZ. COMP. OF DISP. TRANS.#2',29,5.,90.,
     6Y2(N4+1),Y2(N4+2))
      CALL LINE(X,Y2,N4,1,0,0)
      CALL PLOT(8.,-3.,999)
      RETURN
      DEBUG SUBCHK
      END
//
```